

Helicity Modulus and Fluctuating Type II Superconductors: Elastic Approximation and Numerical Simulations

Tao Chen and S. Teitel

Department of Physics and Astronomy, University of Rochester, Rochester, NY 14627

(May 11, 2018)

Abstract

We develop the helicity modulus as a criterion for superconducting order in the mixed phase of a fluctuating type II superconductor. We show that there is a duality relation between this helicity modulus and the superfluid density of a system of analog 2D bosons. We show that the vortex line lattice exhibits a perfect Meissner effect with respect to a shearing perturbation of the applied magnetic field, and this becomes our criterion for “longitudinal superconductivity” parallel to the applied field. We present arguments based on the 2D boson analogy, as well as the results of numerical simulations, that suggest that longitudinal superconductivity can persist into the vortex line liquid state for systems of finite thickness, comparable to those commonly found in experiments.

74.60.Ge,64.60.-i,74.40.+k

Typeset using REVTeX

I. INTRODUCTION

The mixed state of a type II superconductor in an applied magnetic field \mathbf{H} is characterized, in *mean field* theory, by a spatially varying order parameter $\psi(\mathbf{r})$ whose amplitude vanishes continuously as $T_{c2}(H)$ is approached from below.¹ While this description is adequate for traditional superconductors, the importance of thermal fluctuations in determining the behavior of the high temperature superconductors² now requires one to find a reasonable criterion for superconducting coherence in the mixed state, that is defined in terms of an average over all fluctuating configurations $\psi(\mathbf{r})$. One possibility is the correlation function $\langle\psi^*(\mathbf{r})\psi(0)\rangle$. However controversy has arisen over the proper gauge invariant definition for this correlation function;³⁻⁷ the most straightforward definition leads in three dimensions (3D) to correlations which decay exponentially^{3,4} (albeit with a long decay length) even within the Abrikosov vortex line lattice state, once harmonic elastic fluctuations of the vortex lines are included. The flux flow resistance of an unpinned vortex lattice in a completely clean material also is contrary to the conventional idea of a superconductor as a state with zero resistance. In this paper we propose using the helicity modulus as a clear equilibrium quantity that can distinguish superconducting from normal behavior in the mixed state. We will show that the helicity modulus, which for a *neutral* superfluid is proportional to the superfluid density,⁸ is in a superconductor (or *charged* superfluid) related to the magnetic susceptibility of the system to a small perturbation in applied magnetic field, about the uniform applied \mathbf{H} . Recall that it is the magnetic response, rather than electrical resistivity, that gives the true defining equilibrium signature of the Meissner transition in either a type I or type II superconductor. Here we will show that for the mixed state of a type II superconductor, the vortex line lattice displays (in the absence of dislocations) a perfect Meissner effect with respect to a certain type of *shear* perturbation of the applied field, for which the screening currents run parallel to \mathbf{H} . Such a shear Meissner effect, also referred to as *longitudinal superconductivity*,⁹ we will take as the defining equilibrium criterion for superconducting order within the mixed state. We will then give a set of arguments, including the

results of numerical simulations, that suggest that for system sizes of experimental interest, longitudinal superconductivity can persist above the vortex line lattice melting transition, into the vortex line liquid state. Some of our results have been briefly presented earlier,^{7,10} for the case of an isotropic system. Here we provide much greater detail, and generalize our formalism to the uniaxial anisotropic case.

The rest of this paper is organized as follows. In Sec. II we define our London model for a continuous anisotropic superconductor, giving the mapping of the Hamiltonian from its representation in terms of the wavefunction phase angle, to its representation in terms of interacting vortex lines. In Sec. III we define the helicity modulus $\Upsilon_{\mu\nu}(\mathbf{q})$, discuss its relation to the magnetic susceptibility, and describe the important physical parameters that may be extracted from it. We also discuss in some detail the mapping between the interacting vortex lines and an analog system of interacting two dimensional (2D) bosons.¹¹ We show that an interesting duality exists between the helicity modulus of the 3D superconductor model and the helicity modulus of the 2D analog bosons, for both the superconductor with a finite magnetic penetration length λ (our main concern in this work), and the superconductor in the $\lambda \rightarrow \infty$ approximation. In Sec. IV we analyze the helicity modulus within the elastic approximation^{12,13} for a vortex line lattice, and demonstrate the existence of the shear Meissner effect. We calculate how the penetration length for the shear perturbation increases with temperature, due to second order elastic fluctuations. In Sec. V we consider the vortex line liquid, and show how the hydrodynamic approximation¹⁴ yields the disappearance of the perfect shear Meissner effect. We discuss how the Kosterlitz–Thouless transition¹⁵ of the analog 2D bosons can yield a cross-over from a normal vortex line liquid to a line liquid with longitudinal superconductivity, and estimate this cross-over temperature as a function of system thickness and applied magnetic field. In Sec. VI we discuss our numerical Monte Carlo (MC) simulations. We define the Hamiltonian and helicity modulus for a discretized *lattice superconductor*,^{16,17} discuss our MC algorithm, and present our numerical results for an isotropic model. We compute the helicity modulus and other measures of vortex fluctuations, and find evidence for longitudinal superconductivity within the vortex line

liquid state. In Sec. VII we present our conclusions and discussion.

II. LONDON SUPERCONDUCTOR MODEL

We will model our uniaxial superconductor as a three dimensional continuum with the weak coupling direction parallel to the $\hat{\mathbf{z}}$ axis. The bare magnetic penetration length along this weak direction is λ_z , while λ_\perp is the penetration length within the more strongly coupled xy planes. $\eta \equiv \lambda_z/\lambda_\perp$ is the anisotropy parameter.

The Ginzburg-Landau Hamiltonian for the Gibbs ensemble, in the London approximation, can then be written as,

$$\mathcal{H}[\theta, \mathbf{A}] = \frac{1}{2} J_\perp \int d^3r \left[\sum_{\mu=x,y,z} \eta_\mu^{-2} (\nabla_\mu \theta - A_\mu)^2 + \lambda_\perp^2 |\nabla \times (\mathbf{A} - \mathbf{A}^{\text{ext}})|^2 \right], \quad (1)$$

where

$$J_\perp \equiv \phi_0^2 / (16\pi^3 \lambda_\perp^2) \quad (2)$$

is the coupling within the xy plane ($\phi_0 = hc/2e$ is the flux quantum),

$$\eta_x = \eta_y \equiv 1, \quad \eta_z \equiv \eta = \lambda_z/\lambda_\perp \quad (3)$$

define the anisotropy, and $(\phi_0/2\pi)\mathbf{A}$ and $(\phi_0/2\pi)\mathbf{A}^{\text{ext}}$ are the vector potentials for the internal and applied magnetic fields,

$$\nabla \times \mathbf{A} = 2\pi\mathbf{b}, \quad \nabla \times \mathbf{A}^{\text{ext}} = 2\pi\mathbf{h}, \quad (4)$$

where $\mathbf{b} = \mathbf{B}/\phi_0$ and $\mathbf{h} = \mathbf{H}/\phi_0$ are the densities of flux quanta of the magnetic field $\mathbf{B}(\mathbf{r})$ inside the superconductor, and the externally applied field $\mathbf{H}(\mathbf{r})$. In Eq.(1), $\theta(\mathbf{r})$ and $\mathbf{A}(\mathbf{r})$ are thermally fluctuating variables to be averaged over in a partition function sum, while $\mathbf{A}^{\text{ext}}(\mathbf{r})$ is a fixed (quenched) field.

It will be useful to introduce the induced magnetic vector potential,

$$\mathbf{A}^{\text{ind}} \equiv \mathbf{A} - \mathbf{A}^{\text{ext}}, \quad \nabla \times \mathbf{A}^{\text{ind}} = 2\pi(\mathbf{b} - \mathbf{h}) = 2\pi\mathbf{b}^{\text{ind}}, \quad (5)$$

in terms of which the Hamiltonian becomes,

$$\mathcal{H}[\theta, \mathbf{A}] = \frac{1}{2} J_{\perp} \int d^3r \left[\sum_{\mu} \eta_{\mu}^{-2} (\nabla_{\mu} \theta - A_{\mu}^{\text{ext}} - A_{\mu}^{\text{ind}})^2 + \lambda_{\perp}^2 |\nabla \times \mathbf{A}^{\text{ind}}|^2 \right], \quad (6)$$

and the partition function is to be viewed as a sum over \mathbf{A}^{ind} .

The Hamiltonian of Eq.(6) can now be mapped onto to a model of interacting vortex lines. If we define the superfluid velocity,

$$\mathbf{v} = \nabla \theta - \mathbf{A}^{\text{ext}} - \mathbf{A}^{\text{ind}} = \nabla \theta - \mathbf{A}, \quad (7)$$

then by Eq.(4) we have

$$\nabla \times \mathbf{v} = 2\pi(\mathbf{n} - \mathbf{h} - \mathbf{b}^{\text{ind}}) = 2\pi(\mathbf{n} - \mathbf{b}), \quad (8)$$

where $\mathbf{n} \equiv \frac{1}{2\pi} \nabla \times \nabla \theta$ is the vortex line density, consisting of singular lines of integer vorticity in the phase angle $\theta(\mathbf{r})$.

Defining the Fourier transforms,

$$\mathbf{v}_q = \int d^3r e^{i\mathbf{q}\cdot\mathbf{r}} \mathbf{v}(\mathbf{r}), \quad \mathbf{v}(\mathbf{r}) = \frac{1}{\mathcal{V}} \sum_q e^{-i\mathbf{q}\cdot\mathbf{r}} \mathbf{v}_q \quad (9)$$

(where \mathcal{V} is the system volume), we can then write the Hamiltonian (6) as,

$$\mathcal{H} = \frac{J_{\perp}}{2\mathcal{V}} \sum_{q,\mu} \left[\eta_{\mu}^{-2} v_{q\mu} v_{-q\mu} + 4\pi^2 \lambda_{\perp}^2 b_{q\mu}^{\text{ind}} b_{-q\mu}^{\text{ind}} \right], \quad (10)$$

and solve Eq.(8) as,

$$\mathbf{v}_q = -2\pi i \left[\mathbf{q} \chi_q + \frac{\mathbf{q} \times (\mathbf{n}_q - \mathbf{h}_q - \mathbf{b}_q^{\text{ind}})}{q^2} \right] \quad (11)$$

where $\chi(\mathbf{r})$ is any smooth scalar function. Substituting Eq.(11) into Eq.(10), and completing the square in χ_q , results in,

$$\mathcal{H} = \frac{4\pi^2 J_{\perp}}{2\mathcal{V}} \sum_q \left[[\mathbf{n}_q - \mathbf{h}_q - \mathbf{b}_q^{\text{ind}}] \cdot \mathbf{V}_q^0 \cdot [\mathbf{n}_{-q} - \mathbf{h}_{-q} - \mathbf{b}_{-q}^{\text{ind}}] + (q_{\perp}^2 + \eta^{-2} q_z^2) \delta \chi_q \delta \chi_{-q} + \lambda_{\perp}^2 \mathbf{b}_q^{\text{ind}} \cdot \mathbf{b}_{-q}^{\text{ind}} \right], \quad (12)$$

where

$$\mathbf{V}_q^0 = \frac{1}{q^2} \left[\mathbf{I} - \frac{\lambda_z^2 - \lambda_\perp^2}{\lambda_z^2 q_\perp^2 + \lambda_\perp^2 q_z^2} (\hat{\mathbf{z}} \times \mathbf{q})(\hat{\mathbf{z}} \times \mathbf{q}) \right] \quad (13)$$

is the “bare” vortex line interaction tensor, before screening by magnetic field fluctuations, and $\delta\chi_q \equiv \chi_q - \chi_q^0$ is the fluctuation of χ_q away from the value

$$\chi_q^0 = \frac{(\lambda_z^2 - \lambda_\perp^2) q_z [\mathbf{q} \times (\mathbf{n}_q - \mathbf{h}_q - \mathbf{b}_q^{\text{ind}})]_z}{q^2 (\lambda_z^2 q_\perp^2 + \lambda_\perp^2 q_z^2)}. \quad (14)$$

Substituting χ_q^0 into Eq.(11) gives the superfluid velocity \mathbf{v}_q^0 that minimizes \mathcal{H} for a given configuration of $\mathbf{n}_q - \mathbf{h}_q - \mathbf{b}_q^{\text{ind}}$. $\delta\chi_q$ represents a smooth “spin-wave” fluctuation about this \mathbf{v}_q^0 .

We can now complete the square in $\mathbf{b}_q^{\text{ind}}$ in Eq.(12), subject to the constraint that $\mathbf{q} \cdot \mathbf{b}_q^{\text{ind}} = 0$, to get,

$$\mathcal{H} = \frac{4\pi^2 J_\perp}{2\mathcal{V}} \sum_q \left[[\mathbf{n}_q - \mathbf{h}_q] \cdot \mathbf{V}_q \cdot [\mathbf{n}_{-q} - \mathbf{h}_{-q}] + (q_\perp^2 + \eta^{-2} q_z^2) \delta\chi_q \delta\chi_{-q} + \delta\mathbf{b}_q \cdot \mathbf{U}_q \cdot \delta\mathbf{b}_{-q} \right], \quad (15)$$

where the tensor

$$\begin{aligned} \mathbf{V}_q &= \mathbf{V}_q^0 - \mathbf{V}_q^0 \cdot \mathbf{U}_q^{-1} \cdot \mathbf{V}_q^0 = \lambda_\perp^2 \mathbf{U}_q^{-1} \cdot \mathbf{V}_q^0 \\ &= \frac{\lambda_\perp^2}{1 + \lambda_\perp^2 q^2} \left[\mathbf{I} - \frac{\lambda_z^2 - \lambda_\perp^2}{1 + \lambda_z^2 q_\perp^2 + \lambda_\perp^2 q_z^2} (\hat{\mathbf{z}} \times \mathbf{q})(\hat{\mathbf{z}} \times \mathbf{q}) \right] \end{aligned} \quad (16)$$

is the uniaxial anisotropic generalization¹³ of the familiar London vortex line interaction, and

$$\mathbf{U}_q = \lambda_\perp^2 \mathbf{I} + \mathbf{V}_q^0 \quad (17)$$

is the interaction tensor for fluctuations of magnetic field, $\delta\mathbf{b}_q \equiv \mathbf{b}_q^{\text{ind}} - \mathbf{b}_q^{\text{ind},0}$, about the value

$$\mathbf{b}_q^{\text{ind},0} = \mathbf{U}_q^{-1} \cdot \mathbf{V}_q^0 \cdot [\mathbf{n}_q - \mathbf{h}_q] = \frac{1}{\lambda_\perp^2} \mathbf{V}_q^0 \cdot [\mathbf{n}_q - \mathbf{h}_q] \quad (18)$$

that minimizes \mathcal{H} for a given configuration $\mathbf{n}_q - \mathbf{h}_q$.

Eq.(15) represents the Ginzburg-Landau Hamiltonian written in terms of decoupled spin wave, magnetic field, and vortex line fluctuations. The partition function is to be summed

over all smooth $\delta\chi_q$, all smooth $\delta\mathbf{b}_q$ subject to the constraint $\mathbf{q} \cdot \delta\mathbf{b}_q = 0$, and all singular vortex line distributions \mathbf{n}_q with conserved vorticity $\mathbf{q} \cdot \mathbf{n}_q = 0$.

The interaction \mathbf{V}_q of Eq.(16) is given as a tensor, with non-vanishing off diagonal components. However, as shown by Carneiro *et al.*,¹⁸ one can exploit the conservation of vorticity to rewrite \mathbf{V}_q in a purely diagonal way. Using

$$\begin{aligned} \mathbf{n}_q \cdot (\hat{\mathbf{z}} \times \mathbf{q})(\hat{\mathbf{z}} \times \mathbf{q}) \cdot \mathbf{n}_{-q} &= q_{\perp}^2 \mathbf{n}_{q\perp} \cdot \mathbf{n}_{-q\perp} - [\mathbf{q}_{\perp} \cdot \mathbf{n}_{q\perp}][\mathbf{q}_{\perp} \cdot \mathbf{n}_{-q\perp}] \\ &= q_{\perp}^2 \mathbf{n}_{q\perp} \cdot \mathbf{n}_{-q\perp} - q_z^2 n_{qz} n_{-qz} \quad , \end{aligned} \quad (19)$$

where $\mathbf{n}_{\perp} \equiv (n_x, n_y)$ is the transverse part of the vorticity, and a similar result for \mathbf{h}_q , we can rewrite the vortex line interaction part of the Hamiltonian as,

$$\mathcal{H}_v = \frac{4\pi^2 J_{\perp}}{2\mathcal{V}} \sum_{q,\mu} V_{q\mu} [n_{q\mu} - h_{q\mu}] [n_{-q\mu} - h_{-q\mu}] \quad , \quad (20)$$

where $V_{qx} = V_{qy} \equiv V_{q\perp}$, and,

$$V_{q\perp} = \frac{\lambda_{\perp}^2}{1 + \lambda_{\perp}^2 q_z^2 + \lambda_z^2 q_{\perp}^2} \quad , \quad V_{qz} = \frac{\lambda_{\perp}^2 (1 + \lambda_z^2 q^2)}{(1 + \lambda_{\perp}^2 q^2)(1 + \lambda_{\perp}^2 q_z^2 + \lambda_z^2 q_{\perp}^2)} \quad . \quad (21)$$

In most of this paper we will be considering behavior in the presence of a *uniform* applied magnetic field, for which $\mathbf{h}_{q \neq 0} = 0$ and hence $\mathbf{b}_{q \neq 0}^{\text{ind}} = \mathbf{b}_{q \neq 0}$.

III. HELICITY MODULUS, MAGNETIC SUSCEPTIBILITY, AND 2D BOSONS

A. Definition of the Helicity Modulus

If we define the supercurrent as,

$$j_{\mu} = J_{\perp} \eta_{\mu}^{-2} v_{\mu} = J_{\perp} \eta_{\mu}^{-2} (\nabla_{\mu} \theta - A_{\mu}^{\text{ext}} - A_{\mu}^{\text{ind}}) \quad , \quad (22)$$

then from Eqs.(10) and (22) we see that

$$\langle j_{q\mu} \rangle = -\mathcal{V} \left\langle \frac{\partial \mathcal{H}}{\partial A_{-q\mu}^{\text{ext}}} \right\rangle = -\mathcal{V} \frac{\partial \mathcal{F}}{\partial A_{-q\mu}^{\text{ext}}} \quad , \quad (23)$$

where $\mathcal{F} = -T \ln \mathcal{Z}$ is the total free energy for the partition function $\mathcal{Z} = \int \mathcal{D}\theta \mathcal{D}\mathbf{A}^{\text{ind}} e^{-\mathcal{H}/T}$.

Consider now a small perturbation about a uniform applied magnetic field $h_0\hat{\mathbf{z}}$, with $\mathbf{A}^{\text{ext}} = 2\pi h_0 x \hat{\mathbf{y}} + \delta\mathbf{A}^{\text{ext}}$. We define the helicity modulus $\Upsilon_{\mu\nu}(\mathbf{q})$ as the linear response coefficient between the induced supercurrent and the perturbation $\delta\mathbf{A}^{\text{ext}}$,

$$\langle j_{q\mu} \rangle \equiv -\Upsilon_{\mu\nu}(\mathbf{q})\delta A_{q\nu}^{\text{ext}} \quad (24)$$

From Eqs.(23) and (24) we then have

$$\begin{aligned} \Upsilon_{\mu\nu}(\mathbf{q}) &= -\left. \frac{\partial \langle j_{q\mu} \rangle}{\partial A_{q\nu}^{\text{ext}}} \right|_0 = \mathcal{V} \left. \frac{\partial^2 \mathcal{F}}{\partial A_{q\nu}^{\text{ext}} \partial A_{-q\mu}^{\text{ext}}} \right|_0 \\ &= \mathcal{V} \left\langle \frac{\partial^2 \mathcal{H}}{\partial A_{q\nu}^{\text{ext}} \partial A_{-q\mu}^{\text{ext}}} \right\rangle_0 - \frac{\mathcal{V}}{T} \left\{ \left\langle \frac{\partial \mathcal{H}}{\partial A_{q\nu}^{\text{ext}}} \frac{\partial \mathcal{H}}{\partial A_{-q\mu}^{\text{ext}}} \right\rangle_0 - \left\langle \frac{\partial \mathcal{H}}{\partial A_{q\nu}^{\text{ext}}} \right\rangle_0 \left\langle \frac{\partial \mathcal{H}}{\partial A_{-q\mu}^{\text{ext}}} \right\rangle_0 \right\}, \end{aligned} \quad (25)$$

where the subscript “0” denotes the unperturbed system with $\delta\mathbf{A}_q^{\text{ext}} = 0$. For a uniform system, the third term on the right hand side of Eq.(25) may be ignored as $\langle j_{q\mu} \rangle_0 = -\mathcal{V} \langle \partial \mathcal{H} / \partial A_{-q\mu}^{\text{ext}} \rangle_0 = 0$ (for the mixed state, we are assuming that q is smaller than any of the reciprocal lattice vectors of the vortex lattice).

Applying Eq.(25) to the Hamiltonian (10), and using the definition of Eq.(22), then results in,

$$\Upsilon_{\mu\nu}(\mathbf{q}) = J_{\perp} \eta_{\mu}^{-2} \left[\delta_{\mu\nu} - \frac{J_{\perp} \eta_{\mu}}{\mathcal{V} T \eta_{\nu}} \langle v_{q\mu} v_{-q\nu} \rangle_0 \right], \quad (26)$$

The form of Eq.(26), expressing $\Upsilon_{\mu\nu}(\mathbf{q})$ in terms of a velocity correlation, is familiar as defining the superfluid density of a neutral superfluid, or equivalently the helicity modulus of an XY model.⁸

Alternatively, we could apply the results of Eqs.(23) and (25) to the form of \mathcal{H} in Eq.(1) to get,

$$\langle j_{q\mu} \rangle = -J_{\perp} \lambda_{\perp}^2 \langle [\mathbf{q} \times (\mathbf{q} \times \mathbf{A}_q^{\text{ind}})]_{\mu} \rangle = -2\pi i J_{\perp} \lambda_{\perp}^2 \langle [\mathbf{q} \times \mathbf{b}_q^{\text{ind}}]_{\mu} \rangle, \quad (27)$$

and,

$$\Upsilon_{\mu\nu}(\mathbf{q}) = J_{\perp} \lambda_{\perp}^2 \left[q^2 \delta_{\mu\nu} - q_{\mu} q_{\nu} - \frac{4\pi^2 J_{\perp} \lambda_{\perp}^2}{\mathcal{V} T} \langle [\mathbf{q} \times \mathbf{b}_q]_{\mu} [\mathbf{q} \times \mathbf{b}_{-q}]_{\nu} \rangle_0 \right], \quad (28)$$

where we have used $\mathbf{b}_q = \mathbf{b}_q^{\text{ind}}$ for the unperturbed system, and $\langle \mathbf{b}_q \rangle_0 = 0$ for finite small \mathbf{q} . Eq.(27) is just a statement of Ampère’s law, relating the induced magnetic field to the

flowing supercurrents. Eq.(28) expresses $\Upsilon_{\mu\nu}(\mathbf{q})$ in an explicitly gauge invariant form, in terms of correlations of the fluctuating internal magnetic field \mathbf{b} .

Finally, we can also express $\Upsilon_{\mu\nu}(\mathbf{q})$ in terms of vortex line correlations. Using the form of \mathcal{H} in Eq.(15), substituting in $2\pi\mathbf{h}_q = -i\mathbf{q} \times \mathbf{A}_q^{\text{ext}}$, and taking the appropriate derivatives as in Eq.(25), results in,

$$\Upsilon_{\mu\nu}(\mathbf{q}) = J_{\perp} \left[(\mathbf{q} \times \hat{\nu}) \cdot \mathbf{V}_q \cdot (\mathbf{q} \times \hat{\mu}) - \frac{4\pi^2 J_{\perp}}{\mathcal{V}T} (\mathbf{q} \times \hat{\nu}) \cdot \mathbf{V}_q \cdot \langle \mathbf{n}_{-q} \mathbf{n}_q \rangle_0 \cdot \mathbf{V}_q \cdot (\mathbf{q} \times \hat{\mu}) \right] \quad (29)$$

where \mathbf{V}_q is the vortex line interaction tensor of either Eqs.(16) or (21).

Note that the helicity modulus is Hermitian, $\Upsilon_{\mu\nu}(\mathbf{q}) = \Upsilon_{\nu\mu}^*(\mathbf{q}) = \Upsilon_{\nu\mu}(-\mathbf{q})$. Also note that any longitudinal component of $\delta\mathbf{A}_q^{\text{ext}}$ produces no response in $\langle \mathbf{j}_q \rangle$, since $\Upsilon(\mathbf{q}) \cdot \mathbf{q} = 0$. This is as expected since a longitudinal component of $\delta\mathbf{A}_q^{\text{ext}}$ produces no magnetic field, and can be eliminated by a gauge transformation. Henceforth it will be simplest to work in the London gauge in which $\mathbf{q} \cdot \mathbf{A}_q^{\text{ext}} = 0$.

The tensor products in Eq.(29) can be simplified greatly if we restrict our interest to wavevectors lying along the symmetry directions, i.e. $\mathbf{q} = q\hat{\mathbf{x}}$, $q\hat{\mathbf{y}}$, and $q\hat{\mathbf{z}}$. Changing notation for the sake of clarity, from \mathbf{n}_q to $\mathbf{n}(\mathbf{q})$, and using Eq.(21) for \mathbf{V}_q , we find for the diagonal elements

$$\Upsilon_{\mu}(q\hat{\nu}) \equiv \Upsilon_{\mu\mu}(q\hat{\nu}) = \frac{J_{\perp} \lambda_{\perp}^2 q^2}{1 + \lambda_{\mu}^2 q^2} \left[1 - \frac{4\pi^2 J_{\perp} \lambda_{\perp}^2}{\mathcal{V}T} \frac{\langle n_{\sigma}(q\hat{\nu}) n_{\sigma}(-q\hat{\nu}) \rangle_0}{1 + \lambda_{\mu}^2 q^2} \right], \quad (30)$$

where μ, ν, σ are any cyclic permutation of x, y, z , and λ_{μ} is either λ_z or λ_{\perp} depending on whether $\mu = z$ or $\mu = x, y$. Note that $\Upsilon_{\mu}(q\hat{\nu}) \sim q^2$ as $q \rightarrow 0$.

The off diagonal elements are

$$\Upsilon_{\mu\nu}(q\hat{\sigma}) = \frac{J_{\perp} \lambda_{\perp}^2 q^2}{1 + \lambda_{\mu}^2 q^2} \left[\frac{4\pi^2 J_{\perp} \lambda_{\perp}^2}{\mathcal{V}T} \frac{\langle n_{\nu}(q\hat{\sigma}) n_{\mu}(-q\hat{\sigma}) \rangle_0}{1 + \lambda_{\nu}^2 q^2} \right]. \quad (31)$$

However for $\mathbf{q} = q\hat{\sigma}$, $\mathbf{q} \cdot \mathbf{n}_q = 0$ implies that $n_{\mu}(q\hat{\sigma})$ and $n_{\nu}(q\hat{\sigma})$ fluctuate without constraint, and since the free energy of Eq.(20) is symmetric separately in $n_{\mu} \rightarrow -n_{\mu}$ and in $n_{\nu} \rightarrow -n_{\nu}$, we expect that the off diagonal terms will vanish.

Henceforth we will restrict ourselves to the simple cases given by Eq.(30). For a uniform applied magnetic field along the $\hat{\mathbf{z}}$ direction, and taking here and henceforth μ, ν, σ to be a

cyclic permutation of x, y, z , we have the three distinct cases, (a) $\Upsilon_y(q\hat{\mathbf{z}})$, (b) $\Upsilon_x(q\hat{\mathbf{y}})$, and (c) $\Upsilon_z(q\hat{\mathbf{x}})$. In Fig. 1 we show a schematic of the magnetic field lines corresponding to these three different perturbations. As suggested by these diagrams, we will refer to (a) as the *tilt* perturbation, (b) as the *compression* perturbation, and (c) as the *shear* perturbation. We will find that the first two cases are determined by the transverse and longitudinal magnetic susceptibilities respectively. We will find that the presence of a perfect Meissner effect with respect to the shear perturbation is a convenient measure of superconducting coherence for the mixed state. Because the screening currents involved in the shear perturbation run parallel to the applied magnetic field, a perfect Meissner effect for the shear perturbation has also been termed *longitudinal superconductivity*.⁹

B. Magnetic Susceptibilities and Renormalized Penetration Lengths

As indicated above, the helicity modulus $\Upsilon_{\mu\nu}(\mathbf{q})$ is closely related to the magnetic susceptibility. Combining Ampère's Law (27) with the definition of $\Upsilon_{\mu\nu}(\mathbf{q})$ in Eq.(24), we have

$$\langle \delta \mathbf{A}_q^{\text{ind}} \rangle = -\frac{\Upsilon(\mathbf{q})}{J_{\perp} \lambda_{\perp}^2 q^2} \cdot \delta \mathbf{A}_q^{\text{ext}} . \quad (32)$$

For the three cases of Eq.(30), corresponding to perturbations $\delta \mathbf{A}_{\mu}^{\text{ext}}(q\hat{\nu})$ where μ, ν, σ is a cyclic permutation of x, y, z , $\Upsilon(\mathbf{q})$ is diagonal and so we can substitute into the above $2\pi\delta b_{\sigma}^{\text{ind}}(q\hat{\nu}) = -iq\delta A_{\mu}^{\text{ind}}(q\hat{\nu})$ and $2\pi\delta h_{\sigma}(q\hat{\nu}) = -iq\delta A_{\mu}^{\text{ext}}(q\hat{\nu})$ to get,

$$-\frac{\Upsilon_{\mu}(q\hat{\nu})}{J_{\perp} \lambda_{\perp}^2 q^2} = \left. \frac{\partial \langle b_{\sigma}^{\text{ind}}(q\hat{\nu}) \rangle}{\partial h_{\sigma}(q\hat{\nu})} \right|_0 \equiv 4\pi\chi_{\sigma}(q\hat{\nu}) , \quad (33)$$

where $\mathbf{b}_q^{\text{ind}}/4\pi$ is the induced magnetization, and $\chi_{\sigma}(q\hat{\nu})$ is the magnetic susceptibility at wavevector $q\hat{\nu}$ for a perturbation in applied magnetic field in direction $\hat{\sigma}$.

To get a feel for the information contained in the helicity modulus, or equivalently the magnetic susceptibility, consider first the case of zero field, in the absence of vortex line fluctuations. When $\mathbf{n}_q = 0$, Eq.(30) yields $\Upsilon_{\mu} = J_{\perp} \lambda_{\perp}^2 q^2 / (1 + \lambda_{\mu}^2 q^2)$. Substituting into Eq.(33) gives,

$$4\pi\chi_\sigma(q\hat{\nu}) = \frac{-1}{1 + \lambda_\mu^2 q^2} . \quad (34)$$

This describes a perfect Meissner effect. As $q \rightarrow 0$, $\langle \delta b_\sigma^{\text{ind}}(q\hat{\nu}) \rangle = 4\pi\chi_\sigma(q\hat{\nu})\delta h_\sigma(q\hat{\nu}) = -\delta h_\sigma(q\hat{\nu})$, and so the total field inside the superconductor, $\langle \delta b_\sigma \rangle = \delta h_\sigma + \langle \delta b_\sigma^{\text{ind}} \rangle$ vanishes. The perturbation δh_σ is completely expelled from the system. The length scale on which this expulsion takes place is λ_μ .

In the presence of vortex line fluctuations, we can write a phenomenological form for the helicity modulus at small q ,

$$\Upsilon_\mu(q\hat{\nu}) = \gamma_\mu \frac{J_\perp \lambda_\perp^2 q^2}{1 + \lambda_{\mu R}^2 q^2} . \quad (35)$$

In this case, substituting into Eq.(33) one gets,

$$4\pi\chi_\sigma(q\hat{\nu}) = \frac{-\gamma_\mu}{1 + \lambda_{\mu R}^2 q^2} . \quad (36)$$

Now only a fraction γ_μ of the applied perturbation is expelled from the system; this expulsion takes place on the length scale $\lambda_{\mu R}$. We thus see that $-\gamma_\mu$ gives the long wavelength magnetic susceptibility, while $\lambda_{\mu R}$ is the magnetic penetration length, as renormalized by vortex fluctuations. γ_μ and $\lambda_{\mu R}$ are the important physical parameters to be extracted from the helicity modulus.

Formally, we can define γ_μ and $\lambda_{\mu R}$ in terms of the small q expansion of the vortex line correlation that appears in Eq.(30). If we define,

$$\langle n_\sigma(q\hat{\nu})n_\sigma(-q\hat{\nu}) \rangle_0 \equiv n_{\mu 0} + n_{\mu 1}q^2 + n_{\mu 2}q^4 + \dots , \quad (37)$$

then we have,

$$\gamma_\mu \equiv -\lim_{q \rightarrow 0} 4\pi\chi_\sigma(q\hat{\nu}) = 1 - \frac{4\pi^2 J_\perp \lambda_\perp^2}{\mathcal{V}T} n_{\mu 0} , \quad (38)$$

and,

$$\frac{\lambda_{\mu R}^2}{\lambda_\mu^2} \equiv -\lim_{q \rightarrow 0} \left[\frac{1}{\lambda_\mu^2 \chi_\sigma(q\hat{\nu})} \frac{d\chi_\sigma(q\hat{\nu})}{dq^2} \right] = 1 - \frac{4\pi^2 J_\perp \lambda_\perp^2}{\mathcal{V}T} \frac{(n_{\mu 0} - n_{\mu 1} \lambda_\mu^{-2})}{\gamma_\mu} . \quad (39)$$

Thus $\gamma_\mu = 1$, or equivalently $n_{\mu 0} = 0$, signals a perfect Meissner screening of the perturbation $\delta A_\mu^{\text{ext}}(q\hat{\nu})$. For zero applied magnetic field, this has a simple physical interpretation: one is in the Meissner state if there are no infinitely large vortex rings.

Although the helicity modulus should have the form of Eq.(35) both below and above the superconducting transition, due to the presence of ordinary fluctuation diamagnetism above the transition, we expect that a phase transition will be indicated by singular behavior in the parameters γ_μ and $\lambda_{\mu R}$. In particular, a transition from a state with perfect a Meissner screening of the perturbation $\delta A_\mu^{\text{ext}}(q\hat{\nu})$ will be signaled by a singular decrease of γ_μ from unity, as well, presumably, by a divergence in $\lambda_{\mu R}^2$. For such a case, it is reasonable to interpret $n_s \equiv m_\mu c^2 / 4\pi e^2 \lambda_{\mu R}^2$ as the density of superconducting electrons.

We stress at this point that γ_μ and $\lambda_{\mu R}$ are describing the response of the system to a small spatially varying perturbation about a uniform applied field and not the response to this uniform field itself.

C. 2D Boson Analogy

Much work on vortex line fluctuations has been done utilizing an analogy between the magnetic field induced vortex lines in the mixed phase of a three dimensional superconductor and the imaginary time world lines of two dimensional bosons within a Feynman path integral description of 2D quantum mechanics. Here we will show the explicit connection between the superfluid density of these analog 2D bosons and the helicity modulus $\Upsilon_z(q\hat{\mathbf{x}})$ giving the response to the *shear* perturbation of Fig. 1c.

In this analogy, as introduced by Nelson,¹¹ the energy of vortex line fluctuations is modeled by two pieces: (i) a line tension representing the vortex core energy and self interaction, and (ii) a pairwise interaction between all vortex line segments which lie in the same xy plane at equal heights z . This simplified vortex interaction is expected to be a reasonable approximation when the vortex lines remain, over the length scale λ , approximately parallel to the applied field. This simplified vortex interaction is then mapped into a 2D boson

mass and an instantaneous pairwise boson interaction. The mapping results in the following correspondences (quantities on the left refer to the 2D bosons, those on the right refer to the 3D superconductor): imaginary time, $\tau \leftrightarrow z$, distance in direction of applied field \mathbf{h} ; $\hbar_{\text{boson}}/T_{\text{boson}} \leftrightarrow L_z$, length of system parallel to \mathbf{h} ; $\hbar_{\text{boson}} \leftrightarrow T$, temperature of 3D superconductor; boson mass, $m_{\text{boson}} \leftrightarrow \tilde{\epsilon}_1 \sim \pi J_z$, where $\tilde{\epsilon}_1 = \eta^{-2}\epsilon_1$, and ϵ_1 is the single vortex line tension.

In Appendix A, starting from the standard definition of the superfluid density as the long wavelength limit of the transverse momentum susceptibility,^{19,20} we derive an expression Eq.(A8) for the number density of superfluid bosons, $\rho_{s \text{ boson}}$, for a system of 2D interacting bosons, expressed in the form of a path integral over boson world lines. In Eqs.(A9) and (A10) we show that $\rho_{s \text{ boson}}$ is related to the helicity modulus of the 2D bosons, $\Upsilon_{\text{boson}}(q)$, by $\lim_{q \rightarrow 0} \Upsilon_{\text{boson}}(q) = (\hbar_{\text{boson}}^2/m_{\text{boson}})\rho_{s \text{ boson}}$. We now recast the results of Appendix A into the language of vortex lines.

For a magnetic field induced vortex line i parameterized by its transverse deflection $\mathbf{r}_{i\perp}(z)$ in the xy plane at height z , the vortex line density is given by,

$$\mathbf{n}(\mathbf{r}_\perp, z) = \sum_i \delta^{(2)}(\mathbf{r}_\perp - \mathbf{r}_{i\perp}(z)) \left[\hat{\mathbf{z}} + \frac{d\mathbf{r}_{i\perp}(z)}{dz} \right]. \quad (40)$$

Using the above correspondences between the analog bosons and the superconductor, we then have for the term that appears in the boson path integral of Eq.(A9),

$$\int_0^{\hbar_{\text{boson}}/T_{\text{boson}}} d\tau \sum_i \frac{dr_{iy}}{d\tau} e^{iqx_i} = n_y(q\hat{\mathbf{x}}). \quad (41)$$

Eq.(A10) for the 2D boson helicity modulus can then be written as,

$$\frac{\Upsilon_{\text{boson}}(q)}{T_{\text{boson}}} = \frac{1}{L_\perp^2} \langle n_y(q\hat{\mathbf{x}}) n_y(-q\hat{\mathbf{x}}) \rangle_0, \quad (42)$$

where L_\perp is the length of the system in the xy plane. The vortex correlation that appears in Eq.(42) above is precisely the same correlation that enters Eq.(30) for $\Upsilon_z(q\hat{\mathbf{x}})$, which gives the response to the shear perturbation of Fig.1c. Taking the limit $q \rightarrow 0$ in Eq.(42) and combining with Eqs.(37), (38) and (A10) then gives,

$$\gamma_z = 1 - \frac{4\pi^2 J_\perp \lambda_\perp^2}{L_z T} \left[\frac{\Upsilon_{\text{boson}}(q \rightarrow 0)}{T_{\text{boson}}} \right] = 1 - \frac{4\pi^2 J_\perp \lambda_\perp^2}{L_z T} \left[\frac{\hbar_{\text{boson}}^2 \rho_{s \text{ boson}}}{m_{\text{boson}} T_{\text{boson}}} \right]. \quad (43)$$

This leads to the following identifications, originally pointed out by Feigelman and co-workers:²¹ the 2D boson superfluid phase with $\rho_{s \text{ boson}} > 0$ corresponds to a 3D vortex line normal diamagnetic phase with $\gamma_z < 1$; the 2D boson normal fluid phase with $\rho_{s \text{ boson}} = 0$ corresponds to a 3D vortex line phase with $\gamma_z = 1$, and hence with longitudinal superconductivity characterized by a perfect Meissner effect for shear perturbations.

Having made the above observation, there now exists the possibility, as first suggested by Nelson,¹¹ that a Kosterlitz–Thouless (KT) transition from superfluid to normal fluid in the analog 2D boson system, could appear in the 3D superconductor as a transition from a normal vortex line liquid state to a vortex line liquid with longitudinal superconductivity. Fisher and Lee,²² and more recently Täuber and Nelson,²³ have argued that if one relaxes the periodic boundary conditions along $\hat{\mathbf{z}}$ that is assumed in the boson analogy, and uses instead the free boundary conditions which are more realistic for a bulk 3D superconductor, the sharp KT transition no longer exists. Nevertheless, one might expect that a clear cross-over remnant of this KT transition should still be observable in the superconductor. We will return to discuss this KT cross-over in Sec. VB.

D. $\lambda \rightarrow \infty$ Approximation

Many numerical simulations,^{24–30} as well as other theoretical approaches such as the “lowest Landau level” approximation,³¹ have been based upon the approximation of taking $\lambda_\perp \rightarrow \infty$, while keeping J_\perp finite. This approximation corresponds to taking a spatially uniform internal magnetic field \mathbf{b} which is equal to the applied field \mathbf{h} . Such an approximation can be shown to be exact for modeling the analog system of a 3D neutral (uncharged particles) superfluid in a rotating bucket.^{4,19} It is interesting to see how the helicity modulus and the 2D boson analogy look within this $\lambda \rightarrow \infty$ limit.

In this case, the interaction between vortex lines is given by the “bare” interaction tensor

\mathbf{V}_q^0 of Eq.(13). One can show that the correct helicity modulus $\Upsilon_\mu(q\hat{\nu})$ is obtained by taking the limit $\lambda_\mu \rightarrow \infty$ in Eq.(30), keeping J_\perp and $\lambda_\perp/\lambda_\mu$ constant,

$$\Upsilon_\mu(q\hat{\nu}) = J_\mu \left[1 - \frac{4\pi^2 J_\mu}{\mathcal{V}T} \frac{\langle n_\sigma(q\hat{\nu})n_\sigma(-q\hat{\nu}) \rangle_0}{q^2} \right] , \quad (44)$$

where $J_\mu \equiv J_\perp(\lambda_\perp/\lambda_\mu)^2$ is the coupling in direction $\hat{\mu}$.

Noting that $\mathcal{H}_v = (4\pi^2 J_\perp/2\mathcal{V}) \sum_q \mathbf{n}_q \cdot \mathbf{V}_q^0 \cdot \mathbf{n}_{-q}$ must have a finite thermal average, and since $\mathbf{V}_q^0 \sim 1/q^2$, it must therefore be true that as $q \rightarrow 0$,

$$\langle n_\sigma(q\hat{\nu})n_\sigma(-q\hat{\nu}) \rangle_0 \sim q^2 . \quad (45)$$

Substituting Eq.(45) into Eq.(44) we see that, in contrast to the finite λ_μ case where we found $\Upsilon_\mu(q\hat{\nu}) \sim q^2$ as $q \rightarrow 0$, here we find that $\lim_{q \rightarrow 0} \Upsilon_\mu(q\hat{\nu})$ is in general a finite number. This differing dependence of the helicity modulus on q , in the small q limit, is one of the characteristic differences between a charged superfluid (with a finite λ giving a coupling to a fluctuating vector potential) and a neutral superfluid (with $\lambda \rightarrow \infty$ leading to a frozen vector potential). For the $\lambda \rightarrow \infty$ case of a neutral superfluid, $\Upsilon_\mu(0) \equiv \lim_{q \rightarrow 0} \Upsilon_\mu(q\hat{\nu})$ is just proportional to the number density of superfluid particles, as discussed in Appendix A for the two dimensional case, and used in the preceding section. We therefore expect to find $\Upsilon_z(0) > 0$ for $T < T_c$ in an ordered phase with longitudinal superconductivity, and $\Upsilon_z(0) = 0$ for $T > T_c$ in the normal phase.

We now consider the 2D boson analogy for this $\lambda \rightarrow \infty$ approximation. Combining Eq.(42) for the helicity modulus $\Upsilon_{\text{boson}}(q)$ of the analog bosons with Eq.(45), we see that

$$\Upsilon_{\text{boson}}(q) \sim q^2 \quad \text{for small } q . \quad (46)$$

Thus the analog 2D bosons have a helicity modulus characteristic of a 2D *charged* superfluid! This is in agreement with the results of Feigelman and co-workers,²¹ who show that the system of vortex lines interacting with the true London interaction of Eqs.(20) and (21) (as opposed to the more simplified interaction of Nelson's model) can be viewed as a system of analog 2D bosons whose interaction is mediated by a massive vector potential. As $\lambda \rightarrow \infty$,

the mass associated with this vector potential vanishes, and one has a system of 2D charged bosons interacting with 2D electrodynamics.

We can develop the analogy further. Combining Eqs.(42) with (44) we have,

$$\Upsilon_z(q\hat{\mathbf{x}}) = J_z \left[1 - \frac{4\pi^2 J_z}{L_z T q^2} \frac{\Upsilon_{\text{boson}}(q)}{T_{\text{boson}}} \right] \quad (47)$$

One can then define the proportionality coefficient γ_{boson} of Eq.(46) by,

$$\Upsilon_{\text{boson}}(q) = \gamma_{\text{boson}} T_{\text{boson}} \frac{L_z T q^2}{4\pi^2 J_z} = \gamma_{\text{boson}} \left[\frac{\hbar_{\text{boson}}^2}{4\pi^2 J_z} \right] q^2, \quad (48)$$

where we have used the correspondences between superconducting variables and analog boson variables to arrive at the last equality. Note that when $\gamma_{\text{boson}} = 1$ we have $\Upsilon_z(0) = 0$, and when $\gamma_{\text{boson}} < 1$ we have $\Upsilon_z(0) > 0$.

One can now show,³² at least in the isotropic case, that the term $[\hbar_{\text{boson}}^2/4\pi^2 J] = [\hbar_{\text{boson}}^2 4\pi\lambda^2/\phi_0^2]$ which appears on the right hand side of Eq.(48) is just twice the magnetic energy coupling of the analog magnetic field of the 2D electrodynamics. We can rename this coupling $[J\lambda^2]_{\text{boson}}$ in analogy with the magnetic energy coupling of our original 3D superconductor of Eq.(1). Eq.(48) then becomes,

$$\Upsilon_{\text{boson}}(q) = \gamma_{\text{boson}} [J\lambda^2]_{\text{boson}} q^2 \quad (49)$$

in complete agreement with the small q limit of the form of the helicity modulus for a charged superfluid, given in Eq.(35) (as derived for our original 3D superconductor at finite λ). $-\gamma_{\text{boson}}$ is therefore the magnetic susceptibility of the analog 2D charged bosons. To next order in q^2 we expect, in analogy with Eq.(35), that $\Upsilon_{\text{boson}}(q)$ has the form,

$$\Upsilon_{\text{boson}}(q) = \gamma_{\text{boson}} \frac{[J\lambda^2]_{\text{boson}} q^2}{1 + \lambda_{\text{R boson}}^2 q^2}, \quad (50)$$

where $\lambda_{\text{R boson}}$ is the magnetic penetration length of the analog 2D charged bosons. If we take $\lambda_{\text{R boson}}^2 = 1/(4\pi n_s \text{ boson})$, with $n_s \text{ boson}$ the number density of superfluid charged bosons, then combining Eqs.(47–50) one can recover all the results found in Sec. V B.3 of Blatter *et al.*,³³ which are therefore seen to apply in a strict sense only to the $\lambda \rightarrow \infty$ approximation, rather than to the finite λ case.

We thus have the following amusing duality. For finite λ we have seen in the preceding section that the 3D superconductor, which is a charged superfluid problem, maps onto analog 2D bosons, which is a neutral superfluid problem. The 3D longitudinal superconductivity transition maps onto the 2D superfluid transition. A perfect Meissner effect for shear perturbations in the 3D superconductor, with $\gamma_z = 1$, represents the normal fluid state of the 2D bosons with $\Upsilon_{\text{boson}}(q \rightarrow 0) = 0$; the loss of this perfect Meissner effect, with $\gamma_z < 1$, corresponds to the superfluid state of the 2D bosons with $\Upsilon_{\text{boson}}(q \rightarrow 0) > 0$. For $\lambda \rightarrow \infty$ however, the 3D superconductor, which now behaves like a neutral superfluid problem, maps onto 2D bosons interacting with 2D electrodynamics, which is a charged superfluid problem. The 3D longitudinal superconductivity transition now maps onto a Meissner transition of a 2D superconductor. The normal state of the 3D superconductor, with $\Upsilon_z(q \rightarrow 0) = 0$, corresponds to a perfect Meissner state of the charged 2D bosons, with $\gamma_{\text{boson}} = 1$; the 3D superconducting state, with $\Upsilon_z(q \rightarrow 0) > 0$, corresponds to the loss of this perfect Meissner effect for the 2D charged bosons, with $\gamma_{\text{boson}} < 1$.

Note that for the analog 2D charged bosons of the $\lambda \rightarrow \infty$ approximation, vortices in the 2D condensate wavefunction will interact with a potential that decays exponentially on length scales greater than $\lambda_{\text{R boson}}$, due to the screening by the 2D analog magnetic field. A vortex anti-vortex pair will therefore have a finite energy barrier for unbinding, and so at any finite T_{boson} there must be free vortices which will destroy the 2D Meissner state. Only at $T_{\text{boson}} = 0$ ($L_z \rightarrow \infty$), does there remain the possibility of a sharp Meissner transition in this 2D analog boson system, as \hbar_{boson} varies. Such a transition, if it exists, is driven by quantum and not thermal fluctuations and so it is not in the Kosterlitz–Thouless universality class. We believe that it is this transition at $T_{\text{boson}} = 0$, in the $\lambda \rightarrow \infty$ model, that the work of Feigelman and co-workers²¹ pertains to. Recently, Tešanović has argued³⁴ that such a transition must be driven by the proliferation of closed vortex rings (boson anti-boson virtual pairs), which are left out of the naive 2D boson mapping, and that the transition will be in the universality class of the ordinary 3D XY model.

The above considerations suggest that taking the $\lambda \rightarrow \infty$ limit in our model is rather

subtle and possibly leads to discontinuous changes in the phase diagram, although any such discontinuities will likely be obscured in a finite size system by very strong cross-over effects.

IV. THE VORTEX LINE LATTICE: ELASTIC APPROXIMATION

We consider now the mixed state of a type II superconductor. At low temperatures, such a state is described by the familiar Abrikosov vortex line lattice. In this case, we can evaluate the vortex line correlations that appear in the expression for the helicity modulus by using the well known elastic approximation.^{12,13} It is now convenient to work in the Helmholtz ensemble, with a fixed uniform density b_0 of magnetic field induced vortex lines,

$$b_0 = \frac{B}{\phi_0} \quad , \quad a_v = \left(\frac{4}{3}\right)^{1/4} \frac{1}{\sqrt{b_0}} \quad (51)$$

where a_v is the lattice spacing between lines in their ground state triangular lattice. We will denote thermal averages in this ensemble by $\langle \dots \rangle$, dropping the subscript “0” that we used earlier.

In the elastic approximation, one assumes that vortex line excitations consist only of fluctuations of the magnetic field induced vortex lines, transverse to the direction of the uniform applied field. Such fluctuations are described by the displacement field $\mathbf{u}_i(z)$, which gives the transverse displacement in the xy plane at height z , of the vortex line away from its position \mathbf{R}_i in the ground state vortex lattice. The vortex line density is thus given by Eq.(40), making the substitution $\mathbf{r}_{i\perp}(z) = \mathbf{R}_i + \mathbf{u}_i(z)$.

If we define the Fourier transforms

$$\mathbf{u}_q = \frac{1}{b_0} \int dz \sum_i e^{i(q_z z + \mathbf{q}_\perp \cdot \mathbf{R}_i)} \mathbf{u}_i(z), \quad \mathbf{u}_i(z) = \frac{1}{\mathcal{V}} \sum_q e^{-i(q_z z + \mathbf{q}_\perp \cdot \mathbf{R}_i)} \mathbf{u}_q \quad , \quad (52)$$

where $\mathbf{q}_\perp = (q_x, q_y)$ and the sum over \mathbf{q}_\perp is restricted to the first Brillouin Zone of the Abrikosov lattice, then to lowest order in \mathbf{u} the vortex line density at small finite \mathbf{q} may be written as

$$\mathbf{n}_q = i b_0 [\mathbf{q} \cdot \mathbf{u}_q \hat{\mathbf{z}} - q_z \mathbf{u}_q] \quad . \quad (53)$$

Substituting the expansion for \mathbf{n}_q in terms of the \mathbf{u}_q into Eq.(20), summing over reciprocal lattice vectors, and keeping only terms up to order u_q^2 , results in the free energy functional for elastic vortex line displacements,

$$\begin{aligned} \mathcal{H}_{\text{el}}[\mathbf{u}] &= \frac{1}{2\mathcal{V}} \sum_{q\alpha\beta} u_{q\alpha} \Phi_{\alpha\beta}(\mathbf{q}) u_{-q\beta} \\ &= \frac{1}{2\mathcal{V}} \sum_q \left\{ [c_{44}(\mathbf{q})q_z^2 + c_{11}(\mathbf{q})q_{\perp}^2] u_{qL} u_{-qL} + [c_{44}(\mathbf{q})q_z^2 + c_{66}(\mathbf{q})q_{\perp}^2] u_{qT} u_{-qT} \right\}. \end{aligned} \quad (54)$$

Here $u_{qL} = \hat{\mathbf{q}} \cdot \mathbf{u}_q$ is the longitudinal part of the displacement, and $u_{qT} = |\mathbf{u}_q - \hat{\mathbf{q}}u_{qL}|$ is the transverse part. $c_{44}(\mathbf{q})$, $c_{66}(\mathbf{q})$, and $c_{11}(\mathbf{q})$ are the wavevector dependent tilt, shear, and compression elastic moduli respectively. We can now use Eqs. (53) and (54) to evaluate the vortex correlations of the helicity modulus of Eq.(30), for the three simple cases of Fig. 1.

A. Tilt Perturbation

We first consider $\Upsilon_y(q\hat{\mathbf{z}})$ which gives the response to the tilt perturbation of Fig.1a. Using Eq.(53), the relevant vortex correlation, to lowest order in \mathbf{u}_q , is

$$\langle n_x(q\hat{\mathbf{z}}) n_x(-q\hat{\mathbf{z}}) \rangle = q^2 b_0^2 \langle u_T(q\hat{\mathbf{z}}) u_T(-q\hat{\mathbf{z}}) \rangle = \frac{b_0^2 \mathcal{V} T}{c_{44}(q\hat{\mathbf{z}})}, \quad (55)$$

where we have used \mathcal{H}_{el} of Eq.(54) to evaluate the displacement correlation. Expanding in q^2 we have,

$$n_{y0} = \frac{b_0^2 \mathcal{V} T}{c_{44}(0)}, \quad n_{y1} = - \frac{b_0^2 \mathcal{V} T}{c_{44}^2(0)} \left. \frac{dc_{44}}{dq_z^2} \right|_{q=0}. \quad (56)$$

Combining Eqs.(2), (38), (39), and (51) with (56) above then gives for the helicity modulus parameters,

$$\gamma_y = 1 - \frac{B^2}{4\pi c_{44}(0)}, \quad (57)$$

and,

$$\frac{\lambda_{yR}^2}{\lambda_{\perp}^2} = 1 - \frac{B^2}{4\pi c_{44}(0)\gamma_y} \left[1 + \frac{1}{c_{44}(0)\lambda_{\perp}^2} \left. \frac{dc_{44}}{dq_z^2} \right|_{q=0} \right]. \quad (58)$$

Note that from general thermodynamic arguments³⁵ one has,

$$c_{44}(0) = \frac{B^2}{4\pi} \frac{dH_{\perp}}{dB_{\perp}}, \quad (59)$$

where the dH_{\perp}/dB_{\perp} is evaluated at the average magnetic field $B_0\hat{\mathbf{z}}$. Hence γ_y is determined by the transverse magnetic susceptibility,

$$\gamma_y = 1 - \frac{dB_{\perp}}{dH_{\perp}}, \quad (60)$$

as expected from our discussion in Sec. III B.

Using our explicit results for c_{44} from Appendix B, we have,

$$\gamma_y \simeq \begin{cases} \frac{\phi_0}{8\pi\lambda_{\perp}^2 B} \left[\eta^{-2} \left(\ln \frac{H_{c2}}{B} - 1 \right) + \frac{\phi_0}{4\pi\lambda_{\perp}^2 B} \right] \ll 1 & \text{for large B, } \lambda_{\perp} \gg a_v \\ 1 - \frac{8\pi\lambda_{\perp}^2 B}{\phi_0} \frac{1}{\eta^{-2} [\ln(H_{c2}/B) - 1] + 1} \approx 1 & \text{for intermediate B, } \lambda_{\perp} \ll a_v \ll \lambda_z \\ 1 - \frac{8\pi\lambda_{\perp}^2 B}{\phi_0} \frac{1}{\eta^{-2} [2 \ln(\eta\kappa) - 1] + 1} \approx 1 & \text{for small B, } \lambda_z \ll a_v \end{cases} \quad (61)$$

For λ_{yR} , using Eq.(58) and our results for c_{44} from Appendix B, we have for large magnetic fields, $\lambda_{\perp} \gg a_v$,

$$\frac{\lambda_{yR}^2}{\lambda_{\perp}^2} \simeq \begin{cases} \frac{1}{2\lambda_{\perp}^2 k_0^2} & \text{for strong anisotropy, } \frac{1}{2\lambda_{\perp}^2 k_0^2} \gg \eta^{-2} \ln \left(\frac{H_{c2}}{B} \right) \\ \frac{1}{2\lambda_{\perp}^2 k_0^2} \eta^{-2} \ln \left(\frac{H_{c2}}{B} \right) & \text{for weak anisotropy, } \frac{1}{2\lambda_{\perp}^2 k_0^2} \ll \eta^{-2} \ln \left(\frac{H_{c2}}{B} \right) \end{cases} \quad (62)$$

For intermediate magnetic fields, $\lambda_{\perp} \ll a_v \ll \lambda_z$, (where strong anisotropy is by definition implied) we have

$$\frac{\lambda_{yR}^2}{\lambda_{\perp}^2} \simeq 1 - \lambda_{\perp}^2 k_0^2, \quad (63)$$

and for weak magnetic fields, $\lambda_z \ll a_v$, we have

$$\frac{\lambda_{yR}^2}{\lambda_{\perp}^2} \simeq \begin{cases} 1 - 2\lambda_{\perp}^2 k_0^2 & \text{for strong anisotropy, } \frac{1}{2} \gg \eta^{-2} \ln \eta \kappa \\ 1 - \frac{\lambda_{\perp}^2 k_0^2}{\eta^{-2} \ln \eta \kappa} & \text{for weak anisotropy, } \frac{1}{2} \ll \eta^{-2} \ln \eta \kappa \end{cases} \quad (64)$$

where $k_0^2 = 4\pi B/\phi_0 \sim 1/a_v^2$.

For strong magnetic fields, $\lambda_{\perp} \gg a_v$, Eq.(62) gives $\lambda_{yR} \simeq 1/\sqrt{2}k_0 \lesssim a_v$, independent of the bare λ_{\perp} . Since our definition of λ_{yR} in Eq.(35) was based on an expansion in small q , it is doubtful that we should take such a small λ_{yR} too seriously as a screening length, without considering higher terms in an expansion in q , as well as considering the response \mathbf{j}_{q+K} to the perturbation $\mathbf{A}_q^{\text{ext}}$ (where \mathbf{K} is a reciprocal lattice vector of the vortex lattice).

For weak magnetic fields, $\lambda_{\perp} \ll a_v$, Eqs.(63) and (64) give, $\lambda_{yR} \approx \lambda_{\perp}$.

B. Compression Perturbation

We next consider $\Upsilon_x(q\hat{\mathbf{y}})$ which gives the response to the compression perturbation of Fig. 1b. Using Eq.(53), the relevant vortex correlation, to lowest order in \mathbf{u}_q , is

$$\langle n_z(q\hat{\mathbf{y}})n_z(-q\hat{\mathbf{y}}) \rangle = q^2 b_0^2 \langle u_L(q\hat{\mathbf{y}})u_L(-q\hat{\mathbf{y}}) \rangle = \frac{b_0^2 \mathcal{V}T}{c_{11}(q\hat{\mathbf{y}})}, \quad (65)$$

where we have used Eq.(54) to evaluate the displacement correlation.

We therefore have,

$$\gamma_x = 1 - \frac{B^2}{4\pi c_{11}(0)}. \quad (66)$$

The compression modulus in the vortex line lattice can be written as $c_{11} = c_L + c_{66}$, where c_L is the ‘‘bulk modulus’’ for an isotropic compression. General thermodynamic arguments give,³⁵

$$c_L(0) = \frac{B^2}{4\pi} \frac{dH_z}{dB_z}. \quad (67)$$

Noting from Eqs.(B16) and (B23) that, for large $\lambda_{\perp} \gg a_v$, $c_{66}(0) \ll c_{11}$, we have $c_{11}(0) \simeq c_L(0)$, and so,

$$\gamma_x \simeq 1 - \frac{dB_z}{dH_z} \quad (68)$$

is determined by the longitudinal magnetic susceptibility. For $\lambda_\perp \ll a_v$, Eqs.(B22) and (B23) give $c_{11} = \frac{3}{2}c_L$, and so $\gamma_x = 1 - \frac{2}{3}(dB_z/dH_z)$.

Using our explicit results for c_{11} from Appendix B, we find,

$$\gamma_x \simeq \begin{cases} -\frac{\phi_0}{16\pi\lambda_\perp^2 B} & \text{for large B, } \lambda_\perp \gg a_v \\ -\frac{16\sqrt{2\pi}\lambda_\perp^2 B}{9\phi_0} \left(\frac{\lambda_\perp}{a_v}\right)^{3/2} e^{a_v/\lambda_\perp} & \text{for small B, } \lambda_\perp \ll a_v \end{cases} \quad (69)$$

$\gamma_x < 0$ implies that the magnetic field induced in the material is *larger* than the applied perturbation, so there is *negative* screening. This may be understood from Eq.(68) by noting that in the mixed phase one always has $dB_z/dH_z > 1$.

For the screening length, we find

$$\frac{\lambda_{xR}^2}{\lambda_\perp^2} \simeq \begin{cases} -\frac{1}{4\lambda_\perp^2 k_0^2} & \text{for large B, } \lambda_\perp \gg a_v \\ -\frac{5 a_v^2}{72\lambda_\perp^2} & \text{for small B, } \lambda_\perp \ll a_v \end{cases} \quad (70)$$

Since $k_0^2 = 4\pi B/\phi_0 \sim 1/a_v^2$, both cases give $\lambda_{xR} \sim ia_v$. It is tempting to interpret this imaginary λ_{xR} as indicating the rearrangement of vortex lines on the length scale a_v due to the penetration of the applied field, with no ‘‘healing’’ length at all at the surface of the sample. However our cautionary remarks following Eq.(64), concerning the applicability of our results on the length scale a_v , should again be noted.

C. Shear Perturbation

The preceding two cases of the tilt and the compression perturbations gave information about the transverse and longitudinal magnetic susceptibilities, via γ_y and γ_x . However, since for large B λ_{yR} , $\lambda_{xR} \sim a_v$ is independent of the bare λ_\perp , it is unclear whether they give any information about the density of superconducting electrons, or whether they can

be expected to diverge at the superconducting to normal transition. A more interesting case is therefore given by the third possibility, $\Upsilon_z(q\hat{\mathbf{x}})$, which gives the response to the shear perturbation of Fig. 1c.

The relevant vortex correlation we need to compute is $\langle n_y(q\hat{\mathbf{x}})n_y(-q\hat{\mathbf{x}}) \rangle$, but to lowest order in \mathbf{u}_q , Eq.(53) shows this to vanish identically. This is merely an artifact of our Fourier transform of the displacement field \mathbf{u} , which prohibits vortex lines from having a net tilt away from the $\hat{\mathbf{z}}$ axis. To avoid this difficulty we can evaluate the correlation at $\mathbf{q} = q_x\hat{\mathbf{x}} + q_z\hat{\mathbf{z}}$, with finite q_z , and then take the limit as $q_z \rightarrow 0$. From Eqs.(53) and (54) we get

$$\lim_{q_z \rightarrow 0} \langle n_y(\mathbf{q})n_y(-\mathbf{q}) \rangle = \lim_{q_z \rightarrow 0} \frac{q_z^2 b_0^2 \mathcal{V}T}{c_{66}(\mathbf{q})q_x^2 + c_{44}(\mathbf{q})q_z^2} . \quad (71)$$

For the case of a vortex line lattice with $c_{66} > 0$, taking $q_z \rightarrow 0$ results in a vanishing of the vortex correlation. From Eqs.(38) and (39) we then have $\lambda_{zR} = \lambda_z$, and $\gamma_z = 1$. We will see in the next section that higher order elastic corrections lead to a temperature dependent increase in λ_{zR} , but do not change $\gamma_z = 1$. The vortex line lattice thus exhibits longitudinal superconductivity, with a perfect Meissner effect for shear perturbations.

If one assumes $c_{66} \equiv 0$, as might describe the case of a vortex line liquid, Eq.(71) results in $\langle n_y(q\hat{\mathbf{x}})n_y(-q\hat{\mathbf{x}}) \rangle = b_0^2 \mathcal{V}T / c_{44}(q\hat{\mathbf{x}})$. In this case we have $\gamma_z = 1 - B^2 / 4\pi c_{44}(0) = 1 - dB_\perp / dH_\perp < 1$, exactly as in the case of the tilt perturbation, Eqs.(57) and (60). To summarize,

$$\begin{aligned} \langle n_y(q\hat{\mathbf{x}})n_y(-q\hat{\mathbf{x}}) \rangle &= 0 , & \gamma_z &= 1 & \text{if } c_{66} > 0 \\ \langle n_y(q\hat{\mathbf{x}})n_y(-q\hat{\mathbf{x}}) \rangle &= \frac{b_0^2 \mathcal{V}T}{c_{44}(q\hat{\mathbf{x}})} , & \gamma_z &= 1 - \frac{dB_\perp}{dH_\perp} < 1 & \text{if } c_{66} \equiv 0 \end{aligned} \quad (72)$$

The above arguments suggest that a singular decrease of γ_z from unity (or equivalently the singular increase of n_{z0} from zero), marking the loss of longitudinal superconductivity, serves as a convenient criterion for the superconducting to normal transition in the mixed state of a type II superconductor. This is one of the main results of our paper. If this transition is second order, we expect that λ_{zR} will diverge at the transition with $n_s \sim 1/\lambda_{zR}^2$ the density of superconducting electrons.

In considering the vortex correlation at $\mathbf{q} = q_x \hat{\mathbf{x}} + q_z \hat{\mathbf{z}}$, it is the relative order in which one takes q_x and q_z to zero that distinguishes between the shear and the tilt perturbation. It is the order corresponding to the shear perturbation that is related to the superfluid density of the 2D analog bosons, $\rho_{s \text{ boson}}$. Note that if we had defined $\rho_{s \text{ boson}}$ in terms of the $\mathbf{q} = 0$ winding number of Pollock and Ceperley,³⁶ rather than in terms of the $\mathbf{q} \rightarrow 0$ transverse momentum correlation function as we have done in Appendix A, the connection of $\rho_{s \text{ boson}}$ to the shear, as opposed to the tilt, perturbation would become ambiguous.

The preceding discussion has been based upon elastic fluctuations about a perfect dislocation free vortex line lattice. Recently, Frey *et al.*³⁷ have argued that, at sufficiently high magnetic field in a layered superconductor, the proliferation of dislocations can result in the loss of longitudinal superconductivity even in the vortex line lattice state.

D. Second Order Corrections

Our analysis in the preceding sections is based on Eq.(53), which gives an expansion of the vortex line density \mathbf{n} to *linear* order in the displacement field \mathbf{u} . In this section, we consider the effect of higher orders, by continuing the expansion in \mathbf{u} ,

$$\begin{aligned}
\mathbf{n}_q &= ib_0[\mathbf{q} \cdot \mathbf{u}_q \hat{\mathbf{z}} - q_z \mathbf{u}_q] \\
&- \frac{b_0}{V} \sum_{q'} \left\{ \frac{1}{2} [\mathbf{q} \cdot \mathbf{u}_{q'}] [\mathbf{q} \cdot \mathbf{u}_{q-q'}] \hat{\mathbf{z}} - (q_z - q'_z) [\mathbf{q} \cdot \mathbf{u}_{q'}] \mathbf{u}_{q-q'} \right\} \\
&- \frac{ib_0}{2V^2} \sum_{q', q''} \left\{ \frac{1}{3} [\mathbf{q} \cdot \mathbf{u}_{q'}] [\mathbf{q} \cdot \mathbf{u}_{q''}] [\mathbf{q} \cdot \mathbf{u}_{q-q'-q''}] \hat{\mathbf{z}} \right. \\
&\quad \left. - (q_z - q'_z - q''_z) [\mathbf{q} \cdot \mathbf{u}_{q'}] [\mathbf{q} \cdot \mathbf{u}_{q''}] \mathbf{u}_{q-q'-q''} \right\} + \dots
\end{aligned} \tag{73}$$

for small but finite \mathbf{q} .

To systematically evaluate vortex correlations using this higher order expansion, one should also in principle extend the elastic energy of Eq.(54) to higher order in \mathbf{u} by taking the expansion above, and substituting into the vortex-vortex interaction Hamiltonian of Eq.(20). The resulting expression is rather complex. For simplicity, we will instead continue to use the quadratic elastic energy of Eq.(54), however we now view the elastic moduli as

appropriately redefined temperature dependent parameters, in the spirit of a self-consistent phonon approximation.

We consider here only the case of $\Upsilon_z(q\hat{\mathbf{x}})$, corresponding to the shear perturbation, for which we need the correlation, $\lim_{q_z \rightarrow 0} \langle n_y(\mathbf{q})n_y(-\mathbf{q}) \rangle$, with $\mathbf{q} = q\hat{\mathbf{x}} + q_z\hat{\mathbf{z}}$. As we have already seen in the preceding section, for $c_{66} > 0$, the contribution to $O(u^2)$ vanishes. By symmetry, the next leading term is $O(u^4)$. Using the expansion of Eq.(73), and factorizing the average of the product of the four u 's into all possible pairs, we find,

$$\begin{aligned} \langle n_y(\mathbf{q})n_y(-\mathbf{q}) \rangle &= b_0^2 T^2 q_\alpha q_\beta \sum_{\mathbf{q}'} \left\{ (q_z - q'_z)^2 \Phi_{\alpha\beta}^{-1}(\mathbf{q}') \Phi_{yy}^{-1}(\mathbf{q} - \mathbf{q}') \right. \\ &\quad \left. + (q_z - q'_z) q'_z \Phi_{\alpha y}^{-1}(\mathbf{q}') \Phi_{\beta y}^{-1}(\mathbf{q} - \mathbf{q}') - q_z^2 \Phi_{yy}^{-1}(\mathbf{q}) \Phi_{\alpha\beta}^{-1}(\mathbf{q}') \right\} , \end{aligned} \quad (74)$$

where summation over $\alpha, \beta = x, y$, is implied, and Φ is the elasticity tensor of Eq.(54). Taking $q_z \rightarrow 0$, keeping only terms of $O(q^2)$, and using the fact that Φ is symmetric in \mathbf{q} as well as its indices, we get,

$$\langle n_y(q\hat{\mathbf{x}})n_y(-q\hat{\mathbf{x}}) \rangle = b_0^2 T^2 \mathcal{V} q^2 I , \quad (75)$$

where I is the integral,

$$I \equiv \frac{1}{\mathcal{V}} \sum_{\mathbf{k}} \frac{k_z^2}{\det \Phi_{\mathbf{k}}} = \frac{1}{\mathcal{V}} \sum_{\mathbf{k}} \frac{k_z^2}{(c_{44}k_z^2 + c_{11}k_\perp^2)(c_{44}k_z^2 + c_{66}k_\perp^2)} . \quad (76)$$

The correlation of Eq.(75) vanishes as q^2 for $q \rightarrow 0$. We therefore continue to find, as in the preceding section, that $n_{z0} = 0$ and $\gamma_z = 1$ giving a perfect Meissner screening of the shear perturbation. It is straightforward to see that this result persists to all orders in u .

However, in contrast to the preceding section, we now find a finite renormalization of the penetration length. Comparing the expansion of Eq.(37) with the result of Eq.(75), we get $n_{z1} = b_0^2 T^2 \mathcal{V} I$. Using this in Eq.(39) then gives,

$$\frac{\lambda_{zR}^2}{\lambda_z^2} = 1 + \frac{B^2}{4\pi\lambda_z^2} IT . \quad (77)$$

Thus the $o(u^4)$ term generates an $O(T)$ correction to λ_{zR}^2 . Continuing the elastic expansion in powers of u will generate corrections to λ_{zR}^2 in the form of a power series in T .

To estimate the magnitude of the correction to λ_{zR} of Eq.(77) we can evaluate the integral I using a crude approximation. The elastic moduli which appear in I are functions of wavevector \mathbf{k} . However the dominant contributions to the integral will come at wavevectors $k_z \simeq \sqrt{(c_{66}/c_{44})} k_\perp$ and $k_z \simeq \sqrt{(c_{11}/c_{44})} k_\perp$, both giving $k_z \simeq \eta k_\perp$. The dominant k_\perp will be $k_\perp \simeq k_0 = \sqrt{4\pi B/\phi_0}$, at the edge of the Brillouin zone. We will therefore approximate the elastic moduli by their values at this dominant wavevector, denoting these values as \tilde{c}_{44} , \tilde{c}_{11} , and \tilde{c}_{66} . Within this approximation one can explicitly calculate the integral to get,

$$I = \frac{k_0}{4\pi \tilde{c}_{44} \sqrt{\tilde{c}_{44}} (\sqrt{\tilde{c}_{11}} + \sqrt{\tilde{c}_{66}})} . \quad (78)$$

Within the same crude approximation we can estimate the vortex lattice melting temperature T_m . Using the Lindemann criterion^{2,6,38} that melting occurs when $\langle u^2 \rangle \simeq c_L^2 a_v^2$ ($c_L \sim 0.15$ is the Lindemann parameter), and keeping only the transverse fluctuations as the dominant soft mode, we get,

$$T_m = \frac{4\pi c_L^2 a_v^2 \sqrt{\tilde{c}_{66} \tilde{c}_{44}}}{k_0} . \quad (79)$$

Combining Eqs. (77), (78), and (79), and using the estimate that $\tilde{c}_{11} \sim \tilde{c}_{66}$ at the Brillouin zone boundary, we find,

$$\frac{\lambda_{zR}^2}{\lambda_z^2} \simeq 1 + \frac{1}{2} c_L^2 \left(\frac{a_v}{\lambda_z} \right)^2 \frac{B^2}{4\pi \tilde{c}_{44}} \frac{T}{T_m} . \quad (80)$$

Using the result of Fisher³⁹ for c_{44} at the zone boundary, for large magnetic fields $\lambda_\perp \gg a_v$,

$$\tilde{c}_{44} \simeq \frac{\phi_0 B}{32\pi^2 \lambda_z^2} \left[1 + \ln \left[\frac{H_{c2}}{B(1 + \eta^{-2})} \right] \right] , \quad (81)$$

we get,

$$\frac{\lambda_{zR}^2}{\lambda_z^2} \simeq 1 + \frac{4\pi c_L^2 \sqrt{4/3}}{1 + \ln \left[\frac{H_{c2}}{B(1 + \eta^{-2})} \right]} . \quad (82)$$

Taking for example $B = 0.2H_{c2}$, and $\eta^{-2} \ll 1$, we estimate a 12% increase in λ_{zR}^2 over λ_z^2 near melting, due to lowest order elastic fluctuations. Since the elastic moduli $c_{\alpha\alpha}(\mathbf{k})$ are in general larger than the values $\tilde{c}_{\alpha\alpha}$, this is an overestimate. The above estimate does not of course include the effects of critical fluctuations near a phase transition, which for a second order transition should result in a divergence of λ_{zR} at T_c .

V. THE VORTEX LINE LIQUID

In the preceding section we considered the vortex line lattice at $T < T_m$. In particular we showed how the response to the shear perturbation, given by $\Upsilon_z(q\hat{\mathbf{x}})$, gives a useful criterion for superconducting phase coherence: $\gamma_z \equiv \lim_{q \rightarrow 0} [\Upsilon_z(q\hat{\mathbf{x}})/J_\perp \lambda_\perp^2 q^2] = 1$, or equivalently $n_{z0} \equiv \lim_{q \rightarrow 0} \langle n_y(q\hat{\mathbf{x}})n_y(-q\hat{\mathbf{x}}) \rangle = 0$, indicates the presence of longitudinal superconductivity. In this section we consider behavior in the vortex line liquid at $T > T_m$. As a measure of superconductivity we focus on the behavior of n_{z0} .

A. Hydrodynamic Approximation

The simplest approximation one can make at high T is to take the Hamiltonian (20) and regard the Fourier components of the vortex line density \mathbf{n}_q as continuous, independently fluctuating variables, subject to the constraint $\mathbf{q} \cdot \mathbf{n}_q = 0$. We refer to this as a hydrodynamic approximation.⁴⁰ This yields $\langle n_y(q\hat{\mathbf{x}})n_y(-q\hat{\mathbf{x}}) \rangle = T\mathcal{V}/[4\pi^2 J_\perp V_\perp(q\hat{\mathbf{x}})]$. Substituting into Eq.(30), we find that $\Upsilon_z(q\hat{\mathbf{x}}) = 0$ for all values of q , reflecting the fact that well above the superconducting transition, an applied magnetic field will induce no supercurrents at all.

For temperatures closer to, but still above T_m , we expect the system to show a finite fluctuation diamagnetism. A better approximation can be obtained by coarse graining the Hamiltonian (20) over a length scale of order the inter-vortex spacing a_v , and then applying the hydrodynamic approximation to average over the resulting coarse grained vortex density. This coarse grained free energy has been given by Marchetti¹⁴ as,

$$\mathcal{H}[\mathbf{n}] = \frac{1}{2b_0^2\mathcal{V}} \sum_{\mathbf{q}} \{c_L(\mathbf{q})\delta n_{qz}\delta n_{-qz} + c_{44}(\mathbf{q})\mathbf{n}_{q\perp} \cdot \mathbf{n}_{-q\perp}\} , \quad (83)$$

where $\delta n_z = n_z - b_0$, c_L is the bulk modulus, and c_{44} is a tilt modulus of the same form as for the vortex lattice. Using this form we find,

$$n_{z0} = \lim_{q \rightarrow 0} \langle n_y(q\hat{\mathbf{x}})n_y(-q\hat{\mathbf{x}}) \rangle = \frac{b_0^2\mathcal{V}T}{c_{44}(0)} > 0 , \quad (84)$$

and from Eqs.(38) and (59),

$$\gamma_z = 1 - \frac{B^2}{4\pi c_{44}(0)} = 1 - \frac{dB_{\perp}}{dH_{\perp}} < 1 . \quad (85)$$

Thus, within this hydrodynamic approximation, the longitudinal superconductivity found in the vortex line lattice is lost for the vortex line liquid. Note that since Eq.(85) gives γ_z strictly less than unity in the vortex line liquid, while $\gamma_z = 1$ in the vortex line lattice, γ_z presumably takes a discontinuous jump at the transition where longitudinal superconductivity is lost.

A more detailed calculation of vortex correlations, averaging over unbounded dislocation loops within a continuum elastic model, has been carried out by Marchetti and Nelson⁴¹ as a model for a hexatic vortex line liquid. In the limit $q \rightarrow 0$, the result of Eq.(84) is again obtained.

Eqs.(84) and (85) are identical to the result we found in Eq.(72) by simply taking $c_{66} \equiv 0$ in the elastic approximation for the vortex line lattice. It is interesting to speculate about the behavior of a “soft” vortex line lattice in which the long wavelength shear modulus vanishes, $c_{66}(\mathbf{q} = 0) = 0$, but in which a finite shear stiffness remains on shorter length scales, $c_{66}(\mathbf{q}_{\perp}, q_z = 0) > 0$ for $\mathbf{q}_{\perp} > 0$. In this case, taking the limit $\mathbf{q} \rightarrow 0$ as in Eq.(71), we find that $n_{z0} = 0$ and longitudinal superconductivity remains.⁴² As Marchetti and Nelson⁴¹ show however, it is not possible to describe an entangled vortex line liquid with such a simple elastic description.⁴³

B. Kosterlitz-Thouless Transition

In Sec.III C we discussed how the KT superfluid transition of the analog 2D bosons could appear in the 3D superconductor as a strong cross-over to a vortex line liquid state with longitudinal superconductivity. In his original model, Nelson¹¹ interpreted this KT transition in terms of a transition from an “entangled” to a “disentangled” vortex line liquid, for sufficiently thin samples. In this section, we estimate the temperature T_c for this KT transition as a function of sample thickness L_z and magnetic field B , and compare this estimate with Nelson’s entanglement criterion.

The 2D KT superfluid transition is characterized¹⁵ by the fact that, exactly at the transition, the boson helicity modulus $\Upsilon_{\text{boson}}(q \rightarrow 0)$ takes a discontinuous jump to zero from the universal finite value $\Upsilon_{\text{boson}}/T_{\text{boson}} = 2/\pi$. Υ_{boson} is given by the vortex correlation of Eq.(42), which for a vortex line liquid can be related to the tilt modulus c_{44} by Eq.(84). Using Eq.(59) for c_{44} and applying the universal jump criterion then gives for the KT transition,

$$T_c = \frac{2 c_{44}(0)}{\pi b_0^2 L_z} = \frac{\phi_0^2}{2\pi^2 L_z} \frac{dH_\perp}{dB_\perp} . \quad (86)$$

Thus as the thickness L_z increases, T_c decreases. In order to observe a vortex line liquid with longitudinal superconductivity we need the system to be thin enough that $T_c > T_m$. If we define the length,

$$\Lambda \equiv \frac{\phi_0^2}{2\pi^2 T_m} , \quad (87)$$

then we can rewrite Eq.(86) as,

$$\frac{T_c}{T_m} = \frac{dH_\perp}{dB_\perp} \frac{\Lambda}{L_z} \equiv \frac{L_{z \text{ max}}}{L_z} . \quad (88)$$

We thus will have $T_c > T_m$ provided,

$$L_z < L_{z \text{ max}} = \frac{dH_\perp}{dB_\perp} \Lambda = \left(\frac{4\pi c_{44}(0)}{B^2} \right) \Lambda . \quad (89)$$

Assuming that $c_{44}(0)$ in the line liquid is not too different from $c_{44}(0)$ in the line lattice, we can use our results from Appendix B to evaluate the length $L_{z \text{ max}}$. For large applied magnetic fields, such that $a_v \ll \lambda_\perp$ or equivalently $H_{c1} \ll B$, we have $dH_\perp/dB_\perp \simeq 1$ and so to leading order,

$$L_{z \text{ max}} = \Lambda . \quad (90)$$

For small magnetic fields, such that $\lambda_z \ll a_v$, we have,

$$L_{z \text{ max}} = \frac{\phi_0}{8\pi \lambda_\perp^2 B} \left\{ \eta^{-2} [2 \ln(\eta \kappa) - 1] + 1 \right\} \Lambda . \quad (91)$$

For an anisotropic material in intermediate magnetic fields, such that $\lambda_{\perp} \ll a_v \ll \lambda_z$, we have to leading order,

$$L_{z \max} = \frac{\phi_0}{8\pi\lambda_{\perp}^2 B} \left\{ \eta^{-2} [\ln(H_{c2}/B) - 1] + 1 \right\} \Lambda . \quad (92)$$

Note that for a melting temperature of $T_m \sim 90^\circ\text{K}$, as in YBCO, one has for large B , $L_{z \max} = \Lambda \simeq 1400\mu\text{m}$. This is much thicker than typical experimental samples, which are generally of the order $50\mu\text{m}$. As B decreases, $L_{z \max}$ only gets *larger*.

The above results may be compared with the original criterion for 2D boson superfluidity given by Nelson¹¹ in terms of the ‘‘entanglement length,’’

$$\xi_z = \frac{\tilde{\epsilon}_1 \phi_0}{2TB} . \quad (93)$$

ξ_z is the length required for a vortex line to have a transverse deflection equal to the average spacing between vortex lines, a_v . Only when $\xi_z < L_z$ can the vortex lines have enough transverse wandering so that they may become geometrically entangled. The cross-over T_{\times} between a disentangled and an entangled vortex line liquid is thus given by,

$$T_{\times} = \frac{\tilde{\epsilon}_1 \phi_0}{2BL_z} = \frac{\phi_0^2}{2\pi^2 L_z} \frac{\phi_0 \eta^{-2} \ln \kappa}{16\lambda_{\perp}^2 B} , \quad (94)$$

where we have used $\tilde{\epsilon}_1 = \epsilon_1 \eta^{-2}$ with $\epsilon_1 = (\phi_0^2/4\pi\lambda_{\perp})^2 \ln \kappa$ for small B . One will have $T_{\times} > T_m$ only for $L_z < L'_{z \max}$, where,

$$L'_{z \max} = \frac{4}{\pi} \left[\frac{\pi^2 \tilde{\epsilon}_1}{\phi_0 B} \right] \Lambda = \frac{\phi_0 \eta^{-2} \ln(\kappa)}{16\lambda_{\perp}^2 B} \Lambda . \quad (95)$$

Except for some numerical factors, $L'_{z \max}$ agrees with $L_{z \max}$ of Eqs.(91) and (92), decreasing as $1/B$, for increasing magnetic field. In the large field limit however, our result in Eq.(90) saturates to the finite value Λ instead of continuing to decrease. The difference between the results of Eqs.(90) and (95) arises because the later is based on the the line tension $\tilde{\epsilon}_1$ for the energy of a single vortex line tilting, while the former is based on the tilt modulus $c_{44}(0)$ for the collective tilting of all lines. This points out an important distinction: geometric vortex line entanglement, i.e. the local wrapping of lines around each other, is not necessarily

equivalent to the global vortex line winding that characterizes the analog 2D boson superfluid phase.³⁶ Nelson's entanglement length of Eq.(95) nevertheless remains the important length scale for local geometric entanglement, which still can have a significant effect on the dynamic behavior of the vortex line liquid if the barriers for vortex line cutting are high.⁴⁴

The above discussion has been based on the familiar KT transition of an ordinary 2D superfluid, and predicts that as $L_z \rightarrow \infty$ at fixed $T > T_m$ ($T_{\text{boson}} \rightarrow 0$ at fixed \hbar_{boson}) $T_c \rightarrow 0$ and so one is always in the boson superfluid state, corresponding to a normal vortex line liquid. Feigelman⁴⁵ and co-workers²¹ however have argued that for $\lambda \rightarrow \infty$, the long range nature of the effective 2D boson interaction can lead to a normal boson fluid, and hence to a vortex line liquid with longitudinal superconductivity, even in the $L_z \rightarrow \infty$ ($T_{\text{boson}} \rightarrow 0$) limit for $T < T_c^\infty$, where T_c^∞ (i.e. the critical \hbar_{boson} in the boson variables) gives the 2D Meissner transition of the analog 2D *charged* bosons of the $\lambda \rightarrow \infty$ approximation, as discussed in Sec. III D. Such a $\lambda \rightarrow \infty$ transition would probably lead to strong cross-over effects in the finite λ case, which would obscure the KT transition when $L_z \ll L_{z \text{ max}}$, where the T_c of Eq.(86) can be very much larger than T_c^∞ .

Searching for longitudinal superconductivity within the vortex line liquid will be one of the main objectives of our numerical investigations, to be discussed in the following section.

VI. NUMERICAL SIMULATIONS

In this section we report the results of numerical Monte Carlo simulations we have carried out in order to study the behavior of the system of fluctuating vortex lines.

A. Lattice Superconductor

To carry out numerical simulations, our first step will be to discretize the continuum to a cubic grid of $N = N_\perp^2 N_z$ sites i . The grid spacing in direction $\hat{\mu}$ is taken to be

$$a_\mu = \begin{cases} a_\perp = \xi_\perp, & \mu = x, y \\ a_z = d, & \mu = z \end{cases} \quad (96)$$

The grid spacing ξ_\perp in the xy plane is meant to approximate the core radius of a vortex, while the spacing d along \hat{z} is meant to simulate the spacing between CuO planes of a layered high T_c superconductor. If one wants to model an anisotropic continuum superconductor, such as in Sec. II, one should take $d \equiv \xi_z$, where the anisotropic Ginzburg Landau free energy functional gives² $\xi_z = \eta^{-1}\xi_\perp$. Discretization of Eq.(1) then leads to the *lattice superconductor* model,^{16,17}

$$\mathcal{H}[\theta_i, A_{i\mu}] = \sum_{i,\mu} \left[\mathcal{U}_\mu(\theta_{i+\hat{\mu}} - \theta_i - A_{i\mu}) + 2\pi^2 C_\mu (b_{i\mu} - h_{i\mu})^2 \right], \quad (97)$$

where θ_i is the phase angle on grid site i ,

$$A_{i\mu} = \int_i^{i+\hat{\mu}} \mathbf{A} \cdot d\ell \quad (98)$$

is the integral of the total magnetic vector potential across the bond at site i in direction $\hat{\mu}$, and if μ, ν, σ is a cyclic permutation of x, y, z , then,

$$2\pi b_{i\mu} = A_{i+\hat{\nu},\sigma} - A_{i\sigma} - A_{i+\hat{\sigma},\nu} + A_{i\nu} \quad (99)$$

is the sum of the $A_{j\nu}$ going counterclockwise around the plaquette at site i in direction $\hat{\mu}$, and gives 2π times the flux of total magnetic field through the plaquette (see Fig. 2); a similar relation defines $h_{i\mu}$ in terms of $A_{i\mu}^{\text{ext}}$. The kinetic energy piece is expressed in terms of the Villain function,⁴⁶

$$e^{-\mathcal{U}_\mu(\phi)/T} = \sum_{m=-\infty}^{\infty} e^{-\bar{J}_\mu \eta_\mu^{-2} (\phi - 2\pi m)^2 / 2T}, \quad (100)$$

with couplings,

$$\bar{J}_\mu = J_\perp \frac{a_\nu a_\sigma}{a_\mu} = \begin{cases} \bar{J}_\perp = J_\perp d, & \mu = x, y \\ \bar{J}_z = J_\perp \frac{\xi_\perp^2}{d}, & \mu = z \end{cases} \quad (101)$$

The couplings of the magnetic energy piece are,

$$C_\mu = J_\perp \lambda_\perp^2 \frac{a_\mu}{a_\nu a_\sigma} = \begin{cases} C_\perp = \bar{J}_z \left(\frac{\lambda_\perp}{\xi_\perp} \right)^2, & \mu = x, y \\ C_z = \bar{J}_\perp \left(\frac{\lambda_\perp}{\xi_\perp} \right)^2, & \mu = z \end{cases} \quad (102)$$

To express the Hamiltonian in terms of vortex line variables, we first perform a standard duality transformation⁴⁷ of the kinetic energy piece, and then, following Carneiro¹⁷ (in complete analogy with Eqs.(15) –(21)), complete the square in $b_{q\mu}^{\text{ind}} = b_{q\mu} - h_{q\mu}$ subject to the constraint that $\mathbf{b}_q^{\text{ind}}$ is divergenceless. Our lattice Fourier transforms are defined by,

$$b_{q\mu} = \sum_i e^{i\mathbf{q}\cdot\mathbf{r}_i} b_{i\mu}, \quad b_{i\mu} = \frac{1}{N} \sum_q e^{-i\mathbf{q}\cdot\mathbf{r}_i} b_{q\mu}, \quad (103)$$

and the constraint that $b_{i\mu}^{\text{ind}}$ is divergenceless can be written as, $\mathbf{Q}^* \cdot \mathbf{b}_i^{\text{ind}} = 0$, where,

$$Q_\mu \equiv 1 - e^{iq_\mu a_\mu}. \quad (104)$$

The vortex part of the resulting Hamiltonian is,

$$\mathcal{H}_v = \frac{4\pi^2 \bar{J}_\perp}{2N} \sum_{q,\alpha} V_{q\alpha} [n_{q\alpha} - h_{q\alpha}] [n_{-q\alpha} - h_{-q\alpha}], \quad (105)$$

where $V_{qx} = V_{qy} \equiv V_{q\perp}$, and,

$$V_{q\perp} = \frac{\left(\frac{\lambda_\perp}{d} \right)^2}{1 + \left(\frac{\lambda_\perp}{d} \right)^2 |Q_z|^2 + \left(\frac{\lambda_z}{\xi_\perp} \right)^2 |\mathbf{Q}_\perp|^2} \quad (106)$$

$$V_{qz} = \frac{\left(\frac{\lambda_\perp}{\xi_\perp} \right)^2 \left[1 + \left(\frac{\lambda_z}{d} \right)^2 |Q_z|^2 + \left(\frac{\lambda_z}{\xi_\perp} \right)^2 |\mathbf{Q}_\perp|^2 \right]}{\left[1 + \left(\frac{\lambda_\perp}{d} \right)^2 |Q_z|^2 + \left(\frac{\lambda_\perp}{\xi_\perp} \right)^2 |\mathbf{Q}_\perp|^2 \right] \left[1 + \left(\frac{\lambda_\perp}{d} \right)^2 |Q_z|^2 + \left(\frac{\lambda_z}{\xi_\perp} \right)^2 |\mathbf{Q}_\perp|^2 \right]}. \quad (107)$$

$n_{q\mu}$ is the Fourier transform of the vorticity $n_{i\mu}$ piercing plaquette $i\mu$. Eqs.(105–107) are the lattice equivalents of the continuum Eqs.(20) and (21).

Note that \mathcal{H}_v/T depends on *four* dimensionless parameters, which may be taken to be \bar{J}_\perp/T , $\eta = \lambda_z/\lambda_\perp$, $\kappa = \lambda_\perp/\xi_\perp$, and $\zeta = \xi_\perp/d$. The ratio the of couplings that appear in the Villain kinetic energy terms of Eq.(100) is then $\bar{J}_z \eta^{-2}/\bar{J}_\perp = (\lambda_\perp \xi_\perp/\lambda_z d)^2 = (\zeta/\eta)^2$. If one wants to model an anisotropic continuum, with $d = \xi_z = \eta^{-1} \xi_\perp$, then one has $\zeta = \eta$ and there are only *three* dimensionless parameters, \bar{J}_\perp/T , η , and κ , with $\bar{J}_z \eta^{-2}/\bar{J}_\perp = 1$.

Both cases are in general different from an earlier derivation of the London lattice vortex line interaction¹⁷ which assumed equal grid spacings in all directions, $a_\mu = a_0$ for all μ , and so with $\zeta = 1$ involves only the three dimensionless parameters, \bar{J}_\perp/T , η , and λ_\perp/a_0 , but with $\bar{J}_z\eta^{-2}/\bar{J}_\perp = \eta^{-2}$. Keeping the distinction $a_z \neq a_\perp$ (i.e. $d \neq \xi_\perp$) is essential to correctly model the effects of the anisotropic vortex core energy in either a continuum or a layered anisotropic superconductor.

We can now define the helicity modulus for the lattice superconductor in complete correspondence with the continuum Eqs.(22–25). The only change needed is to replace the system volume \mathcal{V} with the number of grid sites N , due to the slightly differing definitions of the Fourier transform in the continuum, Eq.(9), and on the lattice, Eq.(103). As in the continuum we restrict ourselves to the three special perturbations of Fig. 1, $A_\mu^{\text{ext}}(q\hat{\nu})$, where μ, ν, σ are a cyclic permutation of x, y, z . Taking the Fourier transform of Eq.(99), we get $2\pi h_\sigma(q\hat{\nu}) = Q_\nu^* A_\mu^{\text{ext}}(q\hat{\nu})$. Substituting for h_σ in terms of A_μ^{ext} in \mathcal{H}_ν of Eq.(105), and then applying the definition of helicity modulus in Eq.(25), we get for the diagonal part of the helicity modulus tensor,

$$\Upsilon_\mu(q\hat{\nu}) = \frac{\bar{J}_\mu \left(\frac{\lambda_\perp}{a_\nu}\right)^2 |Q_\nu|^2}{1 + \left(\frac{\lambda_\mu}{a_\nu}\right)^2 |Q_\nu|^2} \left[1 - \frac{4\pi^2 \bar{J}_\mu \left(\frac{\lambda_\perp}{a_\nu}\right)^2 \langle n_\sigma(q\hat{\nu}) n_\sigma(-q\hat{\nu}) \rangle_0}{TN \left(1 + \left(\frac{\lambda_\mu}{a_\nu}\right)^2 |Q_\nu|^2\right)} \right], \quad (108)$$

and for the off diagonal part,

$$\Upsilon_{\mu\nu}(q\hat{\sigma}) = \frac{\bar{J}_\mu \left(\frac{\lambda_\perp}{a_\sigma}\right)^2 |Q_\sigma|^2}{1 + \left(\frac{\lambda_\mu}{a_\sigma}\right)^2 |Q_\sigma|^2} \left[\frac{4\pi^2 \bar{J}_\nu \left(\frac{\lambda_\perp}{a_\sigma}\right)^2 \langle n_\nu(q\hat{\sigma}) n_\mu(-q\hat{\sigma}) \rangle_0}{NT \left(1 + \left(\frac{\lambda_\mu}{a_\sigma}\right)^2 |Q_\sigma|^2\right)} \right]. \quad (109)$$

Eqs.(108) and (109) are the lattice equivalents of the continuum Eqs.(30) and (31). The primary difference between continuum and lattice expressions is the substitution, $q_\mu^2 \rightarrow |Q_\mu/a_\mu|^2 = (2 - 2 \cos q_\mu a_\mu)/a_\mu^2$.

Expanding the vortex correlation at small q ,

$$\langle n_\sigma(q\hat{\nu}) n_\sigma(-q\hat{\nu}) \rangle_0 = n_{\mu 0} + n_{\mu 1} |Q_\nu|^2 + n_{\mu 2} |Q_\nu|^4 + \dots \quad (110)$$

we can again write the diagonal part as,

$$\Upsilon_\mu(q\hat{\nu}) = \gamma_\mu \frac{\bar{J}_\mu \left(\frac{\lambda_\pm}{a_\nu}\right)^2 |Q_\nu|^2}{1 + \left(\frac{\lambda_{\mu R}}{a_\nu}\right)^2 |Q_\nu|^2}, \quad (111)$$

where, analogous to Eqs.(38) and (39),

$$\gamma_\mu = 1 - \frac{4\pi^2 \bar{J}_\mu \left(\frac{\lambda_\pm}{a_\nu}\right)^2}{NT} n_{\mu 0} \quad (112)$$

and,

$$\left(\frac{\lambda_{\mu R}}{\lambda_\mu}\right)^2 = 1 - \frac{4\pi^2 \bar{J}_\mu \left(\frac{\lambda_\pm}{a_\nu}\right)^2 \left[n_{\mu 0} - n_{\mu 1} \left(\frac{\lambda_\mu}{a_\nu}\right)^{-2}\right]}{NT \gamma_\mu}. \quad (113)$$

Noting that $Q_\nu \simeq -iq_\nu a_\nu$ for small q , that $N = \mathcal{V}/(\xi_\perp^2 d)$, and that there is a slight distinction between Fourier components defined on the lattice versus in the continuum, $n_{q\mu}^{\text{lattice}} = a_\mu^{-1} n_{q\mu}^{\text{continuum}}$, all the above expressions agree completely with their continuum counterparts, in the limit $q \rightarrow 0$.

B. Monte Carlo Method and Parameters

To carry out Monte Carlo simulations of the lattice superconductor model, we start with a fixed density $b_0 = \xi_\perp^2 B/\phi_0$ of magnetic field induced straight vortex lines, parallel to the $\hat{\mathbf{z}}$ axis. Following Carneiro, Cavalcanti, and Garter,³⁰ we update the system, heating from the ground state, by adding elementary closed vortex rings that surround only a single bond of the discretizing grid (i.e. rings of area ξ_\perp^2 in the xy plane, or area $\xi_\perp d$ in the xz or yz planes). The rings are added one at a time, at random positions with random orientations, and then accepted or rejected according to the standard Metropolis algorithm. When a side of such a ring coincides with, and is oppositely oriented to, a segment of one of the initial magnetic field induced vortex lines, these two segments will cancel out resulting in a net fluctuation of the vortex line. This procedure provides for a complete sampling of phase space for the vortex variables $n_{i\mu}$ which are subject to the constraints that vorticity is locally conserved, $\sum_\mu [n_{i\mu} - n_{i-\hat{\rho},\mu}] = 0$, and that the average internal magnetic field is kept constant, $(1/N) \sum_i \mathbf{n}_i = b_0 \hat{\mathbf{z}}$ (i.e. we are using the Helmholtz ensemble).

Our simulation uses periodic boundary conditions in all directions. The periodicity along $\hat{\mathbf{z}}$ makes our simulation map exactly onto the 2D boson problem. In order to compute energy changes for the Metropolis acceptance test, it is convenient to use,⁴⁸

$$\Delta E = 2\pi^2 \bar{J}_\perp \sum_{i\mu} F_{i\mu} \Delta n_{i\mu} , \quad (114)$$

where $\Delta n_{i\mu}$ is the change in vorticity due to the vortex ring excitation, and

$$F_{i\mu} \equiv \sum_j V_\mu(\mathbf{r}_j - \mathbf{r}_i) n_{j\mu} \quad (115)$$

represents the “potential” field of all other vortices. $V_\mu(\mathbf{r}_i) = (1/N) \sum_q e^{-i\mathbf{q}\cdot\mathbf{r}_i} V_{q\mu}$ is the Fourier transform of the vortex line interaction of Eqs.(106) and (107), where the sum is over all \mathbf{q} satisfying periodic boundary conditions, $q_\mu = 2\pi\ell_\mu/N_\mu a_\mu$, $\ell_\mu = 0, 1, \dots, N_\mu - 1$. In this way, the computation of ΔE is a *local* computation, involving only the sites of the elementary vortex ring excitation. Only when an excitation is accepted is it necessary to update the potentials $F_{i\mu}$, a calculation of order N . Since acceptance rates are generally low below the transition, this method is significantly faster than a direct computation involving the long range vortex interactions.

For simplicity, we have only simulated the completely isotropic case with $\lambda \equiv \lambda_\perp = \lambda_z$, $a_0 \equiv \xi_\perp = d$, and hence $\bar{J}_0 \equiv \bar{J}_\perp = \bar{J}_z$. Hence forth all lengths will be measured in units of the grid spacing $a_0 \equiv 1$, and temperatures in units of \bar{J}_0 . Our simulations are for the fixed vortex density $b_0 = 1/15$ whose ground state, shown in Fig. 3, is a close approximation to a perfect triangular lattice with sides of length $\sqrt{18} \times \sqrt{17} \times \sqrt{17}$. We choose $\kappa = \lambda/a_0 = 5$, comparable to the vortex line spacing $a_v/a_0 \simeq 1/\sqrt{b_0} = 2.87$. We study system sizes $N_\perp = 30$ in the xy plane, and $N_z = 15$ and 30 parallel to the applied magnetic field.

Our simulations are carried out heating from the ground state. At each temperature we use typically 5000 sweeps to equilibrate, followed by another 8 – 16000 sweeps to compute averages. Each “sweep” refers to $N = N_\perp^2 N_z$ attempts to add an elementary vortex ring. Statistical errors are estimated using the standard block averaging method.

C. Results: Helicity Modulus

In an earlier report¹⁰ we presented an analysis of our data based on Eqs.(110-113), fitting our computed correlations $\langle n_\sigma(q\hat{\nu})n_\sigma(-q\hat{\nu}) \rangle_0$ to an expansion in $|Q_\nu|^2$. Here we take a different approach. Plotting $\bar{J}_0\lambda^2|Q_\nu|^2/\Upsilon_\mu(q\hat{\nu})$ versus $|Q_\nu|^2$, Eq.(111) shows that at small q we should find a straight line with intercept γ_μ^{-1} and slope $\gamma_\mu^{-1}\lambda_{\mu R}^2$.

In Figs. 4a – c we show such plots for the three types of perturbations shown in Fig. 1, for $N_z = 30$ and selected values of temperature. $\mu = y, x, z$ correspond to the tilt, compression, and shear perturbations respectively. The straight lines through the data result from least squares fits, using the smallest eight values of $q > 0$. In virtually all cases, the fit is quite reasonable. In Figs. 5a – c and 6a – c we show the values of γ_μ and $(\lambda_{\mu R}/\lambda)^2$ obtained from these fits. In each case we show the result of fits to the smallest eight, seven, six, and five values of $q > 0$. As is seen, our results are virtually insensitive to the number of values of q used, except for the case of the compression perturbation in the vicinity of $T_m \simeq 1.2$, where our data is rather scattered and statistical errors are large (see data for $T = 1.2$ in Fig. 4b and the corresponding dashed line fit). We have also obtained values of γ_μ and $(\lambda_{\mu R}/\lambda)^2$ by fitting $\bar{J}_0\lambda^2|Q_\nu|^2/\Upsilon_\mu(q\hat{\nu})$ to a second order polynomial in $|Q_\nu|^2$. We have found the results from such quadratic fits to be essentially unchanged from the values obtained from the linear fits.

In Figs. 7a – b we show γ_μ and $(\lambda_{\mu R}/\lambda)^2$ respectively for all three types of perturbations, comparing the finite size effects for $N_z = 30$ and $N_z = 15$. The results shown are for fits to the smallest eight values of q , except for the case of the tilt perturbation for $N_z = 15$ where we have used only the smallest four values of q (since the allowed values of q_z are spaced twice as far apart for $N_z = 15$ as compared to $N_z = 30$). We see that finite size effects are in general small, except for the case of the shear perturbation $\mu = z$.

We now discuss our results for γ_μ . From Fig. 7a we see that all three $\gamma_\mu \simeq 1$ at low temperatures. For γ_z , this is in agreement with our expectation that there is a total Meissner effect for shear perturbations in the vortex line lattice phase. However the elastic theory

results given by the first lines of Eqs.(61) and (69) would lead one to expect $\gamma_y, |\gamma_x| \ll 1$. This is because for the relatively large B simulated here, $B \simeq H$ and the susceptibilities dB_σ/dH_σ that enter γ_y and γ_x in Eqs.(60) and (68) are both close to unity. That we find $\gamma_y, \gamma_x \simeq 1$ at low T is, we believe, an artifact of our discretizing grid which acts like a periodic pinning potential for vortex lines. At low T , the vortex lines are locked into a lattice structure commensurate with this pinning potential. Indeed, the fact that the ground state of Fig.3 is not a perfect equilateral triangular lattice is due to this effect. This periodic pinning potential leads to an enhanced stiffness of the effective elastic moduli, greatly reducing the susceptibilities dB_σ/dH_σ from their continuum values, and resulting in the observed $\gamma_y, \gamma_x \simeq 1$ at low T . Indeed the periodic pinning potential of the discretizing grid acts in many ways like the columnar pins of the “Bose glass” model⁴⁹ of a disordered superconductor, and $\gamma_y = 1$ is similar to the “transverse Meissner” effect for tilting the applied magnetic field that is found in that problem. One can wonder whether the decrease of γ_y from unity which begins at $T \simeq 0.6$ is a smooth cross-over due to finite energy barriers for discretized vortex fluctuations, or is rather a sharp transition, being the periodic pinning analog of the Bose glass transition.

At higher temperatures, γ_x and γ_y decrease towards zero at $T_m \simeq 1.2$. We will soon see that this T_m is the melting temperature of the vortex line lattice. It is only when the vortex lattice melts that the vortex lines also depin from the the periodic potential of the grid. Assuming that the effective tilt and compression moduli of the unpinned vortex line liquid are not greatly different from those of the continuum vortex line lattice, one expects from Eq.(61), $0 < \gamma_y \approx 1/(8\pi\lambda^2b_0) = 0.024 \ll 1$, and from Eq.(69), $\gamma_x \approx -1/(16\pi\lambda^2b_0) = -0.012 < 0$. Looking at Figs. 5a – b we see that γ_y is indeed small and positive for $T > T_m$, while γ_x is small and negative. That γ_x is indeed negative and not zero for $T > T_m$ is more clearly seen in Fig.4b by noting that the intercepts of the fitted lines are just γ_x^{-1} . The numerical values we find for γ_x and γ_y in this region are in roughly the same ratio as the above estimates, but approximately two or three times larger in magnitude. This rough agreement of γ_x and γ_y with elastic theory gives us confidence that, above T_m , the

artificial pinning introduced by our discretizing grid is no longer playing a significant role in the vortex line fluctuations.

Returning to Fig. 7a we see that, in contrast to γ_y and γ_x , γ_z remains equal to unity well into the vortex line liquid phase $T > T_m$. γ_z only decreases from unity towards the small value expected from Eq.(85) for the vortex line liquid, $\gamma_z = 1 - dB_\perp/dH_\perp = \gamma_y$, at $T_c \simeq 1.8$. Thus longitudinal superconductivity, indicated by the shear Meissner effect with $\gamma_z = 1$, persists well above T_m into the vortex line liquid. This one of the main observations of our simulations. Comparing results for $N_z = 15$ with $N_z = 30$, we see that the width of this transition clearly sharpens as N_z increases, however the temperature T_c , where γ_z starts to fall below unity, decreases only slightly.

We now consider our results for $(\lambda_{\mu R}/\lambda)^2$. For the tilt perturbation, comparison of Figs. 5a and 6a show that to a very good approximation, $\gamma_y \approx (\lambda_{yR}/\lambda)^2$ for the entire range of T . Such a result follows from Eqs.(57) and (58) if one makes the simple assumption that $c_{44}(\mathbf{q}) \simeq (B^2/4\pi\lambda_\perp^2)V_{q\perp} + b_0\tilde{\epsilon}_1$ where $V_{q\perp}$ is the vortex line interaction of Eq.(21), and $\tilde{\epsilon}_1 = \eta^{-2}\epsilon_1$ where ϵ_1 is the effective q_z independent single vortex line tension. It is interesting that λ_{yR} shows no increase as T_m is approached from below, as is usually associated with a decay length near a transition.

Turning to the compression perturbation we see from Fig. 6b that, in contrast to λ_{yR} , $(\lambda_{xR}/\lambda)^2$ does increase from unity as T_m is approached from below. This increase is clearly noticeable at temperatures sufficiently below T_m so that our data still has good statistical accuracy. This is in contrast to a similar increase in γ_x in Fig. 5b just below T_m , which we do not believe is statistically meaningful, but is rather just a reflection of the scatter in our data. Thus, as the lattice starts to depin from the discretizing grid, a fluctuation in vortex line density decays over an increasing length scale λ_{xR} . Above T_m , our numerical values are consistent with $(\lambda_{xR}/\lambda)^2 \approx \gamma_x$, as expected from Eqs.(69) and (70) for the case $\lambda > a_v$. That λ_{xR}^2 is indeed negative here, and so λ_{xR} is imaginary, can be seen in Fig. 4b by noting that the slopes of the fitted lines are equal to $\gamma_x^{-1}\lambda_{xR}^2$, and that for $T > T_m$, $\gamma_x < 0$.

Finally, we turn to the shear perturbation. Since this perturbation experiences a total

Meissner screening in the superconducting state, we may expect, in analogy with the Meissner effect at $H = 0$, that $\lambda_{zR}^{-2} \sim n_s$ where n_s is the density of superconducting electrons (not to be confused with $\rho_{s \text{ boson}}$, the superfluid density of the analog 2D bosons). Since n_s decreases as T increases, vanishing at the superconducting transition, we expect that λ_{zR}^2 should increase with increasing T , reaching a maximum at T_c (diverging in the case of a second order transition). Precisely such behavior is seen in Fig. 6c. Above T_c , λ_{zR}^2 decreases to roughly the same small values as λ_{yR} , as is expected from Eqs.(55) and (84). Comparing results for $N_z = 15$ with $N_z = 30$ we see that, similar to the behavior of γ_z , the transition width sharpens and the temperature of the peak in λ_{zR}^2 slightly decreases as N_z is increased. It is interesting to note however, that the value of λ_{zR}^2 at its peak has also very slightly decreased as N_z increased.

The possibility that longitudinal superconductivity can persist into the vortex line liquid has been suggested by the 2D boson analogy. We can therefore compare the T_c found here with the predictions of Sec. V B. Rewriting Eq.(86) in terms of the dimensionless parameters of our numerical simulation, and taking $dH_{\perp}/dB_{\perp} \approx 1$, gives $T_c = 8\pi\bar{J}_0\kappa^2/N_z$. Using $\kappa = 5$ and $N_z = 30$ gives $T_c/\bar{J}_0 \simeq 21$, ten times larger than the value 1.8 found numerically. We can also estimate the entanglement cross-over of Nelson. Eq.(94) gives $T_{\times} = \pi\bar{J}_0 \ln \kappa/2b_0N_z$, and using $b_0 = 1/15$, $\kappa = 5$, and $N_z = 30$ gives $T_{\times} = 1.26 \approx T_m$. This is somewhat lower than the observed T_c . Moreover, both the boson superfluid transition temperature and the entanglement temperature T_{\times} should scale with system thickness as $1/N_z$. In contrast, comparing $N_z = 15$ with $N_z = 30$, we see no such dramatic shift in the numerically observed $T_c \simeq 1.8$.

D. Results: Vortex Line Fluctuations

To elucidate the nature of the transitions in our model, we have measured other properties to characterize the vortex line fluctuations in the system. In Fig. 8 we show snapshot views of the vortex line configurations for $N_z = 15$, at various temperatures $T < T_m$, $T_m < T < T_c$,

and $T_c < T$. We show both a side perspective and a view looking down along the applied field. We see clearly that for $T < T_m$ there is a vortex line lattice. For $T_m < T < T_c$ the lattice is disordered but the vortex lines remain for the most part disentangled. For $T_c < T$ the lines are highly entangled.

For a quantitative determination of the vortex line lattice melting temperature, we compute the structure function of vortices within the same xy plane,

$$S(\mathbf{q}_\perp) = \frac{1}{L_z} \sum_{i,j} e^{i\mathbf{q}_\perp \cdot (\mathbf{r}_i - \mathbf{r}_j)} \langle n_{iz} n_{jz} \rangle \delta_{z_i, z_j} \quad (116)$$

Below T_m we expect to see Bragg peaks at the reciprocal lattice vectors \mathbf{K} of the vortex line lattice, while above T_m we expect to see approximately circular rings characteristic of a liquid. Let us denote by $\{\mathbf{K}_1\}$ the six smallest non-zero reciprocal lattice vectors, and by $\{\mathbf{K}'_1\}$ the six vectors obtained by reflecting the $\{\mathbf{K}_1\}$ through the $\hat{\mathbf{x}}$ axis. Then since the ground state vortex lattice of Fig. 3 breaks this reflection symmetry, while the vortex line liquid restores it, the quantity $\Delta S \equiv S(\mathbf{K}_1) - S(\mathbf{K}'_1)$, averaged over the six $\{\mathbf{K}_1\}$, serves as a convenient order parameter for the melting transition. We plot ΔS , normalized by $S_0 \equiv S(\mathbf{K} = 0)$, in Fig. 9. We see that ΔS vanishes at $T_m \simeq 1.2$. In an earlier work¹⁰ we have shown intensity plots of $S(\mathbf{q}_\perp)$ in the entire \mathbf{q}_\perp plane. The circular rings seen above T_m verify that T_m is indeed a melting to a liquid, and not a depinning to a floating vortex lattice, or some other vortex lattice structural transition.

As another measure of vortex line fluctuations, we have computed the fluctuation length of the vortex lines in the directions transverse and parallel to the applied magnetic field. The total length of vortex lines in the ground state is $\mathcal{L}_0 = b_0 N_z N_\perp^2$. If, in any configuration, \mathcal{L}_μ is the total length of all vortex lines in direction μ (we count length here as an absolute quantity; oppositely oriented segments do not cancel each other out), then we define the normalized excess vortex line lengths as $\Delta\ell_\perp = (\mathcal{L}_x + \mathcal{L}_y)/(2\mathcal{L}_0)$ and $\Delta\ell_z = (\mathcal{L}_z - \mathcal{L}_0)/\mathcal{L}_0$. We plot $\Delta\ell_\perp$ and $\Delta\ell_z$ in Fig. 10. If we assume that all vortex fluctuations consist of purely transverse motion of the magnetic field induced lines, then $\Delta\ell_\perp$ is the average transverse distance traveled by a vortex line between two adjacent xy planes. If we further assume that

these lines are fluctuating as in a random walk, then the total transverse deflection of a line in traveling down the entire length of the system N_z is, $u = \sqrt{N_z}\Delta\ell_\perp$. Entanglement should occur when $u \simeq a_v$, or when $\Delta\ell_\perp \simeq a_v/\sqrt{N_z}$. From Fig. 10, and using $a_v \simeq 1/\sqrt{b_0} = 3.87$, we would estimate the entanglement temperatures as $T_\times \simeq 2.1$ for $N_z = 15$, and $T_\times \simeq 1.9$ for $N_z = 30$. These are both consistent with the T_c seen in Fig. 7. However, if the transition at T_c is indeed caused by the onset of entanglement due to transverse wandering of magnetic field induced vortex lines, it is necessary to explain how just above T_c , where $\gamma_z \simeq 0$, one can have a $\Upsilon_{\text{boson}}/T_{\text{boson}} \simeq N_z T / (4\pi^2 \bar{J}_0 \kappa^2) \approx 0.06$ (see Eq.(43)) so much smaller than the lower bound $2/\pi$ given by the Kosterlitz–Thouless theory¹⁵ of the analog boson superfluid transition. We further note that in previous simulations^{27,28} with $\lambda \rightarrow \infty$, where samples up to thickness $N_z = 200$ were studied, the above criterion gives a T_\times which is well below the observed T_c .

Returning now to Fig. 10, we see that the above assumption of strictly transverse fluctuations of the field induced lines, while reasonable near the melting T_m where $\Delta\ell_z/\Delta\ell_\perp \simeq 0.035$, is not at all reasonable near T_c , where $\Delta\ell_z/\Delta\ell_\perp \simeq 0.41$. The excess vorticity along $\hat{\mathbf{z}}$ can only come from either field induced lines which wander backwards, or from closed vortex ring excitations. Both these types of excitations are absent from the usual 2D boson analogy.

Using an algorithm we have describe elsewhere,²⁸ we trace out the vortex line paths in our configurations to compute the distribution $q(p)$ of the number of closed rings of perimeter p , normalized by the ground state vortex line length $\mathcal{L}_0 = b_0 N_z N_\perp^2$. In Fig. 11 we compare the total length of all vortex line fluctuations, $\Delta\ell_{\text{tot}} \equiv 2\Delta\ell_\perp + \Delta\ell_z$, with the total length of all vortex ring excitations, $\Delta\ell_{\text{ring}} \equiv \sum_p p q(p)$. We see that $\Delta\ell_{\text{ring}} \ll \Delta\ell_{\text{tot}}$ through the melting T_m , however at $T_c = 1.8$, $\Delta\ell_{\text{ring}}$ has increased to 27% of $\Delta\ell_{\text{tot}}$. In Fig. 12 we show a semi-log plot of $q(p)$ vs. $1/T$. The straight lines found at low T indicate thermal activation with a constant energy barrier that increases with ring size. At high $T \sim 2.8$ the $q(p)$ curves saturate. Note that the thermal activation for rings persists up to temperatures above T_c . This suggests that, although the number of rings is becoming sizable near T_c , the transition at T_c is not directly associated with any critical behavior of the rings. This behavior is the

same that we saw in simulations of a 3D XY model, corresponding to $\lambda \rightarrow \infty$, when we took *anisotropic* couplings;²⁸ for isotropic couplings²⁷ in the XY model, the saturation of the $q(p)$ curves coincided with T_c . In Fig. 13 we plot the specific heat C vs. T , for $N_z = 30$. We see that C rises smoothly through T_c . The peak occurs near $T \sim 3.0$ (we only have enough data at high T to locate it very crudely), where the $q(p)$ curves saturate. The peak in C is thus associated with the proliferation of the closed vortex rings, which we believe to be a non-singular cross-over phenomenon associated with the transition of the zero field $b_0 = 0$ model, which occurs⁵⁰ at $T_{c0} \approx 3$. The peak in C is also probably associated²⁸ with the onset of a strong diamagnetic response in the system, which occurs at the so-called “mean field $H_{c2}(T)$ ” line.

Finally, we consider the entanglement of the magnetic field induced vortex lines. Due to the periodic boundary conditions along $\hat{\mathbf{z}}$, the set of points $\{\mathbf{r}_{\perp i}(N_z)\}$ where the field induced vortex lines pierce the xy plane at $z = N_z$, must be some permutation of the set of points $\{\mathbf{r}_{\perp i}(0)\}$ where the lines pierce the xy plane at $z = 0$. Lines for which $\mathbf{r}_{\perp i}(N_z) = \mathbf{r}_{\perp j}(0)$, with $i \neq j$, form part of an entangled braid when viewed in the periodically repeated system. We can thus classify each magnetic field induced line as belonging to a given braid of order m , according to the number of lines m that are mutually entangled in the preceding sense. We compute the distribution $n(m)$ giving the average number of lines in a braid of order m , where $\sum_m n(m) = b_0 N_{\perp}^2$ is just the total number of field induced lines.

In the 2D boson analogy, such entangled vortex lines represent particle exchanges. A superfluid state of these 2D bosons is expected when there are many such exchanges, and in particular when there is a finite probability to form large exchanges involving a macroscopic fraction of the particles,³⁶ that wrap entirely around the system in the transverse direction and thus contribute to $n_{z0} \equiv \lim_{q \rightarrow 0} \langle n_y(q\hat{\mathbf{x}})n_y(-q\hat{\mathbf{x}}) \rangle$. γ_z is a direct measure of n_{z0} (see Eq.(38)), and hence a measure of the presence of such large exchanges. In Fig. 14 we plot vs. T the fraction of lines $R = n(1)/b_0 N_{\perp}^2$ which are not involved in *any* particle exchanges, i.e. the fraction of unentangled vortex lines for which $\mathbf{r}_{\perp i}(N_z) = \mathbf{r}_{\perp i}(0)$. We see that $R = 1$ and all lines remain unentangled up to $T \simeq T_c$, at which point R decreases towards zero.

The width of the decrease in R is roughly the same as the width of the decrease in γ_z , for both $N_z = 15$ and 30.

In Fig. 15 we plot the entanglement distribution $n(m)$ vs. m , for several values of T near and above $T_c = 1.8$, for $N_z = 30$. We see that the distribution broadens as T increases, indicating larger particle exchanges, however no sharp feature is obvious as T increases through T_c . This is in contrast to what we observed in simulations^{27,28} of the $\lambda \rightarrow \infty$ 3D XY model, where $n(m)$ got dramatically flat and equal to unity over a wide range of intermediate m as T reached T_c ; these XY simulations however used much larger system thicknesses, $N_z \simeq 100 - 200$, and this is one possible reason for the difference in behavior from the present case.

VII. CONCLUSIONS AND DISCUSSION

The main conclusion of our numerical work is that longitudinal superconductivity vanishes at a T_c which lies well within the vortex line liquid, at least for the system sizes we have been able to investigate. We note that our system sizes $N_\perp = 30$, and $N_z = 15, 30$, are large compared to the microscopic length scales of our model, $\lambda/\xi_\perp = 5$ and $a_v/\xi_\perp \simeq \sqrt{15}$. We have discussed a mechanism for this phenomenon in terms of the KT superfluid transition of the analog 2D bosons. However the T_c predicted by Eq.(86) is an order of magnitude larger than the numerically observed value. The entanglement temperature T_\times of Nelson is of the correct order of magnitude as the observed T_c . Figs. 8 and 14 also suggest a connection between geometrical entanglement and T_c . However upon comparing $N_z = 15$ and 30, we failed to see any sign of the dramatic size dependence $T_\times \propto 1/N_z$ that is expected from Eq.(94). A similar size dependence is also expected for the KT prediction of Eq.(86).

In earlier simulations²⁶⁻²⁸ of a 3D XY model, corresponding to the $\lambda \rightarrow \infty$ approximation of Sec. III D, we have studied much thicker systems than reported on here, with N_z as large as 200. We again found longitudinal superconductivity to vanish at a T_c^∞ within the vortex line liquid, with virtually no finite size effects in the apparent value of T_c^∞ as N_z was varied.

An analysis^{27,28} of geometrical entanglement, as done here in connection with Fig. 10, gives a T_\times well below the observed T_c^∞ for the thicker systems, and the dependence of T_c^∞ on the system anisotropy was found²⁸ to be $T_c^\infty \propto 1/\eta$, rather than the $T_\times \propto 1/\eta^2$ predicted by Eq.(94). New simulations⁵¹ have further shown that there is no apparent change in the large N_z limiting value of T_c^∞ when the periodic boundary conditions along the direction \hat{z} of the applied magnetic field are replaced with the more realistic free boundary conditions. We believe that these $\lambda \rightarrow \infty$ simulations are therefore in good agreement with the work of Feigelman and co-workers,^{21,45} who argued for just such a superconducting to normal vortex line liquid transition, with a T_c^∞ which remains finite as $L_z \rightarrow \infty$. We believe that this transition of Feigelman *et al.* applies strictly to the $\lambda \rightarrow \infty$ model, and represents a $T_{\text{boson}} = 0$ Meissner transition, as \hbar_{boson} varies, for the analog 2D charged bosons.

Returning to our present simulations, we believe that our results represent a finite λ cross-over from the above $\lambda \rightarrow \infty$ transition at T_c^∞ . Although we believe that the $\lambda \rightarrow \infty$ limit is extremely subtle, one may imagine the following scenario. When λ is large, although the analog 2D bosons behave like a neutral superfluid on sufficiently long transverse length scales, on small length scales they will have the $\lambda \rightarrow \infty$ behavior of *charged* bosons. We would then expect the 2D boson helicity modulus to have, at finite transverse wavevector q , a piece that looks like that of Eq.(50). We thus expect a form like,

$$\Upsilon_{\text{boson}}(q) = \Upsilon_{\text{boson}}(0) + \gamma_{\text{boson}} \frac{[J\lambda^2]_{\text{boson}} q^2}{1 + \lambda_{\text{R boson}}^2 q^2} . \quad (117)$$

As $q \rightarrow 0$, it is $\Upsilon_{\text{boson}}(0)$ that determines if the 2D bosons are in a superfluid ($\Upsilon_{\text{boson}}(0) > 0$) or a normal fluid ($\Upsilon_{\text{boson}}(0) = 0$) state; but at sufficiently large q it will be the second term that dominates, giving the appearance of a charged boson system. For $T < T_c$, with T_c the 2D neutral boson superfluid transition of Eq.(86), one has $\Upsilon_{\text{boson}}(0) = 0$ and only the second term is present. As $q \rightarrow 0$, this term vanishes, and Eq.(43) then gives $\gamma_z = 1$, i.e. we have the perfect shear Meissner effect that we expect for the 2D boson normal fluid phase, as discussed in Sec. III C. However, if L_z is thin enough that $T_c^\infty \ll T_c$, with T_c^∞ the Meissner transition of the $\lambda \rightarrow \infty$ 2D charged boson model, then as one cools down to T_c^∞ ,

one expects $\lambda_{\text{R boson}}$ will become large, and possibly of order the finite transverse size L_{\perp} of the system. In this case, for all available wavevectors, $q > 2\pi/L_{\perp}$ yields $\lambda_{\text{R boson}}^2 q^2 \gg 1$, and the second term becomes approximately the constant, $\gamma_{\text{boson}}[J\lambda^2]_{\text{boson}}/\lambda_{\text{R boson}}^2$. Eq.(43) then gives $\gamma_z = 1 - [\gamma_{\text{boson}}\lambda_{\perp}^2/\lambda_{\text{R boson}}^2]$. It thus appears as if the perfect shear Meissner effect has been lost at the lower temperature $\sim T_c^{\infty}$. We note that for this scenario to agree with the small values of γ_z that we find at temperatures above our numerically observed value of T_c , it would be necessary to have $\gamma_{\text{boson}}\lambda_{\perp}^2/\lambda_{\text{R boson}}^2 \approx 1$; it is not a priori obvious why this would be so.

Thus for a finite λ simulation to see other than the above $\lambda \rightarrow \infty$ cross-over behavior, it would be necessary to do one of the following. One could increase the transverse size L_{\perp} , keeping L_z constant, until one is in the limit where $\max[\lambda_{\text{R boson}}] \ll L_{\perp}$ (although in the $\lambda \rightarrow \infty$ model $\lambda_{\text{R boson}}$ might diverge at T_c^{∞} , in a finite λ model any such divergence would be rounded out to a finite maximum value). In this limit, the second term in Eq.(117) would be observed to be $\sim q^2$, and so one would find $\gamma_z = 1$. One thus expects the apparent T_c to increase above T_c^{∞} as L_{\perp} increases above $\max[\lambda_{\text{R boson}}]$. One might never actually reach the true 2D boson neutral superfluid transition T_c of Eq.(43), since as temperature increases, thermally excited closed vortex rings will start to proliferate, and vortex lines can make long transverse wanderings between two adjacent xy planes; both such effects are left out of the naive mapping to 2D boson statistical mechanics. Alternatively, one could keep L_{\perp} constant, but increase L_z , so that the T_c of Eq.(43) falls below T_c^{∞} . For our parameters, Eq.(43) suggests that this would require a system of thickness $N_z = \phi_0^2/2\pi^2 T_c^{\infty} = 8\pi \bar{J}_0 \kappa^2/T_c^{\infty} \simeq 320$.

Several other groups have done simulations similar to ours. Most of these^{29,30} have been in the $\lambda \rightarrow \infty$ limit, but at much higher vortex line densities such as $b_0 = 1/6$. In these cases it was found that $T_c \approx T_m$, and so no longitudinal superconductivity was observed in the vortex line liquid. We believe that this is a consequence of the high densities b_0 which have been used. Recently, we have studied²⁸ the phase diagram in such $\lambda \rightarrow \infty$ XY models, as a function of the system anisotropy η . Increasing η at fixed b_0 can be argued to play a role similar to increasing b_0 at fixed η . We found that as η increased, T_c and T_m came

closer together, and eventually became indistinguishable from each other. Similar results have recently been reported in simulations by Koshelev.⁵²

Šášik and Stroud have done simulations⁵³ for the $\lambda \rightarrow \infty$ limit using the lowest Landau level approximation, which treats the xy planes as a continuum and so avoids the artificial pinning of our discretized London model. For all values of anisotropy studied they find $T_c \approx T_m$. However Tešanović³⁴ has argued that the lowest Landau level approximation fails as the magnetic field decreases, and so at such low magnetic fields, the London and the lowest Landau level approaches need not be in agreement. Using a mean field analysis, Tešanović³⁴ has argued that longitudinal superconductivity can persist into the vortex line liquid in this low field limit.

Finite λ simulations have been carried out, for the same discretized London model as considered here, by Carneiro.^{9,54} For large line densities, he finds $T_c \approx T_m$, consistent with the above $\lambda \rightarrow \infty$ results. For line densities comparable to our own, he finds T_c noticeably above T_m , when following our analysis based on the q dependence of the helicity modulus within the Helmholtz ensemble of fixed internal magnetic field b_0 . He has suggested⁵⁴ however that the result may be very sensitive to the $q \rightarrow$ extrapolation implied by fitting to the expansion of Eq.(110), with different results obtained when truncating at different orders of the expansion, or when using a different number of q data points in the fit. However our fits of Figs. 5 and 6 show essentially no sensitivity to the number of q data points used, or when comparing a linear versus a quadratic order fit to the data of Fig. 4. Carneiro has also carried out simulations^{9,54} in a Gibbs ensemble, in which the total transverse magnetic field is allowed to fluctuate. Here he concludes $T_c \approx T_m$, even for dilute densities comparable to our own. However we believe⁵⁵ that in this case, his $\mathbf{q} = 0$ calculation of the fluctuation in the transverse magnetic field cannot distinguish between the shear perturbation of Fig. 1c, which is related to the 2D analog boson superfluid density, and the tilt perturbation of Fig. 1a, which is not. We believe that his results are reflecting the softening of c_{44} that occurs at the depinning/melting transition (as is observed in our Fig. 5a), rather than reflecting the loss of longitudinal superconductivity.

Most recently, simulations at finite λ have been carried out by Nguyen *et al.*,⁵⁶ who extend our work to consider behavior as the anisotropy η is varied. For an isotropic system, they find T_c well above T_m , in good agreement with our results. However as η increases, they find the very intriguing result that T_c decreases, and eventually falls *below* T_m . Such a possibility (not observed in similar $\lambda \rightarrow \infty$ simulations²⁸) has been suggested by Frey *et al.*³⁷ as a result of dislocations proliferating in the vortex line lattice. Glazman and Koshelev⁶ have made similar predictions, based on the effect that vortex lattice elastic fluctuations have in reducing the interplanar Josephson coupling. However Nguyen *et al.* suggest that their result is due to the proliferation of vortex rings between adjacent xy plans, and they find at high anisotropy that $T_c \sim \eta^{-2}$, rather than the $T_c \sim \eta^{-1}$ predicted by Ref.[6] or the $T_c \sim 1/\ln \eta$ predicted by Ref.[37]. It should be noted however that Nguyen *et al.* base their criterion for superconductivity on computing the helicity modulus at the single smallest non-zero value of q allowed by their finite size system. We have argued above that a more careful analysis should be based on parameters extracted from the q dependence of the helicity modulus, as $q \rightarrow 0$. Conclusions based on calculations at specific values of finite q can more easily be led astray by subtle cross-over effects such as we have discussed above. Clearly more systematic studies, using our $q \rightarrow 0$ analysis, and making a more extensive study of finite size dependencies, need to be done for both the isotropic and anisotropic cases.

Our result of Eq.(89) suggests that one should find $T_c > T_m$, and hence longitudinal superconductivity within a region of the vortex line liquid, whenever a sample is thinner than $L_{z_{\max}} \approx 1400\mu\text{m}$, for a $T_m \approx 90^\circ\text{K}$. Virtually all experimental single crystal samples fall below this critical thickness. One can therefore ask whether any experimental evidence favors our conclusions. Naively, one would expect a vortex line liquid with longitudinal superconductivity to show a finite linear resistivity transverse to the applied magnetic field, but zero linear resistivity parallel to the applied field. However, in MC simulations of a $\lambda \rightarrow \infty$ XY model,²⁶ we found that in the intermediate phase $T_m < T < T_c$ vortex density correlations decayed anomalously slowly with time. This suggests that vortex lines may

be moving more slowly than diffusion, and if so, it is not obvious what to expect for the transverse resistivity. Experimentally, it is very difficult to obtain accurate measurements of the longitudinal resistivity, due to the slab geometry of single crystal samples, and the non-uniformity of current distributions. Transverse resistivity measurements are intimately related to the vortex pinning impurities in the sample, and so are also not unambiguously characterized.

Nevertheless, the following suggestive observations have been made. Experiments by Steel *et al.*⁵⁷ on artificially prepared MoGe/Ge layered superconductors, found that the d.c. resistivity parallel to the applied field decreased sharply, and showed an onset of strong nonlinear behavior, at a temperature above that where the transverse resistivity vanished. Experiments by Kwok *et al.*⁵⁸ on YBCO, studying the pinning of vortex lines to twin grain boundaries in a system with a well controlled small number of twin planes, found evidence for a sharp lock-in pinning transition at a temperature above vortex lattice melting (where the melting transition was determined by the observation of a sharp drop in transverse resistivity). Such a lock-in transition within the vortex line liquid may suggest a transition in the nature of vortex line fluctuations, as at our T_c . Early experiments by Safar *et al.*,⁵⁹ using a flux transformer geometry, similarly showed evidence for the onset of coherence parallel to the applied field at a “ T_{th} ” above the temperature where the transverse resistivity vanished. However more recent flux transformer experiments by López *et al.*⁶⁰ showed that these two temperatures merged when the sample was made purer, with all twin grain boundaries eliminated. Moore⁶¹ has recently proposed an interpretation which argues that the single transition observed in these newer transformer experiments is the result of some very rapidly increasing longitudinal length scale, rather than being a first order vortex lattice melting transition, as is the usual interpretation. If correct, such a rapidly increasing longitudinal length scale might be associated with our T_c .

The experimental evidence cited above remains, at best, inconclusive. There are several possible reasons why observing a $T_c > T_m$ might be experimentally difficult. Firstly, as in our simulations, the relevant temperature is likely to be the $\lambda \rightarrow \infty$ transition T_c^∞ ,

rather than the much higher T_c of Eq.(86). In recent simulations²⁸ of the $\lambda \rightarrow \infty$ XY model we found that T_c^∞ and T_m merged as the anisotropy η increased. How far apart the corresponding T_c^∞ and T_m for any particular real material are likely to be, remains unknown. Secondly, real layered high temperature superconductors are likely to have an interplanar Josephson coupling that is proportional to the cosine of the phase angle difference across adjacent planes. The non quadratic nature of such a cosine interaction leads to a coupling between spin wave and vortex fluctuations that is absent in both our continuum model and our discretized model of Eq.(97) using the Villain interaction. As either magnetic field, temperature, or anisotropy increases, large interplanar phase differences can be induced by elastic vortex line fluctuations, leading to a large decrease in the effective interplanar energy coupling constant. Such a “decoupling” cross-over, as discussed by Glazman and Koshelev,⁶ and Daemen *et al.*,⁶² might obscure any true critical behavior at a higher T_c . Finally, the free boundary conditions of a real superconductor, as opposed to the periodic boundary conditions of the 2D boson mapping and of our simulations, might lead to a more effective washing out of the 2D boson superfluid transition²² than we have imagined, for samples of experimental thickness.

ACKNOWLEDGMENTS

In the course of this work we have benefited greatly from discussions with C. Ciordas-Ciurdariu, M. Feigelman, A. E. Koshelev, M. C. Marchetti, P. Muzikar, D. R. Nelson, Z. Tešanović, and A. P. Young. This work has been supported by U.S. Department of Energy Grant DE-FG02-89ER14017.

APPENDIX A: SUPERFLUID DENSITY OF 2D BOSONS IN THE PATH INTEGRAL FORMULATION

The superfluid density of a system of N interacting bosons can be defined in terms of the response of the system to the presence of a heat bath moving with velocity $\mathbf{v}(\mathbf{r})$ (“moving

walls”). In the following, all position, velocity, and wave vectors are two dimensional vectors in the xy plane.

The average momentum density $\langle p_{q\mu} \rangle_v$ that results in linear response to the heat bath velocity $v_{-q\nu} = \frac{1}{L^2} \int d^2r v_\mu(\mathbf{r}) e^{-i\mathbf{q}\cdot\mathbf{r}}$ is given by

$$\langle p_{q\mu} \rangle_v = \chi_{\mu\nu}(\mathbf{q}) v_{-q\nu}. \quad (\text{A1})$$

For an isotropic 2D system, the momentum density susceptibility can be written in terms of its longitudinal and transverse pieces,

$$\chi_{\mu\nu}(\mathbf{q}) = \hat{\mathbf{q}}_\mu \hat{\mathbf{q}}_\nu \chi_L(\mathbf{q}) + [\delta_{\mu\nu} - \hat{\mathbf{q}}_\mu \hat{\mathbf{q}}_\nu] \chi_T(\mathbf{q}). \quad (\text{A2})$$

The number density of superfluid bosons ρ_s is then given in terms of the transverse susceptibility by^{19,20}

$$m\rho_s = m\rho - \lim_{q \rightarrow 0} \chi_T(\mathbf{q}) \quad (\text{A3})$$

where m is the boson particle mass, and $\rho = N/L^2$ is the total boson density.

For a system of interacting bosons in the presence of a moving heat bath, the Hamiltonian in the reference frame of the heat bath is given by,

$$\mathcal{H} = \sum_i \frac{1}{2m} (\mathbf{p}_i - m\mathbf{v}(\mathbf{r}_i))^2 + V(\{\mathbf{r}_i - \mathbf{r}_j\}) \quad (\text{A4})$$

where the interaction V depends only on the bosons relative positions.

The partition function is $\mathcal{Z} = \text{Tr}[e^{-\beta\mathcal{H}}]$, and the free energy is $\mathcal{F} = -T \ln \mathcal{Z}$, with $T = 1/\beta$. Consider now that \mathbf{v} points only in the $\hat{\mathbf{y}}$ direction and varies only in the $\hat{\mathbf{x}}$ direction (so the \mathbf{v} is purely transverse). If we write $\mathcal{H}[\mathbf{v}] = \mathcal{H}[0] + \delta\mathcal{H}[\mathbf{v}]$, then since in the $q \rightarrow 0$ limit that \mathbf{v} becomes a uniform constant $\delta\mathcal{H}$ and $\mathcal{H}[0]$ commute, one has

$$\lim_{q \rightarrow 0} L^2 \frac{\partial^2 \mathcal{F}}{\partial v_y(q\hat{\mathbf{x}}) \partial v_y(-q\hat{\mathbf{x}})} \Big|_{v=0} = m\rho - \lim_{q \rightarrow 0} \chi_T(q\hat{\mathbf{x}}) = m\rho_s \quad (\text{A5})$$

To evaluate ρ_s in terms of the path integral formalism,⁶³ one now writes the Lagrangian associated with the Hamiltonian of Eq.(A4), and transforms from real time t to imaginary time $\tau = it$. One gets

$$\mathcal{L}(\tau) = - \sum_i \frac{m}{2} \left(\frac{d\mathbf{r}_i}{d\tau} \right)^2 - V(\{\mathbf{r}_i - \mathbf{r}_j\}) + im \sum_i \left(\frac{d\mathbf{r}_i}{d\tau} \right) \cdot \mathbf{v}(\mathbf{r}_i). \quad (\text{A6})$$

The partition function is then given by

$$\mathcal{Z} = \int \mathcal{D}[\{\mathbf{r}_i(\tau)\}] e^{\hbar^{-1} \int_0^{\hbar\beta} d\tau \mathcal{L}(\tau)}. \quad (\text{A7})$$

where the sum is over all possible boson world lines $\{\mathbf{r}_i(\tau)\}$ subject to permuted periodic boundary conditions, i.e. $\{\mathbf{r}_i(0)\} = \mathcal{P}\{\mathbf{r}_i(\beta)\}$ where \mathcal{P} is any permutation of the N bosons.

Applying Eq.(A5) to the above form for \mathcal{Z} then results in

$$m\rho_s = \lim_{q \rightarrow 0} \frac{Tm^2}{L^2\hbar^2} \left\langle \left(\int_0^{\hbar\beta} d\tau \sum_i \frac{dr_{iy}}{d\tau} e^{iqx_i} \right) \left(\int_0^{\hbar\beta} d\tau' \sum_j \frac{dr_{jy}}{d\tau'} e^{-iqx_j} \right) \right\rangle_0 \quad (\text{A8})$$

where $\langle \dots \rangle_0$ denotes an average over world lines weighted by the Lagrangian factor as in Eq.(A7), only now taking $\mathbf{v} = 0$ in \mathcal{L} .

Note that the heat bath velocity $\mathbf{v}(\mathbf{r})$ enters the Hamiltonian (A4) and the Lagrangian (A6) with precisely the same form as would a 2D external magnetic vector potential given by $\mathbf{v} = (\hbar/m)\mathbf{A}^{\text{ext}}$ (where, as in Sec. II, the units of \mathbf{A}^{ext} are such that $\nabla \times \mathbf{A}^{\text{ext}} = (2\pi/\phi_0)H\hat{\mathbf{z}}$, with $H\hat{\mathbf{z}}$ the 2D magnetic field). In analogy with Eq.(25) we can thus define the helicity modulus of the 2D bosons as,

$$\begin{aligned} \Upsilon_{\text{boson}}(q) &= L^2 \frac{\partial^2 \mathcal{F}}{\partial A_y(q\hat{\mathbf{x}}) \partial A_y(-q\hat{\mathbf{x}})} = L^2 \frac{\hbar^2}{m^2} \frac{\partial^2 \mathcal{F}}{\partial v_y(q\hat{\mathbf{x}}) \partial v_y(-q\hat{\mathbf{x}})} \\ &= \frac{T}{L^2} \left\langle \left(\int_0^{\hbar\beta} d\tau \sum_i \frac{dr_{iy}}{d\tau} e^{iqx_i} \right) \left(\int_0^{\hbar\beta} d\tau' \sum_j \frac{dr_{jy}}{d\tau'} e^{-iqx_j} \right) \right\rangle_0, \end{aligned} \quad (\text{A9})$$

with,

$$\lim_{q \rightarrow 0} \Upsilon_{\text{boson}}(q) = \frac{\hbar^2}{m} \rho_s = T \langle W_y^2 \rangle_0, \quad (\text{A10})$$

where W_y is the y component of the ‘‘winding number’’ introduced by Pollock and Ceperley³⁶ in their path integral approach to the superfluid transition in boson systems.

Our derivation above can be modified in a straightforward way to deal with a boson interaction mediated by a gauge field, as is the case for the more realistic London interaction between vortex lines.²¹ One just replaces the pair potential $V(\{\mathbf{r}_i - \mathbf{r}_j\})$ with the necessary

coupling to the gauge field, and free field energy terms. However the coupling of the bosons to an external vector potential remains unchanged. Thus the expression for the 2D boson helicity modulus in terms of boson world lines remains unchanged from Eq.(A9).

APPENDIX B: ELASTIC MODULI

In this appendix we summarize some results concerning the elastic moduli which appear in Eq.(54). Although calculations of these moduli have appeared elsewhere,^{12,13,39} our explicit computation of the order q^2 dependence at small q we believe is new.

As shown by Sudbø and Brandt,¹³ the elastic tensor $\Phi_{\alpha\beta}(\mathbf{q})$ can be expressed in terms of the vortex line interaction tensor $V_{\alpha\beta}(\mathbf{q})$, as

$$\Phi_{\alpha\beta}(\mathbf{q}) = \frac{B^2}{4\pi\lambda_{\perp}^2} \sum_{\mathbf{K}} \left\{ q_z^2 V_{\alpha\beta}(\mathbf{K} - \mathbf{q}) + (\mathbf{K} - \mathbf{q})_{\alpha}(\mathbf{K} - \mathbf{q})_{\beta} V_{zz}(\mathbf{K} - \mathbf{q}) - K_{\alpha} K_{\beta} V_{zz}(\mathbf{K}) \right\} \quad (\text{B1})$$

where $\{\mathbf{K}\}$ are the reciprocal lattice vectors of the vortex lattice.

For $\mathbf{B} = B\hat{\mathbf{z}}$ the elastic moduli we are interested in can be expressed in terms of $\Phi_{\alpha\beta}(\mathbf{q})$ as

$$c_{66}(q\hat{\mathbf{y}}) = \frac{1}{q^2} \Phi_{xx}(q\hat{\mathbf{y}}), \quad c_{11}(q\hat{\mathbf{x}}) = \frac{1}{q^2} \Phi_{xx}(q\hat{\mathbf{x}}), \quad c_{44}(q\hat{\mathbf{z}}) = \frac{1}{q^2} \Phi_{xx}(q\hat{\mathbf{z}}). \quad (\text{B2})$$

For the London interaction, the sum over \mathbf{K} in Eq.(B1) is divergent, and some method must be employed to make it converge. As shown by Brandt,¹² this can be achieved for $c_{66}(q\hat{\mathbf{y}})$ and $c_{11}(q\hat{\mathbf{x}})$ by subtracting off the self energy of a line interacting with itself. This then gives,

$$c_{66}(q\hat{\mathbf{y}}) = \frac{B^2}{4\pi\lambda_{\perp}^2} \left\{ \sum_{\mathbf{K}} F_{66}[\mathbf{K}, q] - \frac{\phi_0}{B} \int \frac{d^2k}{(2\pi)^2} F_{66}[\mathbf{k}, q] \right\} \quad (\text{B3})$$

$$c_{11}(q\hat{\mathbf{x}}) = \frac{B^2}{4\pi\lambda_{\perp}^2} \left\{ \sum_{\mathbf{K}} F_{11}[\mathbf{K}, q] - \frac{\phi_0}{B} \int \frac{d^2k}{(2\pi)^2} F_{11}[\mathbf{k}, q] \right\}, \quad (\text{B4})$$

where we find, after expanding Φ_{xx} to $O(q^4)$, averaging over the orientation of the vortex lattice in the xy plane, and substituting in for V_{zz} from Eq.(16)

$$F_{66}[\mathbf{k}, q] = \frac{d}{dk^2} \left\{ \frac{1}{4}k^4 \dot{V}_{zz}(\mathbf{k}) + \left[\frac{1}{8}k^4 \ddot{V}_{zz}(\mathbf{k}) + \frac{1}{24}k^6 \dddot{V}_{zz}(\mathbf{k}) \right] q^2 \right\} \quad (\text{B5})$$

$$= -\frac{1}{2}\lambda_{\perp}^2 \left\{ \frac{1}{(1 + \lambda_{\perp}^2 k^2)^2} - \frac{1}{(1 + \lambda_{\perp}^2 k^2)^3} + \left[\frac{1}{(1 + \lambda_{\perp}^2 k^2)^3} - \frac{3}{(1 + \lambda_{\perp}^2 k^2)^4} + \frac{2}{(1 + \lambda_{\perp}^2 k^2)^5} \right] \lambda_{\perp}^2 q^2 \right\} \quad (\text{B6})$$

and

$$F_{11}[\mathbf{k}, q] = \frac{d}{dk^2} \left\{ k^2 V_{zz}(\mathbf{k}) + \frac{3}{4}k^4 \dot{V}_{zz}(\mathbf{k}) + \left[k^2 \dot{V}_{zz}(\mathbf{k}) + \frac{9}{8}k^4 \ddot{V}_{zz}(\mathbf{k}) + \frac{5}{24}k^6 \dddot{V}_{zz}(\mathbf{k}) \right] q^2 \right\} \quad (\text{B7})$$

$$= -\frac{1}{2}\lambda_{\perp}^2 \left\{ \frac{1}{(1 + \lambda_{\perp}^2 k^2)^2} - \frac{3}{(1 + \lambda_{\perp}^2 k^2)^3} + \left[\frac{1}{(1 + \lambda_{\perp}^2 k^2)^3} - \frac{9}{(1 + \lambda_{\perp}^2 k^2)^4} + \frac{10}{(1 + \lambda_{\perp}^2 k^2)^5} \right] \lambda_{\perp}^2 q^2 \right\} \quad (\text{B8})$$

where $\dot{V}_{zz} \equiv dV_{zz}/dk^2$.

To treat the tilt modulus $c_{44}(q\hat{\mathbf{z}})$, self interactions of the vortex lines are important. One therefore handles the convergence of the sum in Eq.(B1) by introducing a convergence factor into the London interaction of Eq.(B1), $V_{q\alpha\beta} \rightarrow V_{q\alpha\beta}^c \equiv g(\xi_{\perp}^2 q_{\perp}^2 + \xi_z^2 q_z^2) V_{q\alpha\beta}$. Here $g(x) \rightarrow 1$ for $x < 1$, $g(x) \rightarrow 0$ for $x > 1$, and one uses an anisotropic cutoff to model the vortex core, $\xi_z/\xi_{\perp} = \lambda_{\perp}/\lambda_z = 1/\eta$. Averaging over the orientation of the vortex lattice in the xy plane, and substituting in for $V_{\mu\mu}$ from Eq.(16) we find

$$c_{44}(q\hat{\mathbf{z}}) = \frac{B^2}{4\pi\lambda_{\perp}^2} \sum_{\mathbf{K}} F_{44}[\mathbf{K}, q] \quad (\text{B9})$$

where

$$F_{44}[\mathbf{k}, q] = \left\{ V_{xx}^c(\mathbf{k}) + \frac{1}{2}k^2 \dot{V}_{zz}^c(\mathbf{k}) + \left[\dot{V}_{xx}^c(\mathbf{k}) + \frac{1}{4}k^2 \ddot{V}_{zz}^c(\mathbf{k}) \right] q^2 \right\} \quad (\text{B10})$$

$$= \frac{1}{2} \left\{ \frac{\lambda_{\perp}^2 g}{1 + \lambda_z^2 k^2} + \frac{\lambda_{\perp}^2 g}{(1 + \lambda_{\perp}^2 k^2)^2} + \dot{g} - \frac{\dot{g}}{1 + \lambda_{\perp}^2 k^2} - \left[\frac{\lambda_{\perp}^2 g}{(1 + \lambda_z^2 k^2)^2} + \frac{\lambda_{\perp}^2 g}{(1 + \lambda_{\perp}^2 k^2)^3} - \frac{\dot{g}}{1 + \lambda_z^2 k^2} - \frac{\dot{g}}{(1 + \lambda_{\perp}^2 k^2)^2} - \frac{\ddot{g}}{2} + \frac{\ddot{g}}{2(1 + \lambda_{\perp}^2 k^2)} \right] \lambda_{\perp}^2 q^2 \right\} \quad (\text{B11})$$

where $\dot{V}_{\mu\mu}^c \equiv dV_{\mu\mu}^c/dq_z^2$ and $\dot{g} \equiv dg/dq_z^2$.

We consider first the limit of large magnetic fields, $\lambda_{\perp} \gg a_v$ (a_v is the spacing between vortex lines). In this case one can approximate the sum over \mathbf{K} by

$$\sum_{\mathbf{K}} F[\mathbf{K}, q] = F[0, q] + \frac{2\pi}{(\Delta K)^2} \int_{k_0}^{\infty} dk k F[\mathbf{k}, q], \quad (\text{B12})$$

where $(\Delta K)^2 = 4\pi^2 B/\phi_0 \equiv \pi k_0^2$ is the area per reciprocal lattice vector, and $k_0 \sim 1/a_v$ is the edge of an approximate circular Brillouin Zone. Carrying out the integrations, we get

$$c_{66}(q\hat{\mathbf{Y}}) = \frac{B^2}{4\pi} \left\{ \frac{\lambda_{\perp}^2 k_0^2}{4(1 + \lambda_{\perp}^2 k_0^2)^2} - \left[\frac{\lambda_{\perp}^2 k_0^2}{4(1 + \lambda_{\perp}^2 k_0^2)^4} \right] \lambda_{\perp}^2 q^2 \right\} \quad (\text{B13})$$

$$c_{11}(q\hat{\mathbf{X}}) = \frac{B^2}{4\pi} \left\{ 1 - \frac{1}{4(1 + \lambda_{\perp}^2 k_0^2)} - \frac{3}{4(1 + \lambda_{\perp}^2 k_0^2)^2} - \left[1 + \frac{1}{4(1 + \lambda_{\perp}^2 k_0^2)^3} - \frac{5}{4(1 + \lambda_{\perp}^2 k_0^2)^4} \right] \lambda_{\perp}^2 q^2 \right\} \quad (\text{B14})$$

$$c_{44}(q\hat{\mathbf{Z}}) = \frac{B^2}{4\pi} \left\{ 1 + \frac{1}{2\lambda_{\perp}^2 k_0^2} \left[\eta^{-2} \ln \left(\frac{1 + \kappa^2 \eta^2}{1 + \lambda_z^2 k_0^2} \right) + \frac{1}{1 + \lambda_{\perp}^2 k_0^2} - \eta^{-2} \right] \right. \\ \left. - \left[1 + \frac{1}{2\lambda_z^2 k_0^2 (1 + \lambda_z^2 k_0^2)} + \frac{1}{4\lambda_{\perp}^2 k_0^2 (1 + \lambda_{\perp}^2 k_0^2)^2} \right] \lambda_{\perp}^2 q^2 \right\} \quad (\text{B15})$$

where for c_{44} we have taken the cutoff $\xi_{\perp} \rightarrow 0$ in all non-divergent terms, and $\kappa \equiv \lambda_{\perp}/\xi_{\perp}$.

Expanding for large $\lambda_{\perp} k_0$, we get to the lowest non trivial order

$$c_{66}(q\hat{\mathbf{Y}}) = \frac{B^2}{4\pi} \frac{1}{4\lambda_{\perp}^2 k_0^2} \left\{ 1 - \frac{2}{\lambda_{\perp}^2 k_0^2} - \frac{\lambda_{\perp}^2 q^2}{\lambda_{\perp}^4 k_0^4} \right\} \quad (\text{B16})$$

$$c_{11}(q\hat{\mathbf{X}}) = \frac{B^2}{4\pi} \left\{ 1 - \frac{1}{4\lambda_{\perp}^2 k_0^2} - \left[1 + \frac{1}{4\lambda_{\perp}^6 k_0^6} \right] \lambda_{\perp}^2 q^2 \right\} \quad (\text{B17})$$

$$c_{44}(q\hat{\mathbf{Z}}) = \frac{B^2}{4\pi} \left\{ 1 + \frac{1}{2\lambda_{\perp}^2 k_0^2} \left[\eta^{-2} \left(\ln \left(\frac{H_{c2}}{B} \right) - 1 \right) + \frac{1}{\lambda_{\perp}^2 k_0^2} \right] \right. \\ \left. - \left[1 + \frac{1}{2\lambda_z^4 k_0^4} + \frac{1}{4\lambda_{\perp}^6 k_0^6} \right] \lambda_{\perp}^2 q^2 \right\}, \quad (\text{B18})$$

where $H_{c2} \equiv \phi_0/4\pi\xi_{\perp}^2$.

Next we consider the case of small magnetic fields, $\lambda_{\perp} \ll a_v$. Here it is convenient to use

$$\sum_{\mathbf{K}} F[\mathbf{K}, q] = \frac{\phi_0}{B} \sum_{\mathbf{R}} \tilde{F}[\mathbf{R}, q] \quad \text{where} \quad \tilde{F}[\mathbf{r}, q] \equiv \int \frac{d^2 k}{(2\pi)^2} e^{-i\mathbf{k}\cdot\mathbf{r}} F[\mathbf{k}, q] \quad (\text{B19})$$

and $\{\mathbf{R}\}$ are the direct Bravais lattice vectors of the vortex lattice.

For the shear and compression moduli, c_{66} and c_{11} , the subtraction terms in Eqs.(B3) and (B4) cause the $\mathbf{R} = 0$ term of the sum in Eq.(B19) to vanish. Since the range of the interaction V_{zz} is $\lambda_{\perp} \ll |\mathbf{R}|$, it will be a good approximation in the sum over \mathbf{R} to keep only the six smallest vectors with $|\mathbf{R}| = a_v$. The Fourier transforms of Eqs.(B6) and (B8), can now be obtained with the help of

$$\int \frac{d^2k}{(2\pi)^2} \frac{e^{-i\mathbf{k}\cdot\mathbf{r}}}{(1 + \lambda^2 k^2)^n} = \frac{1}{2^n \pi (n-1)! \lambda^2} \left(\frac{r}{\lambda}\right)^{n-1} K_{1-n}\left(\frac{r}{\lambda}\right) \quad (\text{B20})$$

where K_ν is the modified Bessel function of the second kind of order ν , whose asymptotic form at large x is

$$K_\nu(x) \sim \sqrt{\frac{\pi}{2x}} e^{-x} \quad (\text{B21})$$

Keeping only the leading terms in a_v/λ_\perp , we find

$$c_{66}(q\hat{\mathbf{z}}) = \frac{3B\phi_0}{64\sqrt{2\pi^3}\lambda_\perp^2} e^{-a_v/\lambda_\perp} \left(\frac{a_v}{\lambda_\perp}\right)^{3/2} \left[1 - \frac{1}{24}a_v^2 q^2\right] \quad (\text{B22})$$

$$c_{11}(q\hat{\mathbf{x}}) = \frac{9B\phi_0}{64\sqrt{2\pi^3}\lambda_\perp^2} e^{-a_v/\lambda_\perp} \left(\frac{a_v}{\lambda_\perp}\right)^{3/2} \left[1 - \frac{5}{72}a_v^2 q^2\right]. \quad (\text{B23})$$

For the tilt modulus c_{44} there are two cases to consider, depending on the strength of the anisotropy. For very small magnetic fields such that $\lambda_z \ll a_v$, all terms in Eq.(B11) may be treated according to the approximation implied by Eq.(B19). Here the $\mathbf{R} = 0$ term dominates all others, and we find

$$c_{44}(q\hat{\mathbf{z}}) = \frac{B^2}{4\pi} \frac{1}{2\lambda_\perp^2 k_0^2} \left\{ \eta^{-2} [2 \ln(\eta\kappa) - 1] + 1 - \left[\frac{1}{2} + \eta^{-2}\right] \lambda_\perp^2 q^2 \right\}. \quad (\text{B24})$$

For the intermediate case $\lambda_\perp \ll a_v \ll \lambda_z$, we must combine approximations, using Eq.(B12) for terms involving $\lambda_z^2 k^2$, and Eq.(B19) for terms involving $\lambda_\perp^2 k^2$. We find

$$c_{44}(q\hat{\mathbf{z}}) = \frac{B^2}{4\pi} \left\{ \frac{1}{2} + \frac{1}{2\lambda_\perp^2 k_0^2} \left(\eta^{-2} \left[\ln\left(\frac{Hc_2}{B}\right) - 1 \right] + 1 \right) - \left[\frac{1}{2} + \frac{1}{4\lambda_\perp^2 k_0^2} \right] \lambda_\perp^2 q^2 \right\}. \quad (\text{B25})$$

REFERENCES

- ¹ M. Tinkham, *Introduction to Superconductivity*, (R.E. Krieger Co., Malabar, FL, 1980).
- ² D. S. Fisher, M. P. A. Fisher, and D. A. Huse, Phys. Rev. B **43**, 130 (1991).
- ³ R. Ikeda, T. Ohmi and T. Tsuneto, J. Phys. Soc. Jpn. **61**, 254 (1992).
- ⁴ M. A. Moore, Phys. Rev. B **45**, 7336 (1992).
- ⁵ A. Houghton, R. A. Pelcovits and A. Sudbø, Phys. Rev. B **42**, 906 (1990).
- ⁶ L. I. Glazman and A. E. Koshelev, Phys. Rev. B **43**, 2835 (1991).
- ⁷ T. Chen and S. Teitel, Phys. Rev. Lett. **72**, 2085 (1994).
- ⁸ M. E. Fisher, M. N. Barber and D. Jasnow, Phys. Rev. A **8**, 1111 (1973); T. Ohta and D. Jasnow, Phys. Rev. B **20**, 139 (1979); P. Minnhagen and G. G. Warren, Phys. Rev. B **24**, 2526 (1981).
- ⁹ G. Carneiro, Phys. Rev. Lett. **75**, 521 (1995).
- ¹⁰ T. Chen and S. Teitel, Phys. Rev. Lett. **74**, 2792 (1995).
- ¹¹ D. R. Nelson, Phys. Rev. Lett. **60**, 1973 (1988); J. Stat. Phys. **57**, 511 (1989); D. R. Nelson and H. S. Seung, Phys. Rev. B **39**, 9153 (1989).
- ¹² E. H. Brandt, J. Low Temp. Phys. **26**, 735 (1977); A. Sudbø and E. H. Brandt, Phys. Rev. Lett. **66**, 1781 (1991).
- ¹³ A. Sudbø and E. H. Brandt, Phys. Rev. B **43**, 10482 (1991).
- ¹⁴ M. C. Marchetti, Phys. Rev. B **43**, 8012 (1991).
- ¹⁵ D. R. Nelson and J. M. Kosterlitz, Phys. Rev. Lett. **39**, 1201 (1977).
- ¹⁶ C. Dasgupta and B. I. Halperin, Phys. Rev. Lett. **47**, 1556 (1981); S. E. Korshunov, Europhys. Lett. **11**, 757 (1990).

- ¹⁷ G. Carneiro, Phys. Rev. B **45**, 2391 (1992).
- ¹⁸ G. Carneiro, M. M. Doria, S. C. B. de Andrade, Physica C **203**, 167 (1992).
- ¹⁹ G. Baym, in *Mathematical Methods in Solid State and Superfluid Theory*, eds. R. C. Clark and D. H. Derrick (Oliver and Boyd, Edinburgh, 1969), p. 121.
- ²⁰ D. Forster, *Hydrodynamic Fluctuations, Broken Symmetry, and Correlation Functions*, (W. A. Benjamin Inc., Reading, MA, 1975).
- ²¹ M. V. Feigel'man, V. B. Geshkenbein and V. M. Vinokur, Pis'ma Zh. Eksp. Teor. Fiz. **52**, 1141 (1990) [JETP Lett. **52**, 546 (1990)]; M. V. Feigel'man, V. B. Geshkenbein, L. B. Ioffe, and A. I. Larkin, Phys. Rev. B **48**, 16641(1993).
- ²² M. P. A. Fisher and D. H. Lee, Phys. Rev. B **39**, 2756 (1989).
- ²³ U. C. Täuber and D. R. Nelson, Phys. Rep., to be published.
- ²⁴ Y.-H. Li and S. Teitel, Phys. Rev. Lett. **66**, 3301 (1991).
- ²⁵ Y.-H. Li and S. Teitel, Phys. Rev. B **45**, 5718 (1992).
- ²⁶ Y.-H. Li and S. Teitel, Phys. Rev. B **47**, 359 (1993).
- ²⁷ Y.-H. Li and S. Teitel, Phys. Rev. B **49**, 4136 (1994).
- ²⁸ T. Chen and S. Teitel, Phys. Rev. B accepted for publication, cond-mat/9610151.
- ²⁹ R. E. Hetzel, A. Sudbø, and D. A. Huse, Phys. Rev. Lett. **69**, 518 (1992); D. Dominguez, N. Grønbech-Jensen, and A. Bishop, Phys. Rev. B **75**, 4670 (1995); E. A. Jagla and C. A. Balseiro, Phys. Rev. Lett. **77**, 1588 (1996).
- ³⁰ R. Cavalcanti, G. Carneiro, and A. Gartner, Europhys. Lett. **17**, 449 (1992); G. Carneiro, R. Cavalcanti, and A. Gartner, Phys. Rev. B **47**, 5263 (1993).
- ³¹ Z. Tešanović, L. Xing, L. Bulaevskii, Q. Li, and M. Suenaga, Phys. Rev. Lett. **69**, 3563 (1992); Z. Tešanović, Physica C **220**, 303 (1994); I. F. Herbut and Z. Tešanović, Phys.

- Rev. Lett. **73**, 484 (1994).
- ³² C. Ciordas-Ciurdariu and S. Teitel, unpublished.
- ³³ G. Blatter, M. V. Feigel'man, V. B. Geshkenbein, A. I. Larkin, and V. M. Vinokur, Rev. Mod. Phys. **66**, 1125 (1994).
- ³⁴ Z. Tešanović, Phys. Rev. B **51**, 16204 (1995).
- ³⁵ A. M. Campbell and J. E. Evetts, Adv. Phys. **21**, 199 (1972).
- ³⁶ E. L. Pollock and D. M. Ceperley, Phys. Rev. B **36**, 8343 (1987).
- ³⁷ E. Frey, D. R. Nelson, and D. S. Fisher, Phys. Rev. B **49**, 9723 (1994).
- ³⁸ A. Houghton, R. A. Pelcovits and A. Sudbø, Phys. Rev. B **40**, 6763 (1989); E. H. Brandt, Phys. Rev. Lett. **63**, 1106 (1989).
- ³⁹ D. S. Fisher in *Phenomenology and Applications of High Temperature Superconductors*, edited by K. Bedell *et al.* (Addison-Wesley, Reading, MA, 1992), p.287.
- ⁴⁰ D. R. Nelson and P. LeDoussal, Phys. Rev. B **42**, 10113 (1990).
- ⁴¹ M. C. Marchetti and D. R. Nelson, Phys. Rev. B **41**, 1910 (1990).
- ⁴² The importance of non-zero shear for suppressing flux flow in currents parallel to H has earlier been pointed out in E. H. Brandt, J. Low Temp. Phys. **44**, 33 (1981).
- ⁴³ Our earlier claim in Ref.[7], that the hexatic liquid could be described by an elastic model with $c_{66}(\mathbf{q}_\perp) \sim q_\perp^2$, is incorrect. We thank M. C. Marchetti for clarifying this point to us.
- ⁴⁴ M. C. Marchetti and D. R. Nelson, Phys. Rev. B **42**, 9938 (1990) and Physica C **174**, 40 (1991); S. P. Obukhov and M. Rubinstein, Phys. Rev. Lett. **65**, 1279 (1990) and *ibid.* **66**, 2279 (1991).
- ⁴⁵ M. V. Feigel'man, Physica A **168**, 319 (1990).

- ⁴⁶ J. Villain, *J. de Physique* **36**, 581 (1975)
- ⁴⁷ E. Fradkin, B. Huberman and S. Shenker, *Phys. Rev. B* **18**, 4789 (1978)
- ⁴⁸ G. S. Grest, *Phys. Rev. B* **39**, 9267 (1989).
- ⁴⁹ D. R. Nelson and V. M. Vinokur, *Phys. Rev. B* **48**, 13060 (1993).
- ⁵⁰ For the case $b_0 = 0$ and $\lambda = 3$, P. Olsson and S. Teitel (unpublished) find $T_{c0} \simeq 2.9$. For $b_0 = 0$ and $\lambda = \infty$, $T_{c0} \simeq 3.03$, see H. Kleinert, *Gauge Fields in Condensed Matter*, v.1, p. 520, (World Scientific, Singapore, 1989).
- ⁵¹ C. Ciordas-Ciurdariu and S. Teitel, unpublished.
- ⁵² A. E. Koshelev, unpublished.
- ⁵³ R. Šašik and D. Stroud, *Phys. Rev. Lett.* **72**, 2462 (1994) and *Phys. Rev. B* **52**, 3696 (1995).
- ⁵⁴ G. Carneiro, *Phys. Rev. B* **53**, 11837 (1996).
- ⁵⁵ see Comment and Reply pair, T. Chen and S. Teitel, *Phys. Rev. Lett.* **76**, 714 (1996); G. Carneiro, *Phys. Rev. Lett.* **76**, 715 (1996).
- ⁵⁶ A. K. Nguyen, A. Sudbø, and R. E. Hetzel, *Phys. Rev. Lett.* **77**, 1592 (1996).
- ⁵⁷ D. G. Steel, W. R. White and J. M. Graybeal, *Phys. Rev. Lett.* **71**, 161 (1993).
- ⁵⁸ W. K. Kwok, J. Fendrich, U. Welp, S. Fleshler, J. Downey, and G. W. Crabtree, *Phys. Rev. Lett.* **42**, 1088 (1994).
- ⁵⁹ H. Safar, P. L. Gammel, D. A. Huse, S. N. Majumdar, L. F. Schneemeyer, D. J. Bishop, D. López, G. Nieva, and F. de la Cruz, *Phys. Rev. Lett.* **72**, 1272 (1994); see also F. de la Cruz, D. López, and G. Nieva, *Phil. Mag. B* **70**, 773 (1994); D. López, G. Nieva, and F. de la Cruz, *Phys. Rev. B* **50**, 7219 (1994).
- ⁶⁰ D. López, E. F. Righi, G. Nieva, and F. de la Cruz, *Phys. Rev. Lett.* **76**, 4034 (1996).

⁶¹ M. A. Moore, preprint cond-mat/9608105.

⁶² L. L. Daemen, L. N. Bulaevskii, M. P. Maley, and J. Y. Coulter, Phys. Rev. Lett. **70**, 1167 (1993).

⁶³ For a simple introduction see, A. Das, *Field Theory, a Path Integral Approach*, (World Scientific, Singapore, 1993).

FIGURES

FIG. 1. Schematic representation of three possible perturbations of the external magnetic field: (a) the tilt perturbation, (b) the compression perturbation, and (c) the shear perturbation.

FIG. 2. Labeling conventions for the lattice superconductor. $A_{i\mu}$ are directed *outwards* from site i on the bonds of the direct lattice. $b_{i\mu}$ are directed *inwards* towards the dual site i on the bonds of the dual lattice, piercing the plaquettes of the direct lattice as shown.

FIG. 3. Ground state for vortex line density $b_0 = 1/15$ on a cubic grid. Solid circles indicate the locations of the straight vortex lines as they pierce the xy plane.

FIG. 4. Helicity modulus plotted as $\bar{J}_0\lambda^2|Q_\nu|^2/\Upsilon_\mu(q\hat{\nu})$ vs. $|Q_\nu|^2$ for various values of T . The straight lines are fits to Eq.(111), and determine the parameters γ_μ and $(\lambda_{\mu R}/\lambda)^2$ for (a) the tilt, (b) the compression, and (c) the shear perturbations of Fig. 1.

FIG. 5. Plots of γ_μ vs. T as obtained from the straight line fits of Fig. 4, fitting to the 8, 7, 6, and 5 smallest values of q , for (a) the tilt, (b) the compression, and (c) the shear perturbations of Fig. 1. Little sensitivity is seen to the number of values of q used in the fit.

FIG. 6. Plots of $(\lambda_{\mu R}/\lambda)^2$ vs. T as obtained from the straight line fits of Fig. 4, fitting to the 8, 7, 6, and 5 smallest values of q , for (a) the tilt, (b) the compression, and (c) the shear perturbations of Fig. 1. Little sensitivity is seen to the number of values of q used in the fit.

FIG. 7. Finite size comparison of the parameters (a) γ_μ and (b) $(\lambda_{\mu R}/\lambda)^2$, for the tilt (Δ), the compression (\circ), and the shear (\diamond) perturbation. Open symbols are data for $N_z = 15$, while solid symbols are data for $N_z = 30$.

FIG. 8. Snapshots of vortex line configurations for $N_z = 15$, for (a) $T = 1.0 < T_m$, (b) $T_m < T = 1.6 < T_c$, and (c) $T_c < T = 2.2$. The bottom row is the view looking down along the applied magnetic field.

FIG. 9. Plot of structure function peak heights, $\Delta S(\mathbf{K}_1)/S_0$, vs. T for $N_z = 15$ and 30.

FIG. 10. Average normalized fluctuation length of vortex lines $\Delta\ell_z$ and $\Delta\ell_\perp$, parallel and transverse to the applied magnetic field, vs. T . We see that $\Delta\ell_z \ll \Delta\ell_\perp$ for $T < T_m$, indicating that there are only transverse fluctuations of the magnetic field induced vortex lines. This is no longer true near T_c . Open symbols are for $N_z = 15$, solid symbols are for $N_z = 30$, and the solid lines are guides to the eye.

FIG. 11. Average normalized length of all vortex line fluctuations $\Delta\ell_{\text{tot}}$, and average length in closed vortex ring excitations $\Delta\ell_{\text{ring}}$, vs. T . Open symbols are for $N_z = 15$, and solid symbols are for $N_z = 30$.

FIG. 12. Semi-log plot of $q(p)$, the distribution of closed vortex rings of perimeter p , vs. $1/T$, for several values of p . Straight lines at low T indicate thermal activation. $q(p)$ saturates at a temperature above T_c . Open symbols are for $N_z = 15$, and solid symbols are for $N_z = 30$.

FIG. 13. Specific heat C vs. T for $N_z = 30$. The peak in C occurs above T_c .

FIG. 14. Fraction of unentangled magnetic field induced vortex lines R vs. T , for $N_z = 15$ and 30. Lines start to entangle at T_c .

FIG. 15. Distribution of entanglement of the magnetic field induced vortex lines. $n(m)$ is the number of lines that participate in entanglement braids of order m . Data is shown for several temperatures near $T_c = 1.8$, for $N_z = 30$.

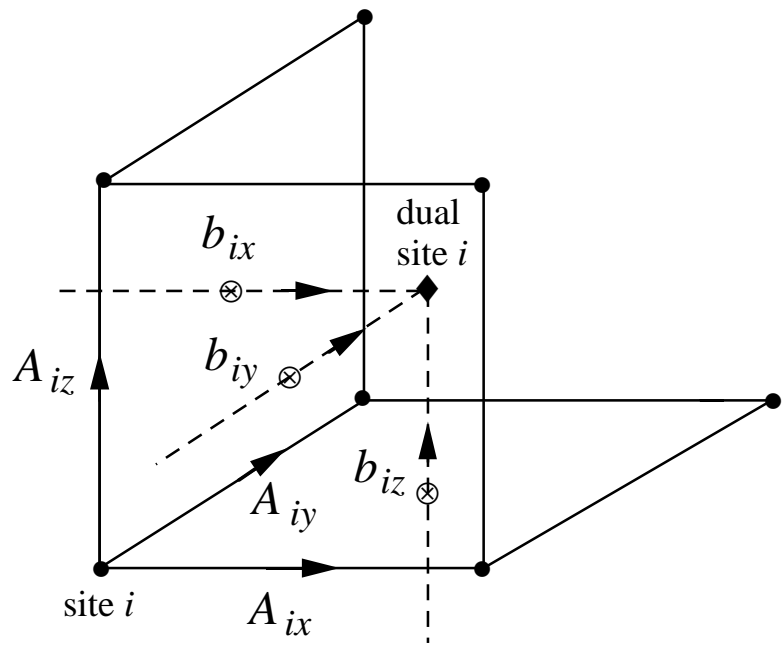


Fig. 2

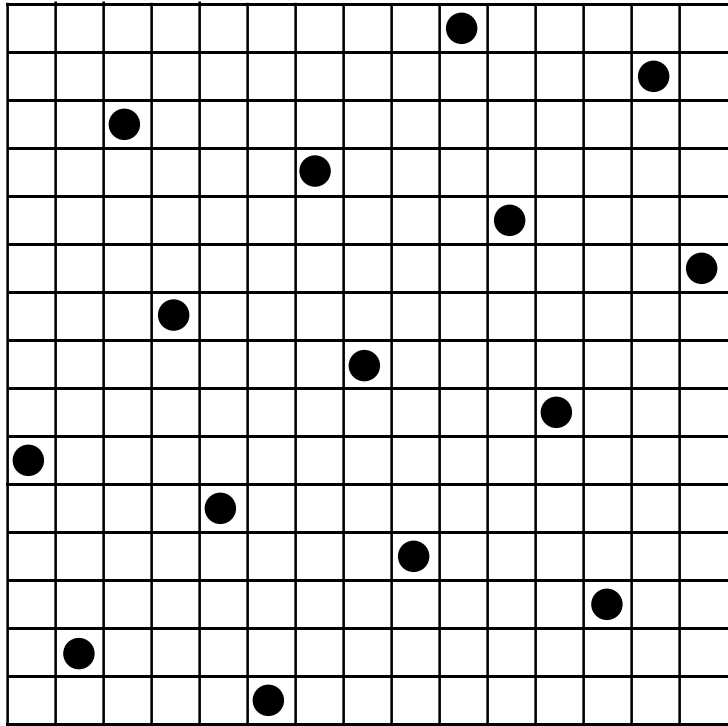


Fig. 3

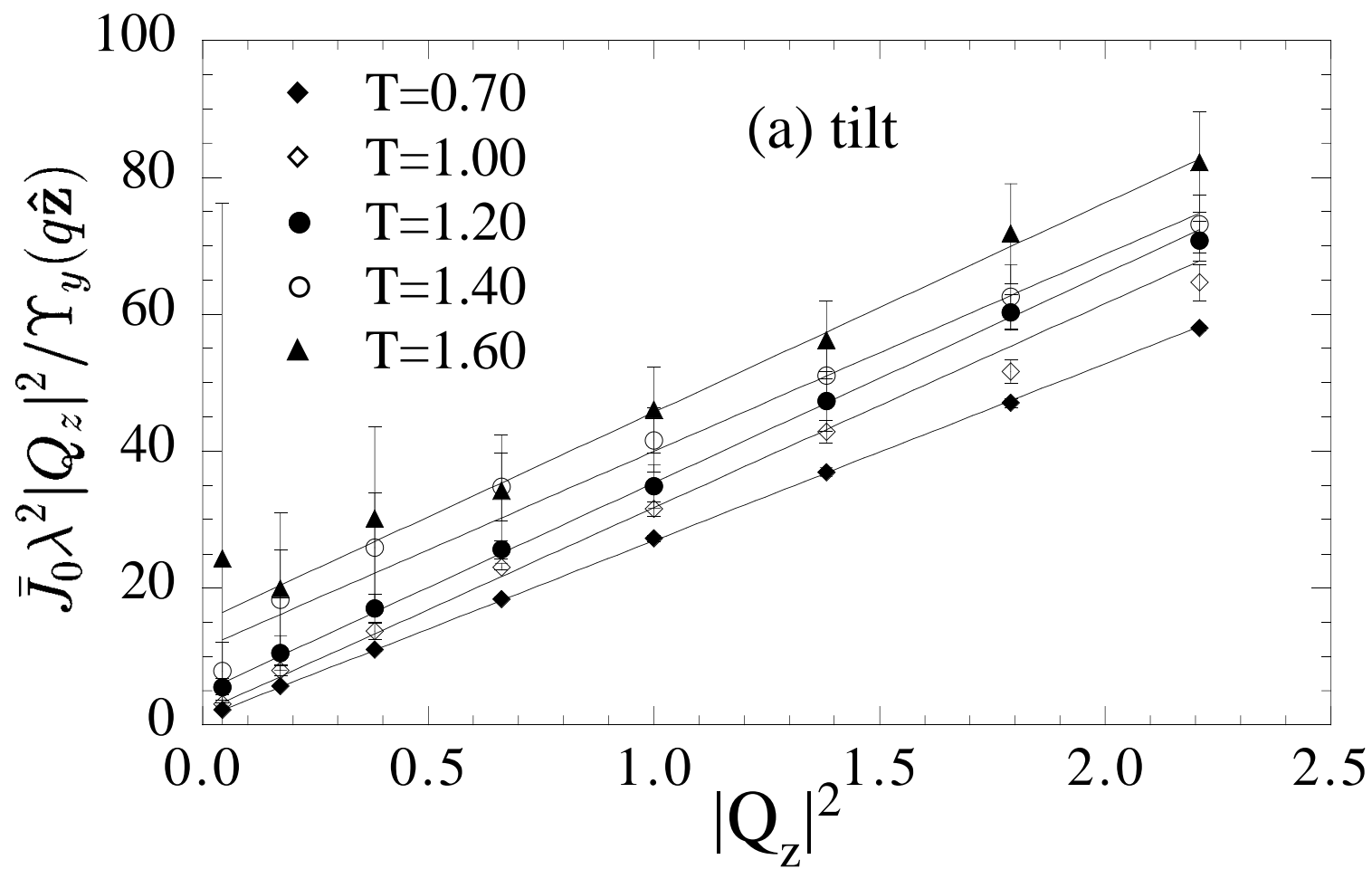


Fig. 4a

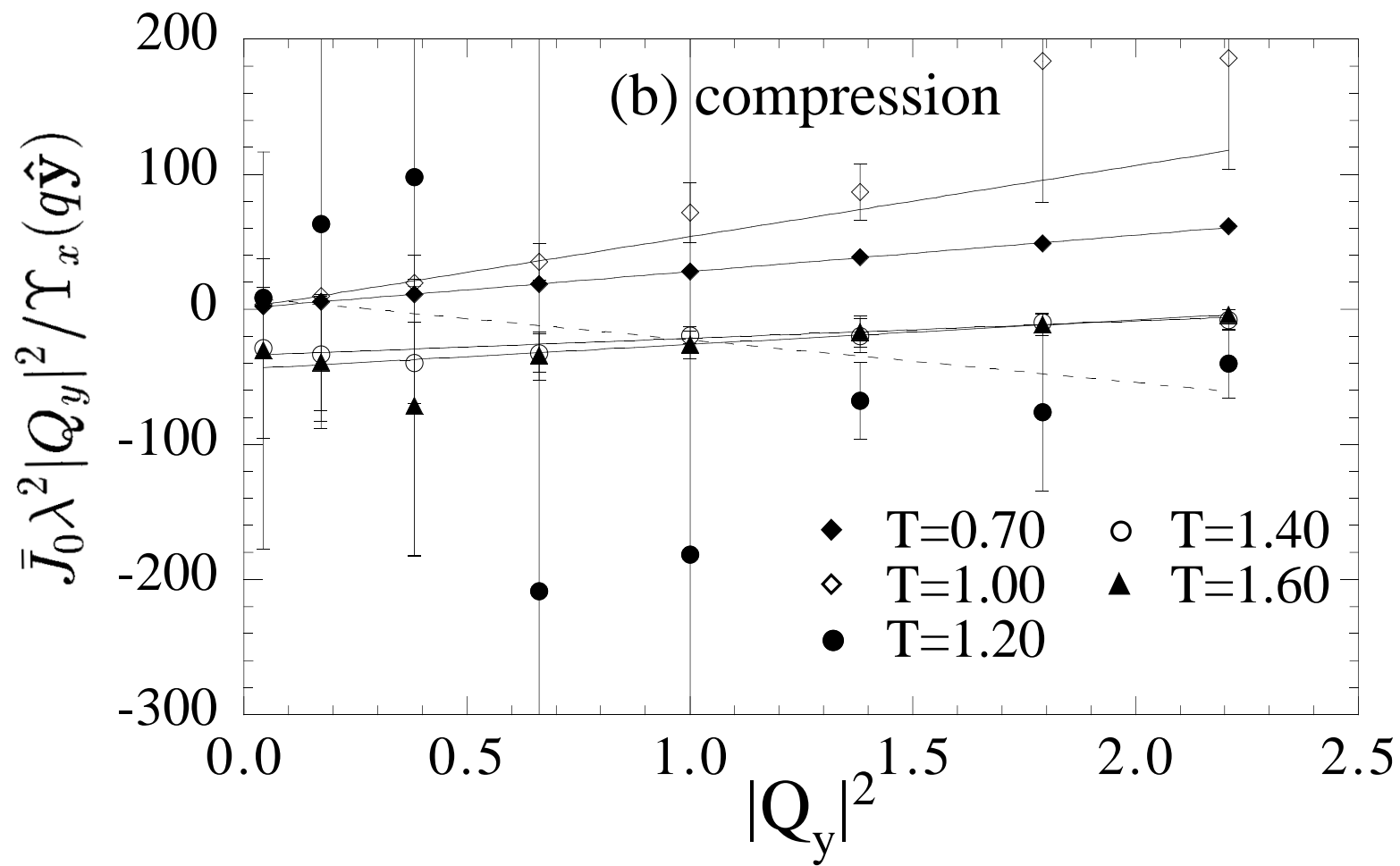


Fig. 4b

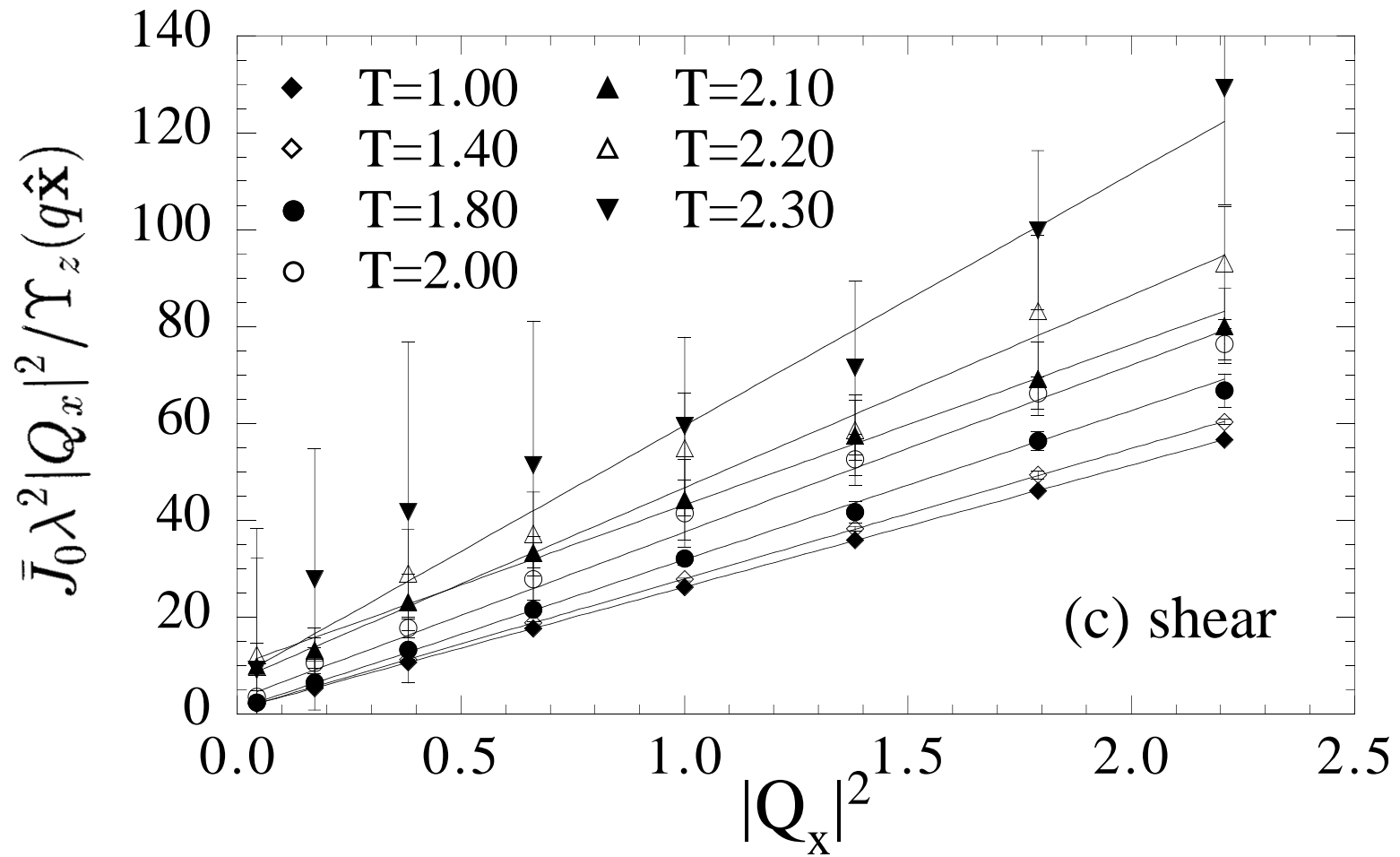


Fig. 4c

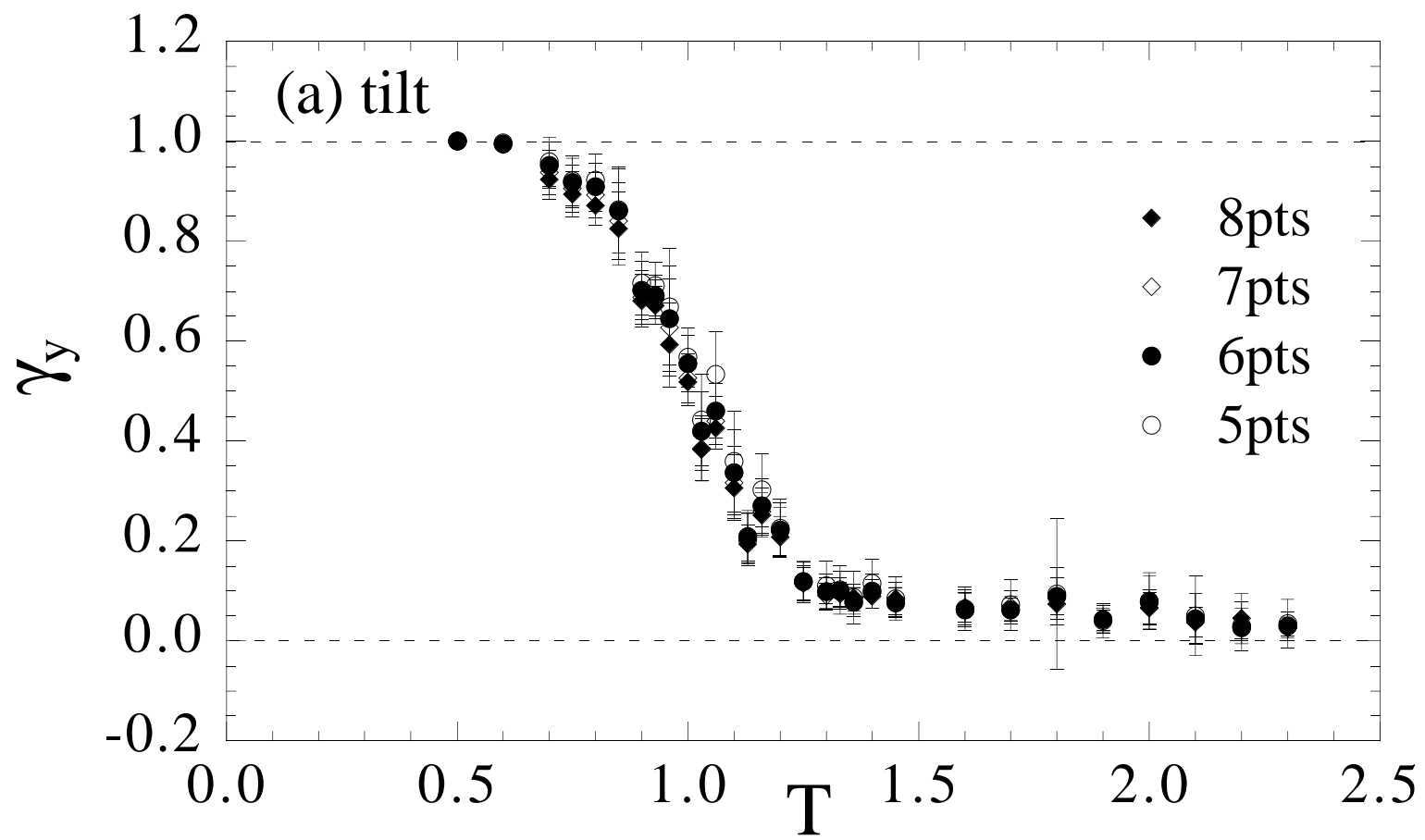


Fig. 5a

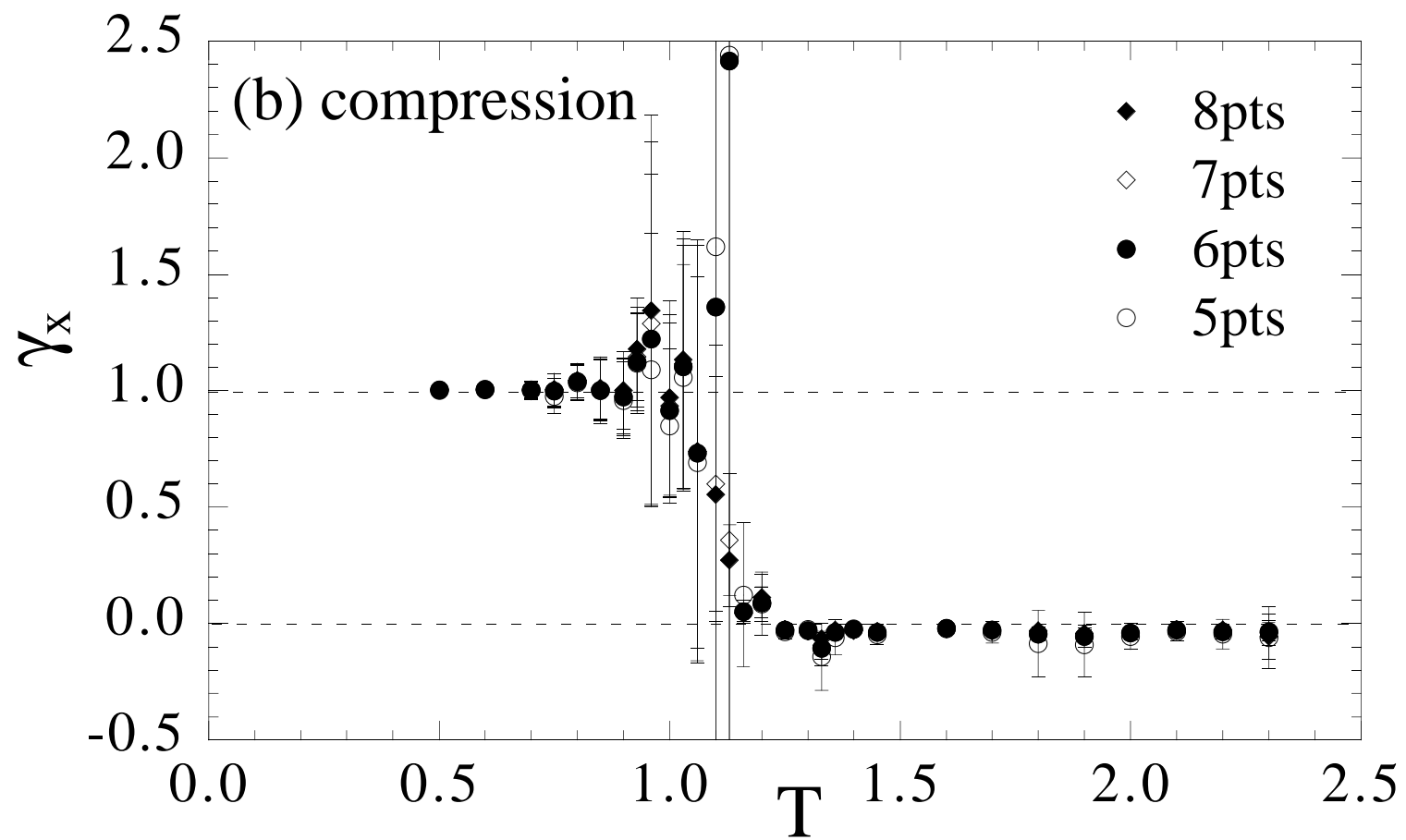


Fig. 5b

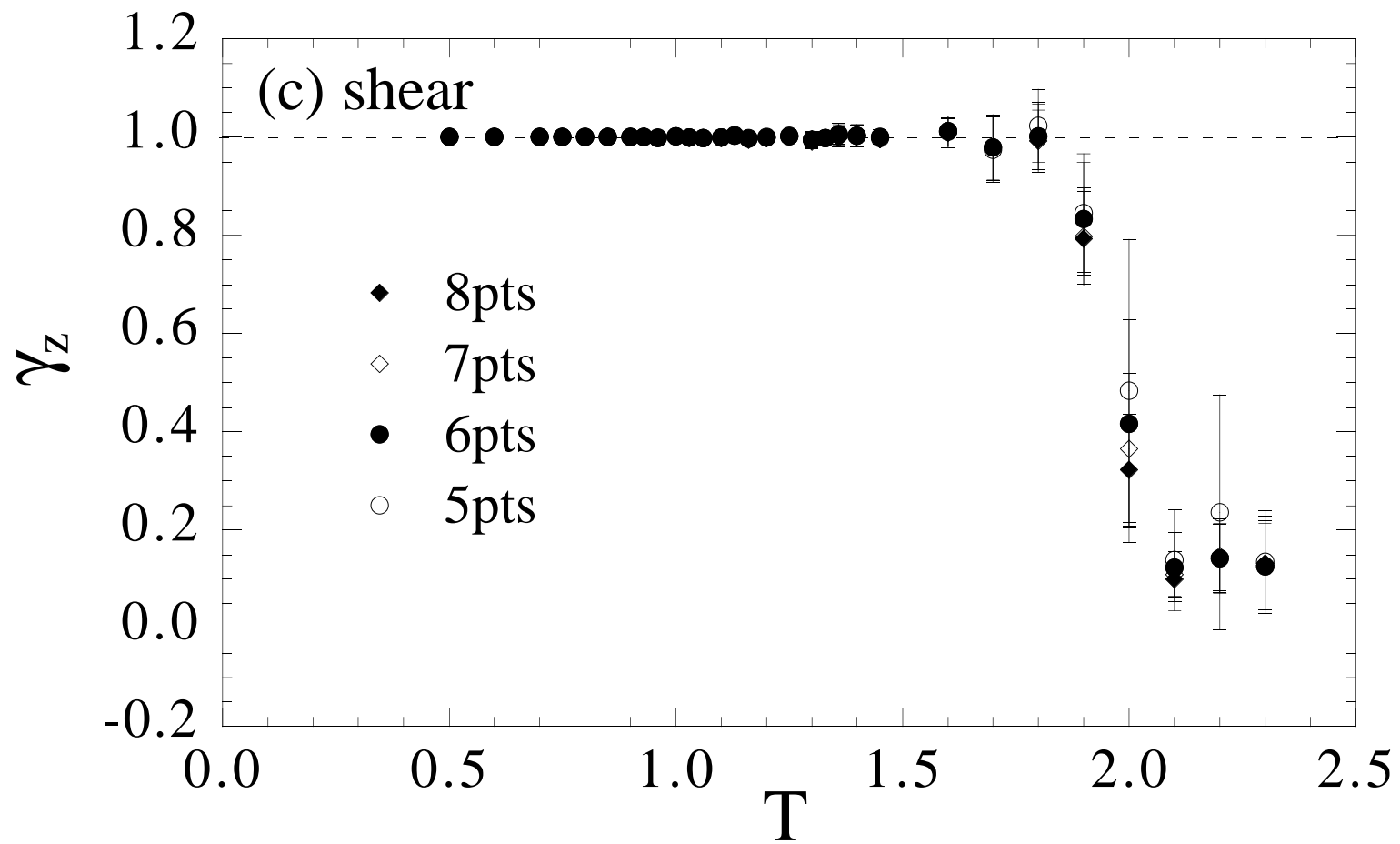


Fig. 5c

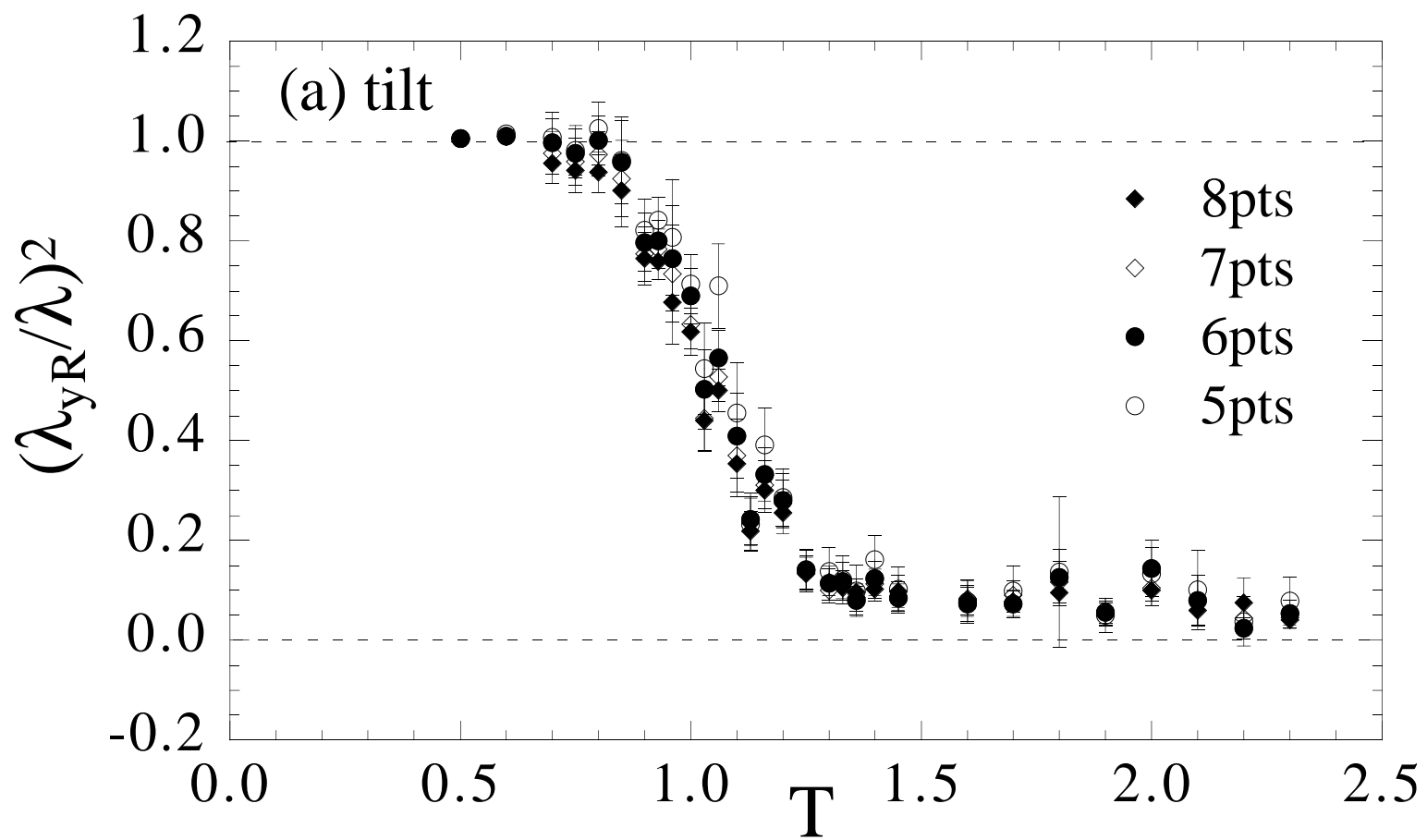


Fig. 6a

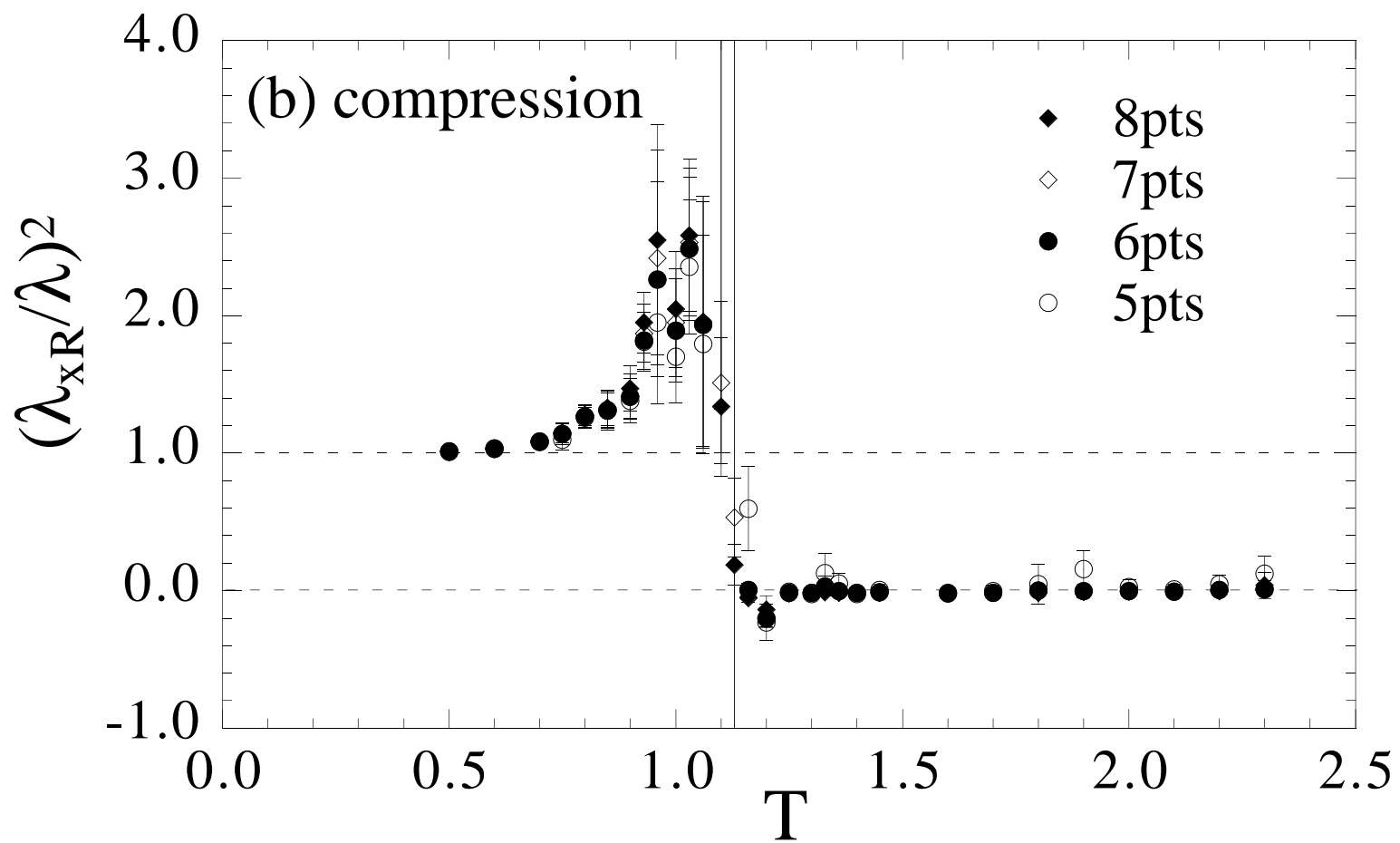


Fig. 6b

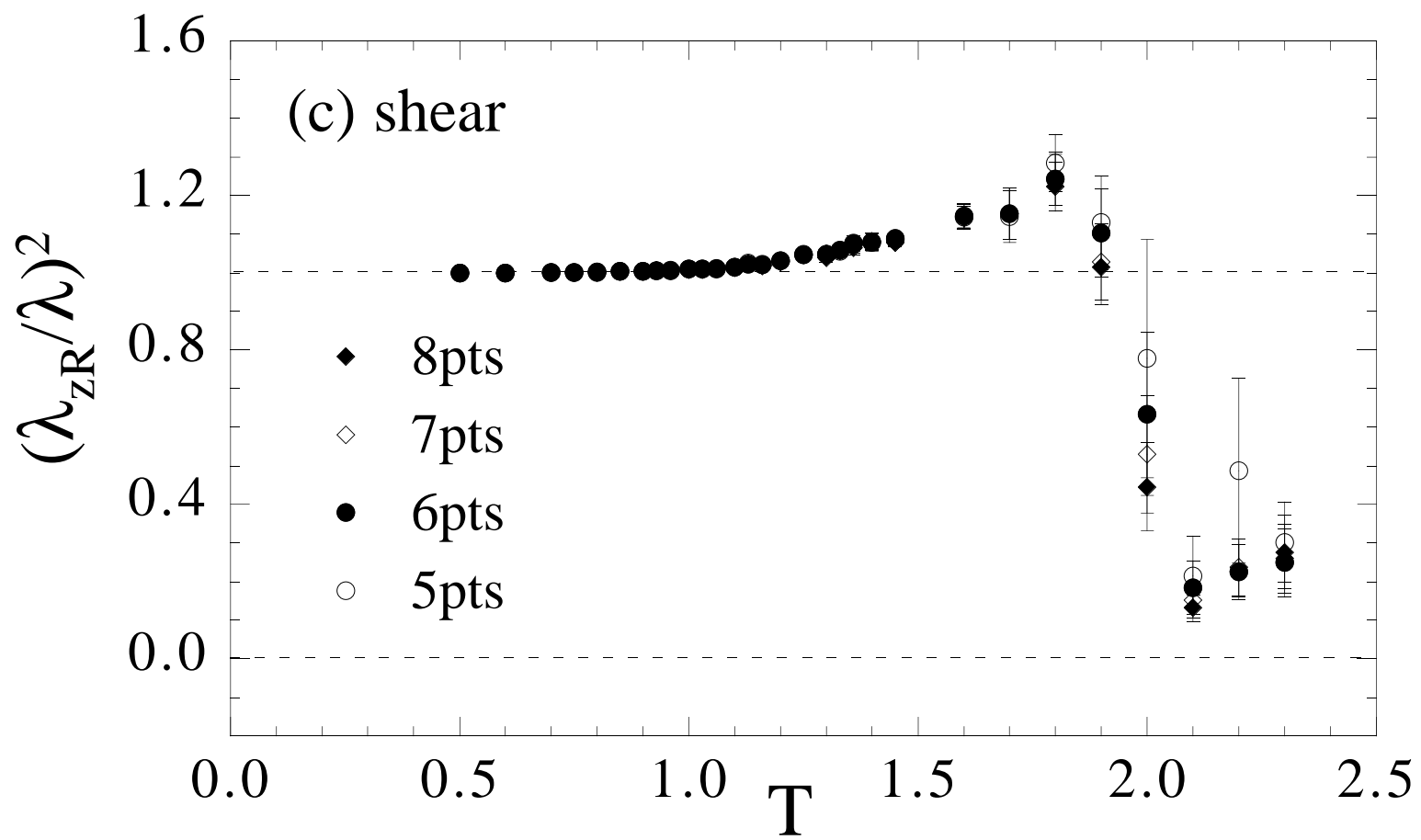


Fig. 6c

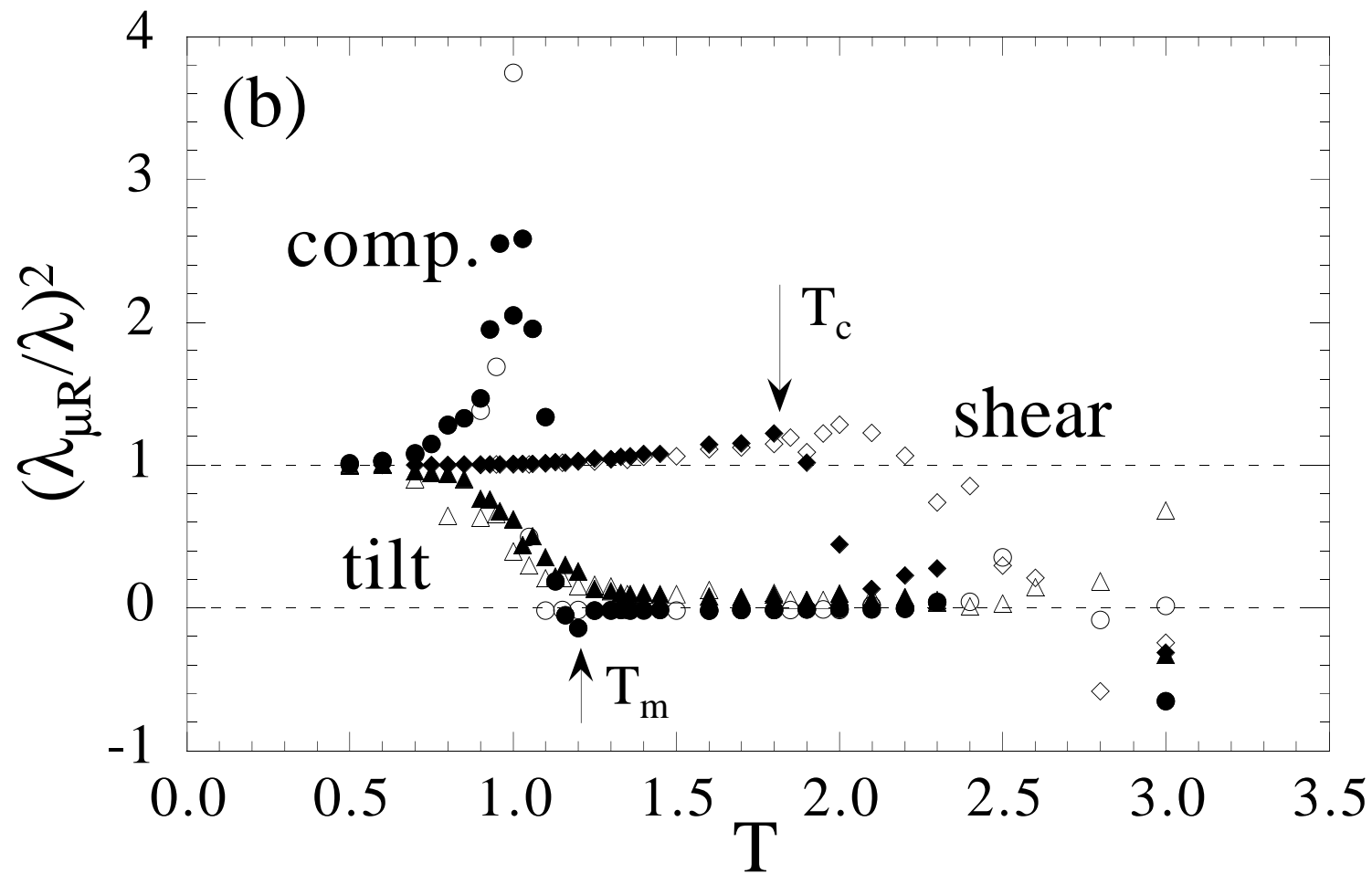
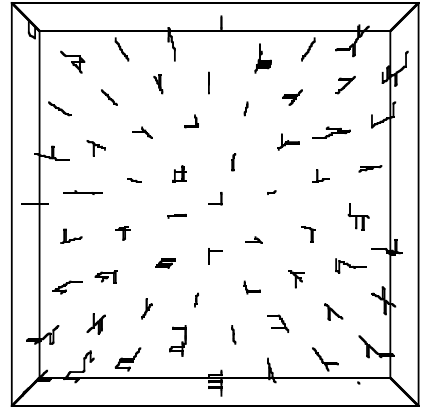
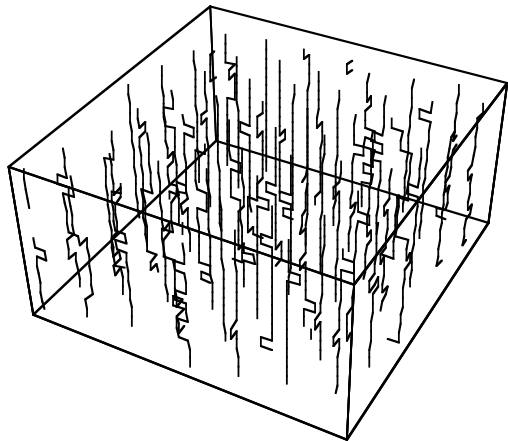
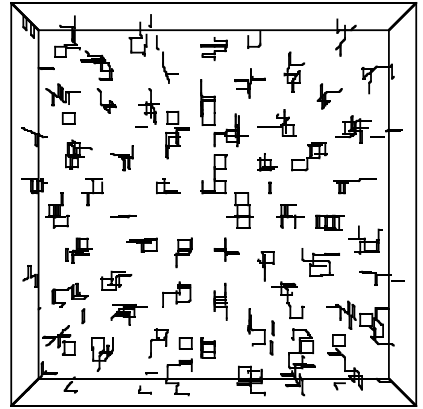
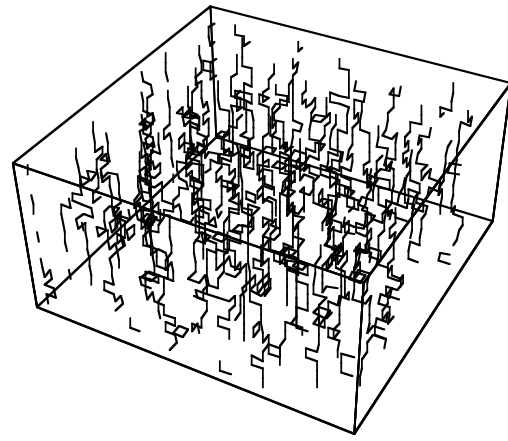


Fig. 7b

a) $T=1.0 < T_m$



b) $T_m < T=1.6 < T_c$



c) $T_c < T=2.2$

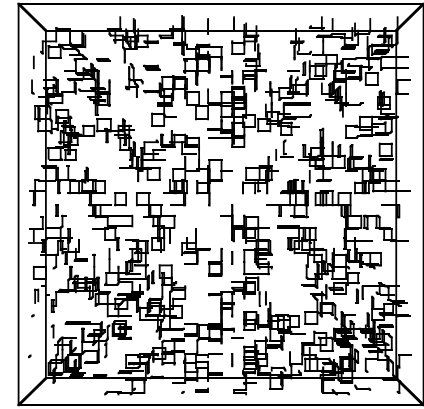
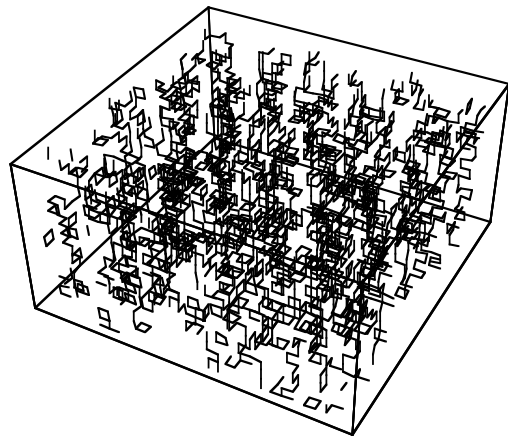


Fig. 8

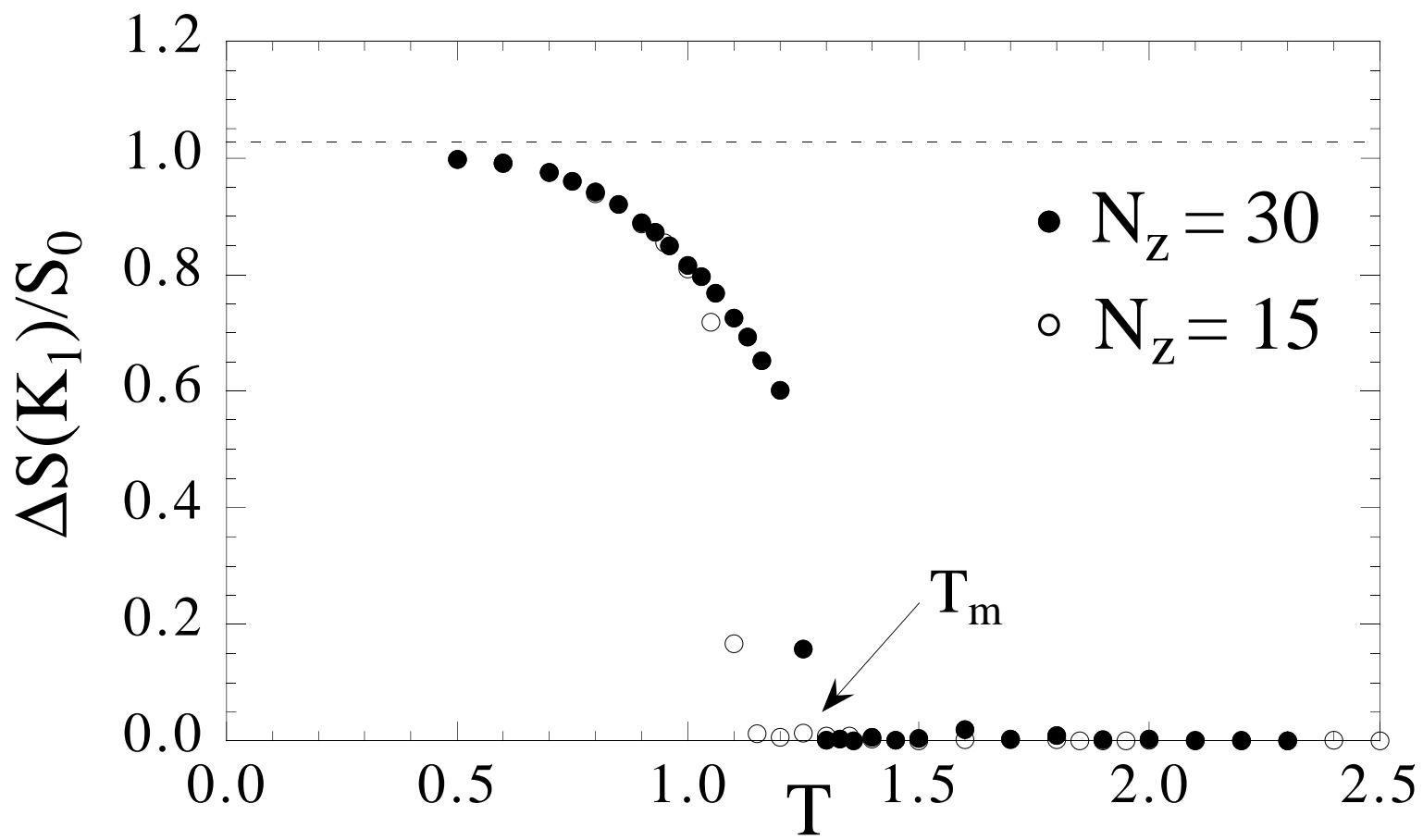


Fig. 9

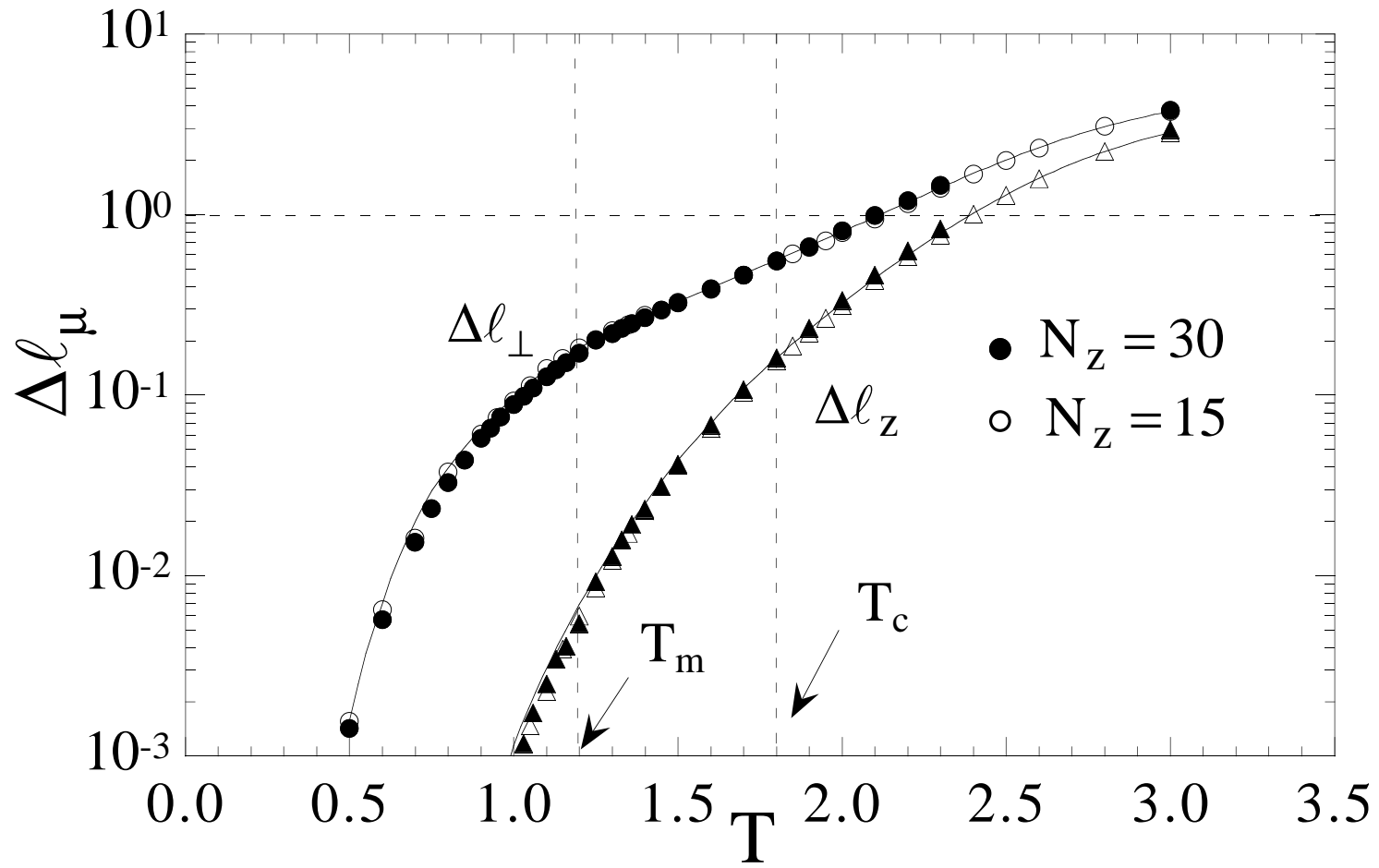


Fig. 10

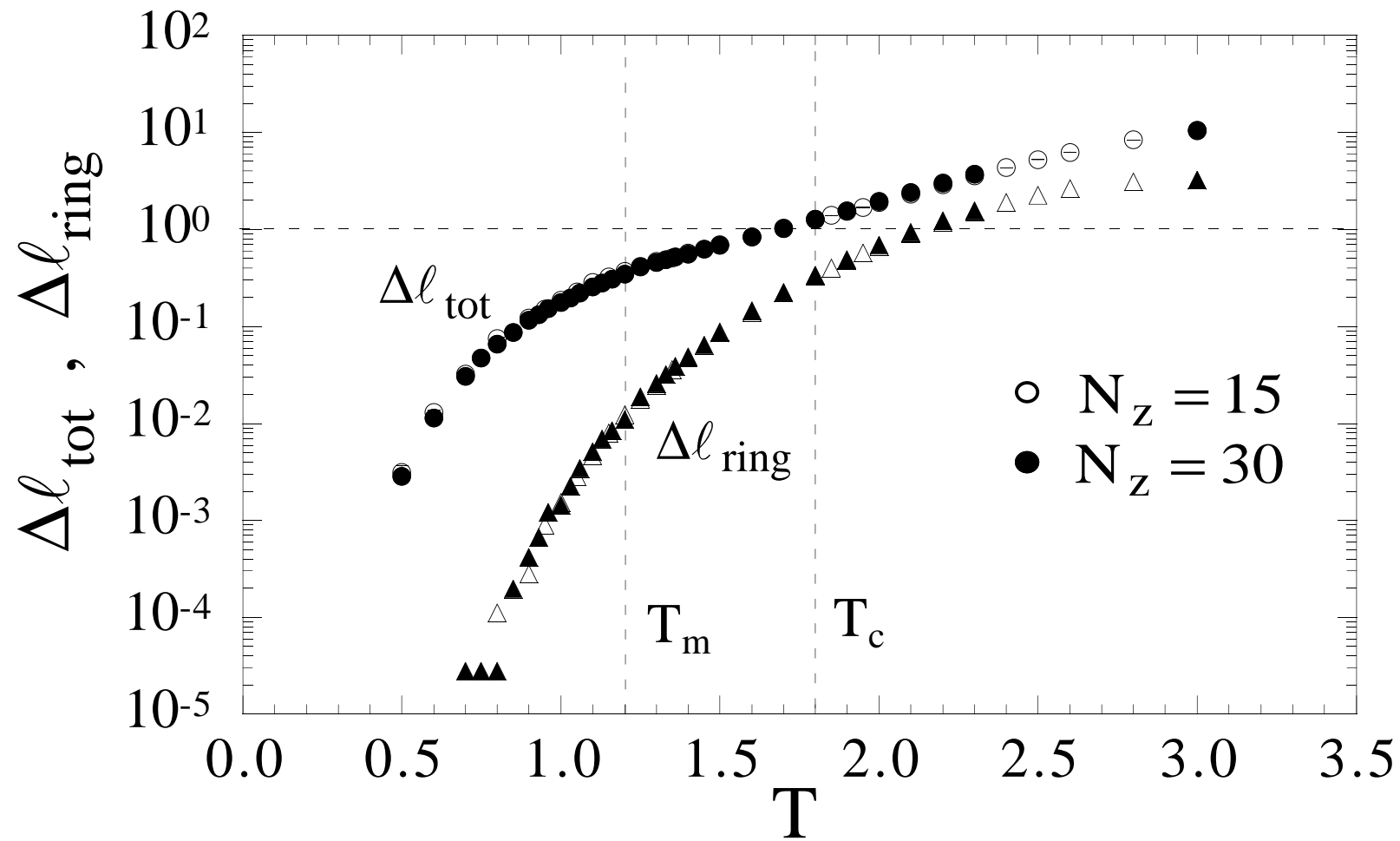


Fig. 11

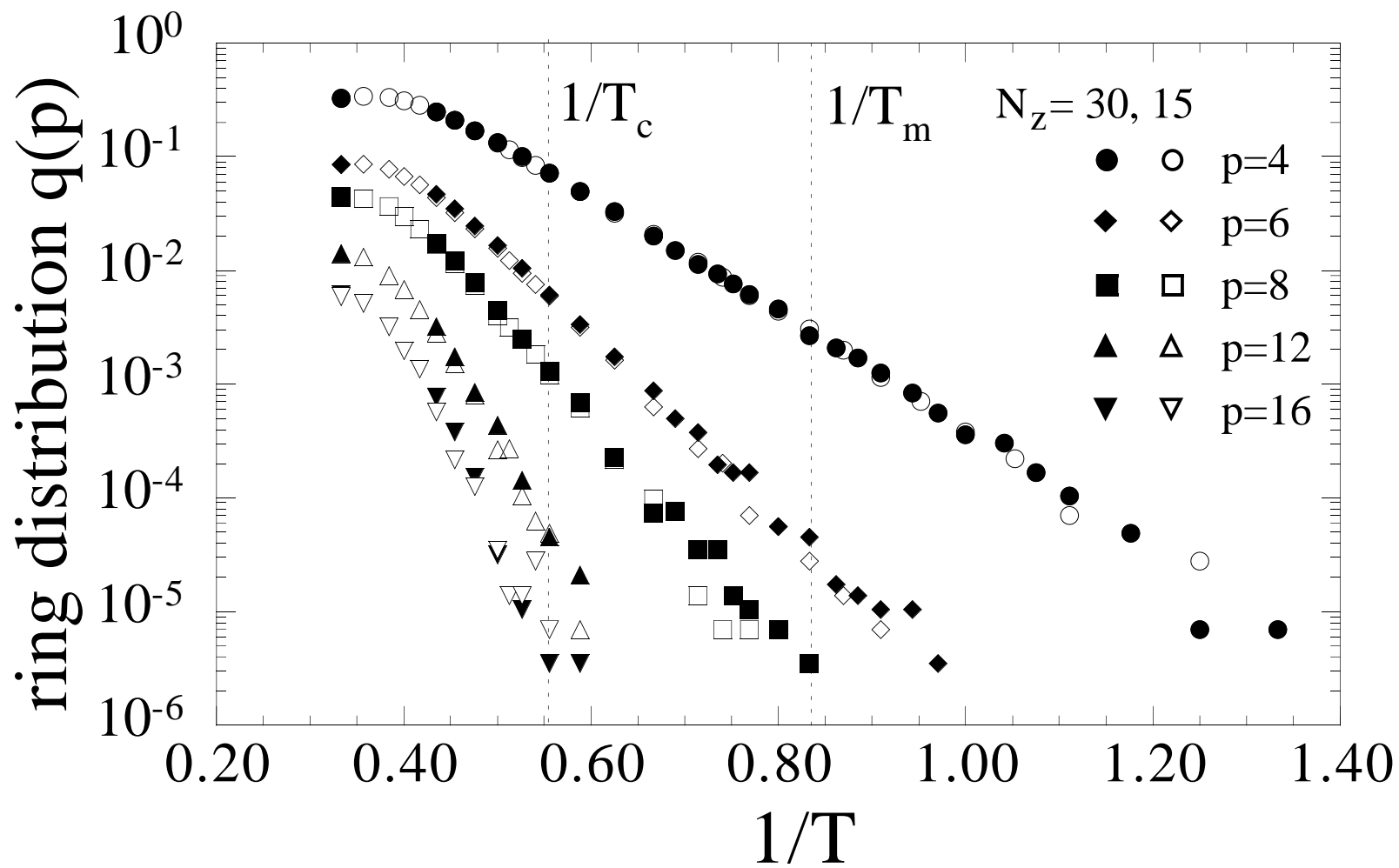


Fig. 12

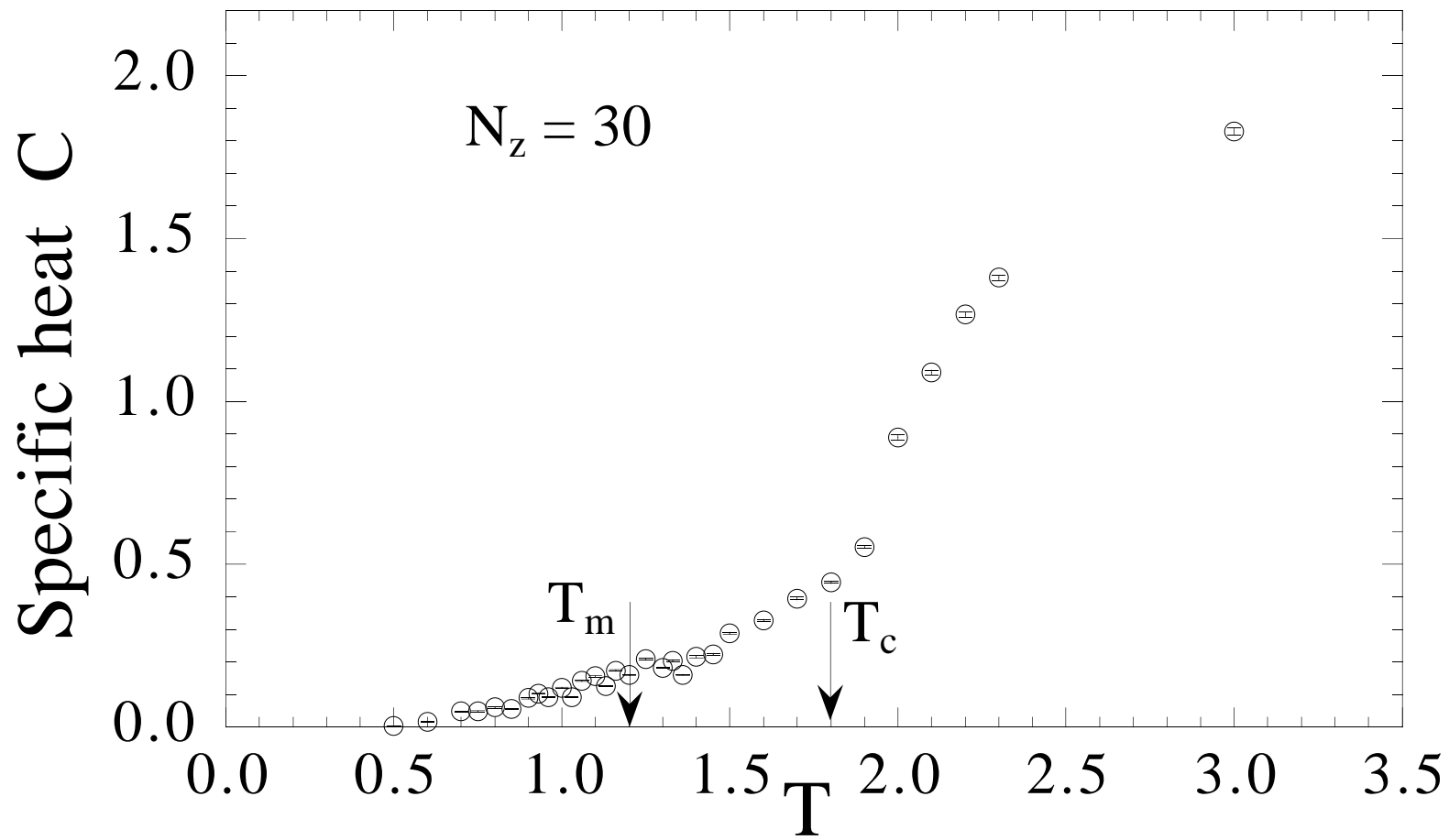


Fig. 13

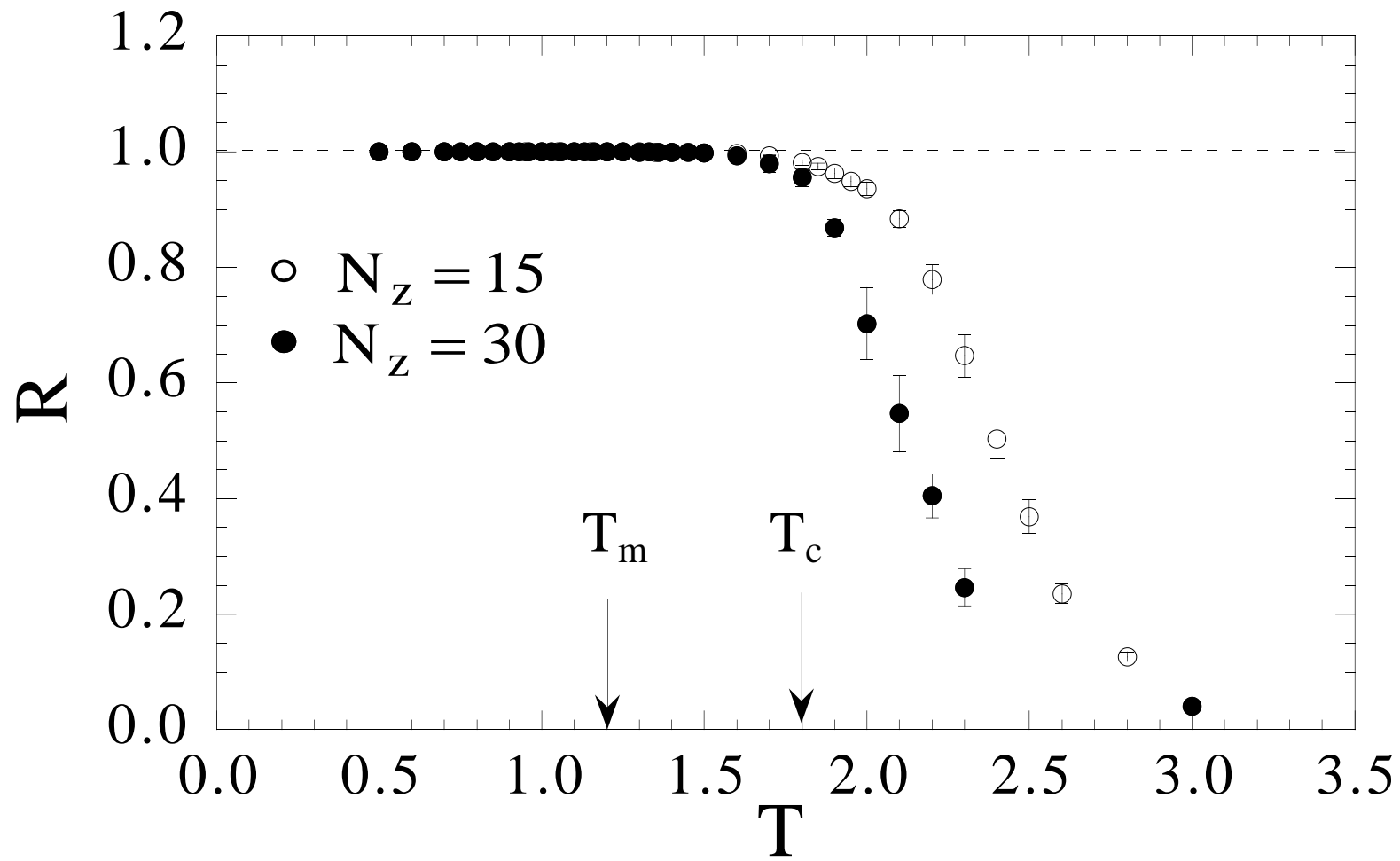


Fig. 14

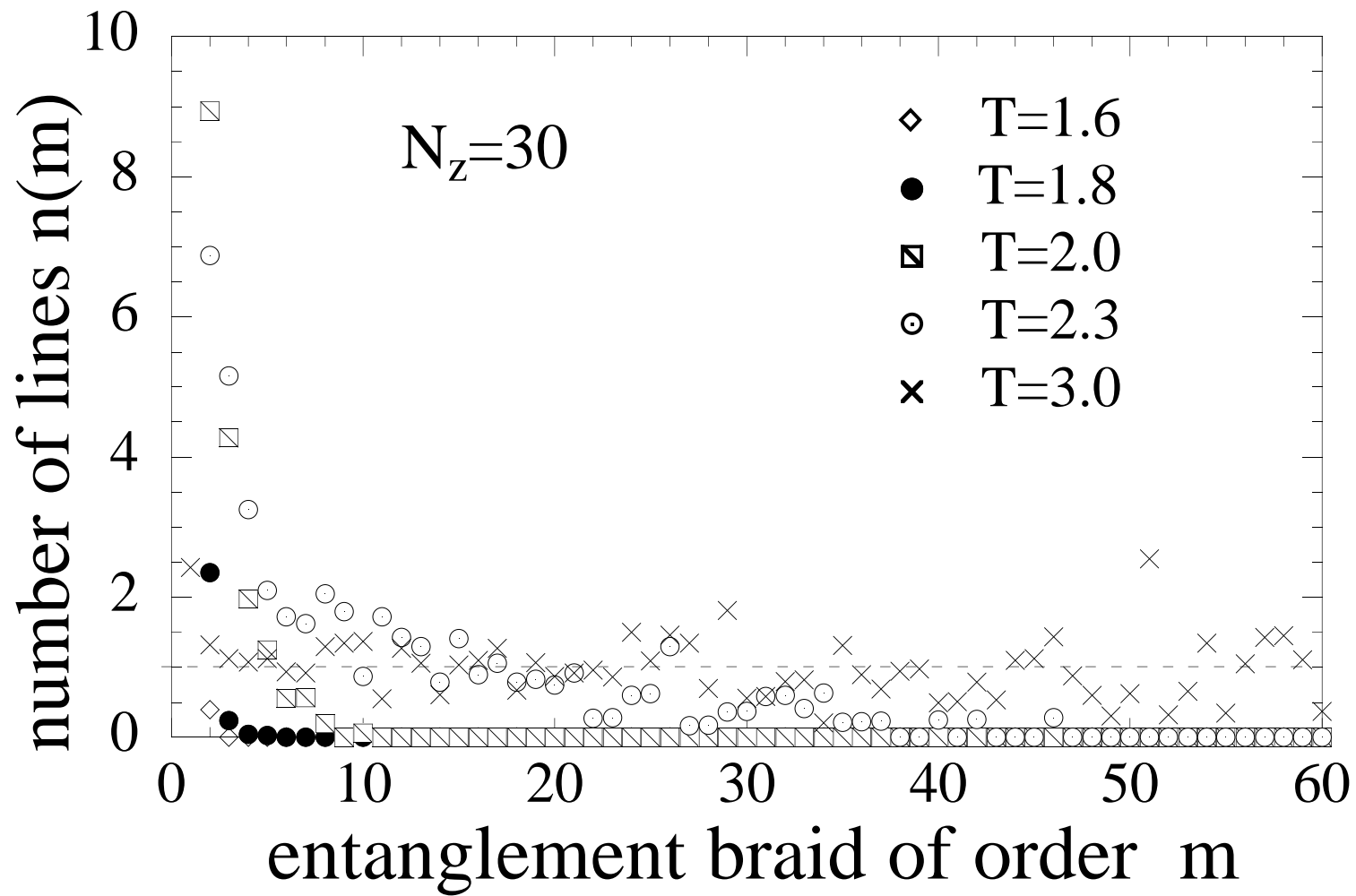


Fig. 15